



REPUBLIC OF IRAQ
MINISTRY OF HIGHER EDUCATION AND SCIENTIFIC
RESEARCH

AL-FURAT AL-AWSAT TECHNICAL UNIVERSITY
ENGINEERING TECHNICAL COLLEGE NAJAF

EFFECT OF VARIABLE CONDITIONS ON COMBUSTION
PARAMETERS BY USING CONSTANT VOLUME CHAMBER

SALAM HASAN MAHDI

M.TECH
IN MECHANICAL ENGINEERING TECHNIQUES
OF POWER

2022



**EFFECT OF VARIABLE CONDITIONS ON COMBUSTION PARAMETERS
BY USING CONSTANT VOLUME CHAMBER**

THESIS

SUBMITTED TO THE DEPARTMENT OF MECHANICAL
ENGINEERING TECHNIQUES OF POWER

IN PARTIAL FULFILLMENT OF THE REQUIREMENTS FOR
THE DEGREE OF MASTER OF THERMAL TECHNOLOGIES IN MECHANICAL
ENGINEERING TECHNIQUES OF POWER

(M.TECH)

BY

SALAM HASAN MAHDI

Supervised by

Asst. prof. Dr. Zaid Maan Hasan Al-Dulaimi

September/2022

بِسْمِ اللَّهِ الرَّحْمَنِ الرَّحِيمِ

وَقَدْ عَلِمْتُمُ

SUPERVISORS CERTIFICATION

We certify that the thesis entitled “EFFECT OF VARIABLE CONDITIONS ON COMBUSTION PARAMETERS BY USING CONSTANT VOLUME CHAMBER“ Submitted by Slam Hassan Mahdi has been prepared under our supervision at the Department of Mechanical Engineering Techniques of power. College of Technical Engineering – Najaf. AL. Furat Al –Awsat Technical University, as partial fulfilment of the requirements for the degree of Master of Techniques of Thermal Engineering.

Signature:

Name: Asst. Prof. Dr. Zaid Maan Hasan Al-Dulaimi

(Supervisor)

Date: / /2022

In view of the available recommendation. We forward this thesis for debate by the examining committee.

Signature:

Name: Dr. Ahmed Salim Naser Almurshdi

Head mechanical Eng.Tech. Of power Dept.

Date: / /2022

COMMITTEE CERTIFICATION

We certify that we have read the thesis entitled "**Effect of variable conditions on combustion parameters by using constant volume chamber** " submitted by **Salam Hasan Mahdi** and, as examining committee, examined the student's thesis in its contents. And that, in our opinion, it is adequate as a thesis for the degree of Master of Techniques in Thermal Engineering.

Signature:

Name: Asst. Prof. Dr. Zaid Maan Hasan Al-Dulaimi

(Supervisor)

Date: / / 2022

Signature:

Name: Asst. Prof. Dr. Adel A. Eidan

(Member)

Date: / / 2022

Signature:

Name: Asst. Prof. Dr. Adel M. Saleh

(Member)

Date: / / 2022

Signature:

Name: Asst. Prof. Dr. Hyder H. Abed Balla

(Chairman)

Date: / / 2022

Approval of the Engineering Technical College- Najaf

Signature:

Name: Asst. Prof. Dr. Hassanain Ghani Hameed

Dean of Engineering Technical College- Najaf

Date: / / 2022

LINGUISTIC CERTIFICATION

This is to certify that this thesis entitled “**Effect of variable conditions on combustion parameters by using constant volume chamber**” was reviewed linguistically. Its language was amended to meet the style of the English language.

Signature:

Name: Dr. Suzanne Abdul-hady Kadhim

Date:

ABSTRACT

This study is very important for combustion, combustion is one of the biggest problems in our lives, and it has a fundamental role in the environment and the economy. One of the most important properties that determine combustion is calculating the fundamental flame speed. To determine this speed, the laminar flame speed is calculated.

The laminar flame speed is one of the most essential parameters that determined the type of fuel used in combustion. The flame speed depends mainly on the unburned to burned density ratio. In this study, the laminar flame speed and burning velocity of premixed flames for various fuels are studied both experimentally and numerically.

In this study, Tracker 5.1.5 software was used to analyze stretched flame speed and CHEMKIN-PRO software to calculate the adiabatic flame temperature and the density ratio, which are utilized to calculate the laminar burning velocity. First, we evaluated the laminar burning velocities of the methane/air blend to confirm the outcomes of the experimental design. The comparison revealed a strong agreement with the findings in the literature, confirming the excellent accuracy of the experimental design and measurement techniques.

The laminar burning velocity (LBV) of premixed $\text{CH}_4/\text{H}_2/\text{CO}_2/\text{air}$ blends were numerically evaluated using CHEMKIN-PRO. Initial temperatures of (303 K), pressures of (0.1 MPa, 0.15 MPa, and 0.2 MPa), and equivalency ratios of (0.8-1.2).

The experimental study was the design and building of a centrally ignited constant volume chamber (CVC) has been designed with different equivalence ratios of air/fuel mixture range from 0.8-1.2 un-stretched flame speed (S_l), a stretched flame speed (S_n), and laminar burning velocity (S_u). The combustion process is recorded by a high-speed camera using the schlieren technique.

The experiments were carried out in a constant volume bomb with a 150 mm internal radius and 510 mm length, using various pure fuels (methane) and methane/hydrogen blends with blending ratios ranging from 10% to 30% by volume. The experiments are conducted at initial pressures of 0.1 MPa, initial temperatures of 303 ± 3 K, and equivalence ratios of 0.8 to 1.2 for the air/fuel mixture.

It is found that adding Carbon dioxide to the methane /air mixture by 30% of fuel volume will reduce the laminar LBV burning velocity by 36% (38cm/s - 28cm/s). While, It is found that adding hydrogen to the methane /air mixture by 30% of fuel volume will rise the LBV by 29% (38cm/s - 48cm/s) . On the other hand, it is concluded that hydrogen must be added by more than 30% of methane/air mixture volume to exceed the negative effect of doubling the initial pressure. Finally, increasing initial pressure is found to decelerate LBV. In such a way, double the initial pressure will element adding hydrogen with the maximum percentage used in the present work

ACKNOWLEDGMENT

Praise is to Allah, the most compassionate and the most merciful, for giving me the persistence and potency to accomplish this study. I would like to show my greatest appreciation to AL-Furat AL-Awsat Technical University- Engineering Technical College Najaf for their support and encouragement of this project.

I would like to express my special thanks to my supervisor, Dr. Zaid Maan H. Al-Dulaimi, for his scientific and moral support, everlasting guidance, and endless inspiration. His assistance and sage advice have been invaluable and have been of significant input to this study.

I would like to express my special thanks to Dr. Mohammed A. Al- Faham for their advisement and support of this work. Also, I would like to express my appreciation to Dr. Ahmed Abdulameer Abdulraheem for his guidance and input during the course of this research and his support for the manufacturing of parts and the purchase of the equipment used.

My thanks are also extended to the head and the staff of the Department of Mechanical Engineering techniques of power at the AL-Furat AL-Awsat Technical University. A special thanks to Mr. Ahmed Sh. Yasiry and Mr. Mohammed Abd AL-Amir Khadem, for helping me during the study period. Finally, my deep gratitude to my family for their patience and support in being what I am now.

Salam Hasan Mahdi

2022

DISCLAIMER

I confirm that the work submitted in this thesis is my own work and has not been submitted to another organization or any other degree.

Salam Hasan Mahdi

/ / 2022

CONTENTS

SUPERVISORS CERTIFICATION	i
COMMITTEE CERTIFICATION.....	ii
LINGUISTIC CERTIFICATION	iii
ABSTRACT	v
ACKNOWLEDGMENT	vii
DISCLAIMER.....	viii
CONTENTS	ix
LIST OF TABLES	xiv
LIST OF FIGURES	xv
NOMENCLATURE.....	xx
CHAPTER ONE.....	1
1.1 INTRODUCTION.....	1
1.2 Flame Speed	2
1.3 Laminar burning velocity (S_u)	2
1.4 Fuels used In this study	3
1.5 Problem statements.....	5
1.6 Research objectives	6
1.7 Scope of study	6

1.8 Thesis Structure	7
CHAPTER TWO	8
LITERATURE REVIEW	8
INTRODUCTION	8
2.1 Introduction	8
2.2 Flame Stretch	8
2.3 Fundamental and Characteristic of Flame Parameters	10
2.4 Experimental devices utilized for determining laminar burning velocity	11
2.4.1 Stationary flame	11
2.4.1.1 Bunsen burner method	11
2.4.1.2 Flat flame burner with Heat Flux method	12
2.4.1.3 Diverging channel method	13
2.4.1.4 Annular diverging tube method	14
2.4.1.5 Stagnation flame method	15
2.4.1.6 Nozzle burner method	16
2.4.2 Non-stationary flame	16
2.4.2.1 Tube method	17
2.4.2.2 Constant volume bomb method (CVC)	17
2.5 Measurement techniques for Burning Velocity and Laminar Flame Speed	22
2.6 Factors Influencing Flame Speed and Laminar Burning Velocity	24

2.6.1 Initial Pressure	24
2.6.2 Initial Temperature	28
2.6.3 Fuel type	29
2.6.4 Thermal Diffusivity and Specific Heat.....	30
2.6.5 Equivalence ratio (ϕ).....	31
2.6.6 Diluents.....	32
2.6.7 Fuel blends.....	35
2.7 Factors affecting Flame Speed Measuring Accuracy in CVC Method	36
2.7.1 Ignition energy.....	36
2.7.2 Flame instabilities.....	38
2.7.3 Buoyancy	38
2.7.4 Nonlinearity of the stretch rate-flame speed relationship.....	39
2.8 Summary.....	40
CHAPTER THREE	46
EXPPERIMENTAL SETUP	46
3.1 INTRODUCTION	46
3.2 1-D Analysis	46
3.3 Analysis Assumptions	47
3.4 Calculation of Equivalence Ratio	48
3.5 Adiabatic Flame Temperature	49

3.6 Density Ratio Calculations	50
3.7 Stretched flame speed analysis	51
3.8 Flame Stretched Rate and Markstein Length	52
3.9 Laminar Burning Velocity	53
3.10 The Experimental Rig's Components	53
3.11 Constant Volume Unit	56
3.11.1 Combustion chamber	56
3.11.2 Temperature measurement and control	58
3.11.3 Pressure transmitter	59
3.11.4 Gasket	59
3.12 Ignition System Unit	60
3.13 Gas injection unit	61
3.13.1 The manifold	61
3.13.2 Fuel tank	62
3.13.3 Air compressor	63
3.13.4 Vacuum System	63
3.14 Electrical Control Board Unit	64
3.15 Photographing Unit	65
3.15.1 Optical path	66
3.15.2 Camera and Source of Light	67

3.16 Calibration	68
3.17 Methods of Experimentation and Data Collection	69
CHAPTER FOUR	71
4.1 INTRODUCTION	71
4.2 Program Validation	71
4.3 Adiabatic Flame Temperature	74
4.4 Experimental Results	78
4.4.1 Repeatability Test	79
4.4.2 Ignition energy	80
4.4.3 Flame Speed Analysis	81
4.4.4 Stretched Laminar Flame Speed	84
4.4.4.1 Influence of stoichiometry	86
4.4.4.2 Influence of hydrogen blending ratio	89
4.4.5 Stretch Rate and Un-stretched Flame Speed	90
4.4.5.1 Influence of Stoichiometry	94
4.4.5.2 Influence of hydrogen blending ratio	95
4.4.6 Laminar Burning Velocity	96
4.4.6.1 Influence of Stoichiometry	97
4.4.6.2 Influence of hydrogen blending ratio	98
4.5 Simulation of Laminar Burning Velocity	99

4.5.1 Comparison of Laminar Burning Velocity	100
4.5.2 Adiabatic flame temperature for different Syngas Blends	100
4.5.3 Influence of initial Pressure	102
4.6 Correlation of Laminar Burning Velocity	106
CHAPTER FIVE	107
5.1 Conclusions	107
5.2 Suggestions for Future Work.....	108
REFERENCE:	110
APPENDIXES	124
Appendix (A): Calibration Certificate	124
Appendix (B): List of Publications.....	129
الخلاصة	

LIST OF TABLES

CHAPTER ONE

Table 1.1: Physical and Chemical Properties of Used Fuels	5
---	---

CHAPTER TWO

Table 2.1- Summary of some prior research	42
---	----

CHAPTER THREE

Table 3.1- Tracker Software Settings for Measuring Flame Speed	52
--	----

CHAPTER FOUR

Table 4.1- Adiabatic flame temperature versus equivalence ratio for CH₄/H₂ /air mixtures at T_i=303±3K with different initial pressures. (a) P_i=0.1MPa (b) P_i=0.2MPa (c) P_i=0.3MPa	76
--	----

Table 4.2- Adiabatic flame temperature vs equivalence ratio for methane with various initial pressures at T_i =303±3 K	78
---	----

LIST OF FIGURES

CHAPTER TWO

Figure 2.1- depicts the stretch and curvature of a flame [17].....	9
Figure 2.2 (a) Bunsen flame , (b) Bunsen burner [14]	12
Figure 2.3- Flat flame burner method [31].....	13
Figure 2.4 - Diverging channel externally heating [32]	14
Figure 2.5- Development of annular step-wise diverging tube [35]	15
Figure 2.6- Schematic diagram of Stagnation flame method [14]	16
Figure 2.7- Constant volume combustion chamber [14].....	17
Figure 2.8- Outwards expanding spherical flame [14].....	18
Figure 2.9- The LBV of methane/air blends with various assessment methods [35].....	22

Figure 2.10- Influence of initial pressure and dilution on CH ₄ /air mixture [77]	27
Figure 2.11- The LBV of C ₃ H ₈ /H ₂ /Air blend Vs with Changing P_i and T_i [93].....	29
Figure 2.12- Variation of S_u with carbon's number atoms in fuel molecules [68].....	30
Figure 2.13- Unstretched LBV for CH ₄ /H ₂ /air mixture versus equivalence ratio [110].....	33
Figure 2.14- Flame Speed vs. Radius for Various Ignition Energies [122].	37
Figure 2.15- Schlieren images of NH ₃ /O ₂ /N ₂ flames at $\phi=1$, $P_i = 1$ atm [126].....	39

CHAPTER THREE

Figure 3.1- Photography for the experimental rig used in the study	54
Figure 3.2- Schematic layout for experimental setup.....	55
Figure 3.3 - Photography for the carbon-steel CC unit	58
Figure 3.4- a) Digital temperature controller, b) Temperature sensor.....	58
Figure 3.5- Pressure transmitter, DPA-Mpa.....	59
Figure 3.6- Gasket	60
Figure 3.7- Schematic diagram of an electronic circuit for the ignition unit	61
Figure 3.8- The gas manifold	62
Figure 3.9- Pressure organizer valve	62
Figure 3.10- Air compressor.....	63
Figure 3.11- Electrical control board unit	65

Figure 3.12- Schematic diagram of Photographing Unit.....	66
Figure 3.13: Convex lens.....	67
Figure 3.14- High-speed camera (AOS -Q PRI)	68
Figure 3.15.a: Thermocouple calibration	69
Figure 3.15.b: Pressure gauge calibration	69

CHAPTER FOUR

Figure 4.1- Experimental and simulation data for LBV of methane at $P_i=0.1\text{MPa}$ compared to published results	72
Figure 4.2- Error of burning velocity of methane for current study with different equivalence ratio.....	73
Figure 4.3- A comparison of adiabatic flame temperature with earlier methane tests under normal settings at $T_i=303\pm 3\text{ k}$ and $P_i=0.1\text{ MPa}$	74
Figure 4.4- Adiabatic flame temperature versus equivalence ratio for $\text{CH}_4/\text{CO}_2/\text{air}$ mixtures at $T_i=303\pm 3\text{K}$ with different initial pressures. (a) $P_i=0.1\text{MPa}$ (b) $P_i=0.2\text{MPa}$ (c) $P_i=0.3\text{MPa}$	77
Figure 4.5- Schlieren Radius vs. stretched Flame Speed for four consecutive methane/air mixture experiments at $T_i=303\pm 3\text{K}$ and $P_i=0.1\text{MPa}$	80
Figure 4.6- Flame propagation photographs for methane at $T_i = 303\pm 3\text{ K}$, $P_i = 0.1\text{MPa}$, and various equivalence ratios.....	82

Figure 4.7- Methane flame radius at stoichiometry as a function of time for various conditions at $T_i=303\pm 3\text{K}$ and $P_i= 0.1\text{MPa}$	83
Figure 4.8- S_n variation with flame radius for methane at $T_i= 303\pm 3\text{ K}$ and $P_i =0.1\text{MPa}$ for various equivalence ratios.....	86
Figure 4.9- Variation of S_n with Equivalence Ratios for Methane with Various Hydrogen Percentages at (2cm) Radius, $T_i= 303\pm 3\text{ K}$ and Atmosphere Pressure	87
Figure 4.10- S_n Variation with flame radius for methane at $T_i= 303\pm 3\text{ K}$ and $P_i =0.1\text{MPa}$ with various hydrogen percentages and stoichiometry : (a) $\phi=0.8$ (b) $\phi=1$ and (c) $\phi=1.2$	88
Figure 4.11- S_n Variation with Flame Radius for Methane with Different Hydrogen Mixtures for Stoichiometric Mixture ($\phi=1$) at Atmospheric Pressure.....	89
Figure 4.12- S_n Variation with Hydrogen Percent for various Equivalence Ratio at a radius of 2 cm , at $T_i= 303\pm 3\text{ K}$ and 0.1MPa initial pressures	90
Figure 4.13- S_n stoichiometric CH_4/air values against at $T_i= 303\pm 3\text{ K}$ and $P_i =0.1\text{MPa}$ with a linear relationship	92
Figure 4.14- Stretched flame speed vs. stretch rate for methane at $T_i= \pm 303\text{ K}$ and $P_i =0.1\text{MPa}$ for various equivalence ratios.....	92
Figure 4.15- Stretched flame speed vs. stretch rate for methane at $T_i= 303\pm 3\text{ K}$ and $P_i =0.1\text{MPa}$ for various equivalence ratios: (a) $\phi=0.8$ (b) $\phi=1$ (c) $\phi=1.2$	93

Figure 4.16- Unstretched flame propagation speed versus equivalence ratios for methane/hydrogen/air mixtures at an initial pressure of 0.1MPa at different hydrogen blends.....	94
Figure 4.17- Flame propagation speed vs. hydrogen blend for different equivalence ratios at $T_i = 303 \pm 3$ K and $P_i = 0.1$ MPa.....	95
Figure 4.18- Burning velocity vs. hydrogen fraction at various equivalency ratios, $T_i = 303 \pm 3$ K and $P_i = 0.1$ MPa	97
Figure 4.19- Equivalence Ratio vs. LBV for Different Hydrogen Blends at $T_i = 303 \pm 3$ K and $P_i = 0.1$ MPa.....	98
Figure 4.20- S_u versus H_2 concentrations and adiabatic flame temperature at $\phi = 1$, $T_i = 303 \pm 3$ K and $P_i = 0.1$ MPa	101
Figure 4.21- S_n versus CO_2 concentrations and adiabatic flame temperature at $\phi = 1$, $T_i = 303 \pm 3$ K and $P_i = 0.1$ MPa.....	102
Figure 4.22- S_u versus equivalence ratio concentrations at 303 ± 3 K and (a) $P_i = 0.1$ MPa, (b) $P_i = 0.15$ MPa and (c) $P_i = 0.2$ MPa	103
Figure 4.23- S_u versus equivalence ratio concentrations at 303 ± 3 K and (a) $P_i = 0.1$ MPa, (b) $P_i = 0.15$ MPa and (c) $P_i = 0.2$ MPa	104
Figure 4.24- LBV vs. Hydrogen Blend at Stoichiometric Mixture for Different Initial Pressures	105
Figure 4.25- LBV vs. Carbon dioxide Blend at Stoichiometric Mixture for Different Initial Pressures	105

NOMENCLATURE

Character	Definition	Unit
A	Flame Surface Area	m^2
C_p	Molar Heat Capacity at Constant Pressure	J/mol.K
D_T	Thermal diffusivity	m^2/s
d	Diameter	mm
K	Karlovitz number	-
l	Length	mm
L	Litre	m^3
L_b	Markstein Length	mm
Le	Lewis number	-
M	Molar Mass	kg/mol
m	Total Mass	kg
n_t	Number of Mole of Component	mol
n_i	Number of Mole of Initial	mol
n_a	Number of Mole of Air	mol
n_f	Number of Mole of Fuel	mol
p	Pressure	MPa
P_i	Initial pressure	MPa
P_{max}	Maximum combustion pressure	MPa
P_t	Total pressure	MPa
P_i	Initial pressure	MPa

R	Gas constant	KJ/kg.K
r_i	Radius Prior to Combustion	mm
r_f	Flame radius	mm
S_u	Stretched laminar burning velocity	cm/s
S_l	Unstretched laminar burning velocity	cm/s
S_n	Stretched laminar Flame speed	cm/s
T_{ad}	Adiabatic flame temperature	K
T_i	Initial temperature	K
T_u	Unburned temperature	K
t	Time	s
h	Enthalpy	KJ/Kg
V	Volume	m^3
X_i	Molar ratio	-
x_i	Volume fraction	-
Greek Symbols		
ρ	Density	kg/m ³
ρ_b	Burned density ratio	kg/m ³
ρ_u	Unburned density ratio	kg/m ³
\emptyset	Equivalence ratio	-
α	Flame stretch rate	1/s
τ	thermal conductivity	W/mk
Subscripts		

Symbols	Description
Act	Actual
ad	Adiabatic
Ave	Average
B	Burned
F	Fuel
I	Initial condition
L	Unstretched
Prod	Products
React	Reactants
Stoich	Stoichiometric
U	Unburned
Abbreviations	
Symbols	Description
AFR	Air-fuel ratio
ADT	Annular diverging tube
CC	Constant Chamber
CPM	Constant Pressure Method
CVM	Constant Volume Method
CVCM	Constant Volume Chamber Method
CVC	Constant Volume Chamber
DM	Dissociated methanol
LBV	laminar burning velocity

LBVs	laminar burning velocities
LPG	Liquid Petroleum Gas
RP-3	Aviation kerosene

Chapter One

Introduction

CHAPTER ONE**INTRODUCTION****1.1 Introduction**

Combustion is a chemical reaction that is exothermic and produces enough heat to support the combustion process [1]. This technique typically produces heat in addition to light in the form of flame. The nature of the chemical reaction itself causes the reactants to mix quickly. The combustion process also produces heat, which raises the temperature of the reactants and accelerates the pace of the reaction.

The combustion process starts with a source of ignition, such as heat or a spark. As soon as the combustible combination reaches the temperature of self-ignition, it begins. Each point of this burning layer serves as an ignition source for the subsequent adjacent layer as combustion spreads from the source of ignition to the next layer of unburned mixture, and so on. It is impossible to derive an equation for forecasting combustion phenomena for various combustion settings due to the rapid changes in the concentrations and temperatures of the combustible mixture as well as the complexity of the mechanism associated with the combustion reaction. For particular reaction conditions, empirical correlations are utilized as an alternative.

Flames are defined as visible, localized exothermic chemical reaction that produces heat [2]. It can be categorized into premixed and diffusion flames based on how the reactants are combined, as well as stationary and non-stationary flames based on how the flame moves. Depending on the flow regime, each of them can be further separated into a laminar and turbulent flame.

Improving combustion efficiency and combustion system performance is of the utmost importance given the anticipated limitation of fossil fuels and the issue of global environmental pollution. The flame propagation and its formation have a significant impact on both variables. This study is an attempt to clarify flame generation and speed for various fuels essential to internal combustion engines.

1.2 Flame Speed

In combustion, the phrase "flame speed" by itself is ambiguous. Since this term might indicate different things in different situations. To make clear what is meant by the flame speed and what is being measured or is intended to be measured, there are frequently multiple definitions provided. The concept of flame speed is therefore based on how the viewer perceives the flame's movement inside the unburned mixture. The flame speed is traditionally described as the rate at which a flame front moves for the fresh gases [3]. The flame speed is divided into two types, laminar and turbulent, as will be explained in detail.

1.3 Laminar Burning Velocity (S_u)

It is the velocity at which unburned gases pass through the combustion wave in a direction normal to the wave surface [4]. It is a key characteristic of fuel that is calculated from chemical kinetics processes as well as the movement of molecular mass and heat. Another important factor in determining the fuel's properties during combustion and establishing the chemical kinetics is laminar burning velocity. As a result, it is crucial for predicting the output and emissions of any combustion system [5]. Even though turbulent combustion occurs in the majority of combustion systems,

laminar burning velocity research is still necessary since many turbulent combustion systems use it as input data.

The constant volume chamber method is one of the experimental techniques used to gauge the laminar burning speed for non-stationary flames (CVC). The following advantages of this strategy above others are the reasons it was chosen for this study:

- (a) The combustion happens instantly, and not much fuel is used.
- (b) It mimics how combustion works in spark-ignited engines (SIE).
- (C) It has the best control over the accurate initial condition setup and combination composition.
- (d) Flame stretch rates that are well characterized due to spherical flame propagation.

1.4 Fuels Used In This Study

The depletion of fossil fuels and the tightening of regulations on vehicle emissions encourage researchers to focus more on the investigation of alternative (clean) fuels while also enhancing combustion [6]. Table (1.1) lists the fuels that have been chosen for this investigation.

➤ Methane (CH₄)

It is the primary component of natural gas, one of the alternative fuels that will be used in spark ignition engines in the future. Additionally, among hydrocarbon fuels, it has the smallest chain structure. Methane has thus been used in this research [7].

➤ Hydrogen (H₂)

A diatomic gas that is colourless, odourless, tasteless, non-toxic, non-metallic, and highly flammable. It has a fast flame speed, a broad flammability range [8], low minimum ignition energy, and no HC or CO₂ emissions [9].

➤ Carbon dioxide (CO₂)

Carbon dioxide is a chemical compound composed of one carbon atom and two oxygen atoms in each molecule. At room temperature, it exists in the gaseous state. Visible light cannot pass through carbon dioxide in the atmosphere. The burning of fossil fuels is the main contributor to both these elevated CO₂ concentrations and the development of both global warming and climate change [10].

Table 1.1: Physical and Chemical Properties of Used Fuels [8,9,11]

Property	Methane	Hydrogen	Carbon dioxide
Chemical formula	CH ₄	H ₂	CO ₂
Molecular weight (g/mol)	16.043	2.016	664
Max. laminar burning velocity at 100 °C (cm/s)	55	230	0
Auto ignition temperature (°C)	580	585	-
Density at 20 °C (kg/ m ³)	0.667	0.09	1.779
Boiling point (°C)	-161.5	-252.9	-78.46

1.5 Problem Statements

Due to the worldwide constantly-increasing demand for energy, fuel consumption and the global pollution problem, it is critical to improving combustion efficiency and system performance. Flame formation and propagation speed have a big impact on each of these factors. This study is an experiment to learn more about flame creation and speed for various fuels relevant to internal combustion engines.

1.6 Research Objectives

Flame parameters such as flame speed and LBV must be studied to build and optimize combustion systems. They have a significant impact on engine power output, performance, and pollutant emissions since they indicate a fuel's reactivity. Controlling these two factors under varied settings is therefore critical, and the following are the study's objectives:

- 1- Investigating the laminar burning velocity (S_u), the stretched (S_n) and un-stretched flame speeds (S_l) by creating a new cylindrical combustion chamber with a centrally ignited premixed fuel/air mixture.
- 2- The Schlieren technique is used to investigate the properties of the fundamental flame speed of a CH_4 /air mixture.
- 3- Studying the effect of initial pressure on CH_4 /air blends and CH_4 /syngas/air mixtures on S_u , S_n and S_l .
- 4- Studying the effect of carbon dioxide and hydrogen dilutions ranging from 10% to 30% at various equivalence ratios on S_u , S_n and S_l .
- 5- Numerically simulating the laminar burning velocities by CHEMKIN-PRO using the GRI 3.0 procedure and comparing the experimental findings to the expected results in this study and the literature.

1.7 Scope Of Study

The study was conducted under the following settings and criteria to achieve those goals:

- 1- The CVC will be built with a 250 mm internal diameter and a 510 mm length.
- 2- The initial temperature will be 303 ± 3 K during the tests.
- 3- The initial pressure will be changed (0.1, 0.15 and 0.2) MPa during the tests.
- 4- The equivalence ratios will be (0.8-1.2) during the tests.
- 5- Pure gaseous fuels (methane) will be used in the tests.
- 6- A methane/syngas/air mixture with a blending ratio of 10%, 20%, and 30% will be tested.

1.8 Thesis Structure

The thesis arrangement is shown in this section. Following this brief overview of the study's goals, chapter 2 presents a background of earlier research that has been done to estimate laminar burning velocities (LBVs). This background includes the various approaches and methods that have been used in this area, as well as the variables that affect the combustion process and techniques used to measure burning velocity. The experimental setup is described in detail in Chapter 3 along with the measurement methodology and optical technique employed. Presenting the theoretical calculations required in the experimental part, which is followed by the numerical modelling using CHEMKIN-PRO and the mechanism used in this study. The experimental and numerical findings are presented and discussed in Chapter 4; Chapter 5 summarizes the suggestions and recommendations.

Chapter Two

Literature Review

CHAPTER TWO

LITERATURE REVIEW

2.1 Introduction

The laminar flame speed plays an important role in spark-ignition engines, as well as in many other combustion applications, such as in designing burners and predicting explosions [12]. While The speed at which unburned gases pass through the combustion wave in a direction normal to the wave front is known as laminar burning velocity (S_u) [13]. The Combustion features such as initial temperature, initial pressure, thermal diffusivity, equivalence ratio and diluents. The LBV is one of the most significant combustion characteristics of premixed fuel/air mixtures. This study, a look at experimental methods for determining LBV and analyzing flame structure, as well as data on LBVs, it is given a quick summary of flammability constraints, flame stretch, fuel combustion characteristics, and the importance of laminar flame speed in determining operational fuel stability.

2.2 Flame Stretch

It is the rate of area change of a flame surface element, where the surface points are those that are travelling at gas speed. Since a true one-dimensional flame does not exist, it is vital to analyze how the stretch affects the effects of non-one-dimensionality on the combustion rate [14]. Significant progress has been made in the theoretical description of stretched flames since the 1970s, and as a result, there is now a reasonably mature qualitative understanding of the structure and reaction of laminar

premixed flames to stretch rate variations. Stretch effects are seen by “aerodynamic straining”, “flame motion”, and “flame curvature”, and these influences are most prominent in the existence of blend non-equidiffusion due to the resultant change in flame temperature [15].

Bunkute [16] defined the flame stretch as a change in the flame area of an infinitesimal flame surface element at any location on the flame surface, or the flame stretch is defined as the relative rate of change of area A of the flame sheet as in equation 2.1[12], while Figure 2.1. It illustrates the strain and curvature, with complete arrows indicating gas velocity and dashed-dotted arrows indicating the flame front's progressively stretched area.

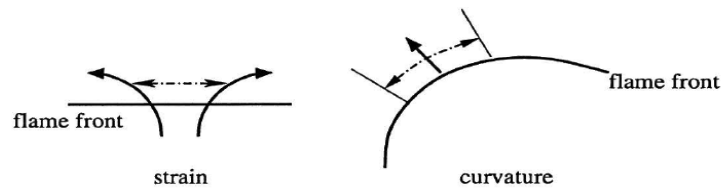


Figure 2.1- depicts the stretch and curvature of a flame [17].

$$\alpha = \frac{1}{A} * \left(\frac{dA}{dt} \right) \quad \dots\dots 2.1$$

Where the stretch rate (α) is measured in seconds. In the equation above, there are two different sources of stretch. The first is the effect of flame surface flow non-uniformity, and the second is stretch, felt by moving the flame, which results in curving the flame. The propagation flame approach for the spherical rate of flame stretch is $\alpha = \frac{2\delta_n}{r_f}$ [18]. To determine the un-stretched flame speed (S_1), the speed of a stretched flame

(S_n) extrapolated to zero stretches is required [1]. As a result, both stationary spherical and propagating planar flames are stretched. However, even if the flame is stationary and is not curved, flow field strain can contribute to stretching [14].

2.3 Fundamental and Characteristic of Flame Parameters

The **adiabatic flame temperature** (T_{ad}) is the highest temperature attained during an adiabatic and constant pressure burning process of a homogeneous reactant mixture under initial circumstances of chemical equilibrium. The initial temperature, initial pressure, equivalency ratio, and mixture composition are some of the factors that affect it. Because of heat losses, the actual temperature is higher than that of the flame. It has an impact on engine efficiency, emissions, and laminar burning velocity [19].

The **self-ignition temperature** is The lowest temperature at which a given substance can self-ignite without the aid of an external ignition source like a spark[20].

The **flammability limits** define the range of fuel concentration in the mixture under specific beginning conditions that allow for the initiation of ignition and the growth and maintenance of flame. It is significantly influenced by the kind of fuel, temperature, pressure, the way the flame expands, and the shape of the combustion vessel [21].

Flame stabilization is the ability of a flame to adapt nimbly to an irregular, temporally changing flow field by adjusting its position, direction, and configuration [19].

The **flashback and liftoff** are significant undesirable design requirements. A flashback occurs when the flame spreads upstream through the burner's tube without being quenched, whereas liftoff occurs when the flame is detached from the burner's port and stabilized at a distance from the port. Until the flame blows out, this distance will grow as the velocity of unburned gases increases [8]. Flashback is not simply a strange occurrence; it can also be dangerous. An explosion could occur if the fuel vessel catches fire due to flame propagation through the burner port.

2.4 Experimental devices utilized for determining laminar burning velocity

Unstretched laminar burning measurement methods are divided into two categories based on the flame: stationary flame and non-stationary flame. The stationary flame is a flow of premixed combustible mixture flows into a constant flame with a speed equivalent to S_u [14]. A non-stationary flame is a flame that propagates through a quiescent combustible mixture[14]. The following sentences will give a summary of it: It will be summarized in the following paragraphs.

2.4.1 Stationary flame

The mixture of gases flows into a steady flame with a speed equal to LBV in this category. It's constructed by continuously injecting a fuel-air mixture into the burner at a steady rate. It is affixed to the burner rim and can be used to calculate the burning velocity. This sort of flame is measured using a variety of methods.

2.4.1.1 Bunsen burner method

This simple approach employs a stretched cone flame mounted on the top of a cylindrical (or generally Bunsen) burner, as shown in Figure 2.2. This method was

employed by several researchers, such as Andrade et al. [22], Wu et al. [23], and Rocha et al. [24]. The uniformity of the gas exit velocity is assumed. The LBV is determined by utilizing the half-cone angle of the flame, gaseous mass flow, and burner parameters. Schlieren or chemiluminescent vision techniques can be used to identify the flame surface for velocimetric local speed measurement [25]. Despite an easy approach, it had three problems, which are heat loss, a variation in flame intensity near the cone's tip, and specifying the specific location of the flame front [26]. The laminar burning velocity is calculated by [27]:

$$Su = u_o \sin \alpha_u \quad \dots(2.2)$$

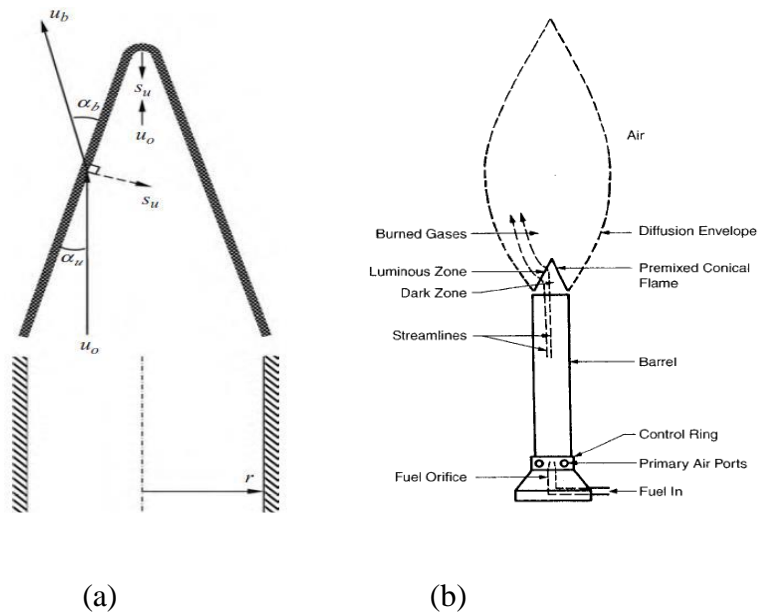


Figure 2.2 (a) Bunsen flame, (b) Bunsen burner [14].

2.4.1.2 Flat flame burner with Heat Flux method

This approach, which is schematically represented in Figure 2.3, is analogous to the stabilized Bunsen flame. The gas flow is controlled until the combustion front is

flat, and the flame is attached to a porosity stopper. To measure the LBV, the burner rim is heated externally to cancel the heat transfer from the flame to the burner and create an adiabatic state, which simplifies data processing because it is unaffected by a stretch. This method was employed by several researchers, such as Sileghem et al. [28], Goswami et al. [29], Chan et al. [30], and Walter et al. [31].

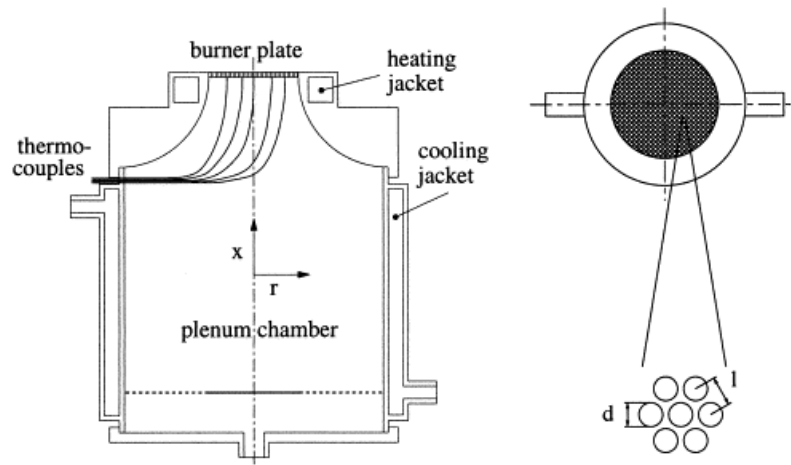


Figure 2.3- Flat flame burner method [31].

2.4.1.3 Diverging channel method

Akram et al. [32], and Katoch et al. [33] proposed a method to find the LBV of various combinations at high temperatures. The method for stabilizing planar flames in a diverging channel is shown in Figure 2.4. This method leads to creating planar flames even for the mixture at non-unity Lewis number (Le). The approach to stabilizing planar flames in an external supply mesoscale diverging channel. The rectangular intake of the channel is fed with a mixture of fuel/air mixtures. When the flow velocity is equal to the reactive mixture's burning velocity, the reactive mixture ignites close to the exit plane and the flame sets [34]. While the flame front's conservation of mass is used to calculate

the laminar adiabatic burning velocity, the flame front must be flat, that is, free of stretch and curvature, to produce proper combustion velocity of fuel/air blends. The flow field has a significant impact on the flame structure. This method has certain drawbacks, such as heat loss and the effect of flame stretching.

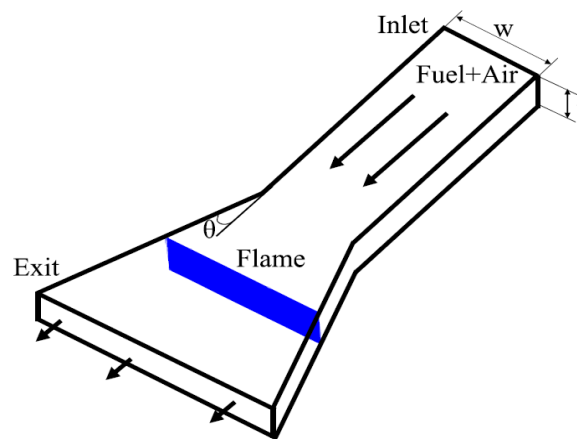


Figure 2.4 - Diverging channel externally heating [32].

2.4.1.4 Annular diverging tube method

This method consists of a tapered core within a quartz tube, creating a two-dimensional parallel channel. An annular diverging tube (ADT) was developed through a series of tests, allowing stationary pre-mixed flames to be hydrodynamically stabilized. As demonstrated in Figure (2.5.a)[35]. When the temperature of the core was not very high, it did not affect the flame propagation velocity. This ADT system has been upgraded by the tapering core, which was first changed to a stepwise core as demonstrated in Figure (2.5.b). The stabilized flame's location has been more precisely characterized, and the quench distance was computed appropriately. The core was combined by Liu and Kim [36] as illustrated in Figure (2.5.c), and each step-unit was

produced independently to achieve greater resolution. This method had some disadvantages due to the heat loss and flame stretch, and flame stretch effect. Which were used by Liu and Kim [36], Jung et al. [37], and Benim and Pfeiffelmann [38].

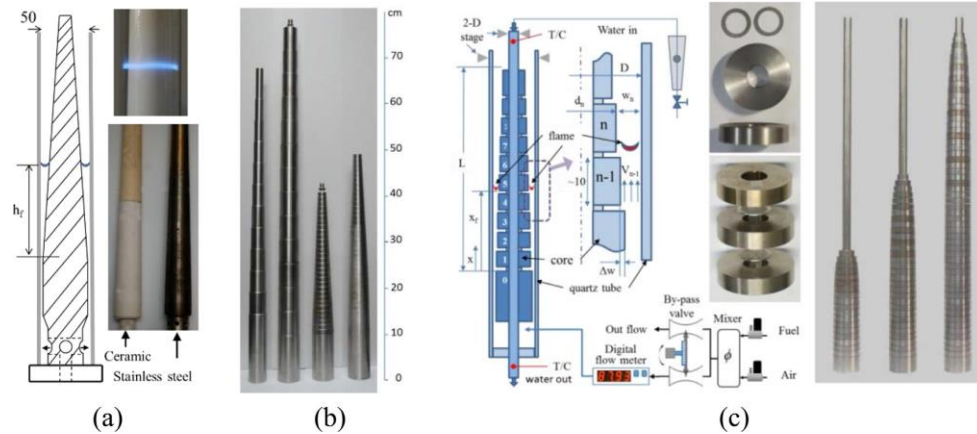


Figure 2.5- Development of annular step-wise diverging tube (ASDT) burners, a- Annular diverging tube (ADT), b- Annular step-wise diverging tube (ASDT), c- Assembled ASDT with a cavity [35].

2.4.1.5 Stagnation flame method

Simmons and Wolfhard (1957), [39], proposed the use of a stagnation/counterflow flame. The Stagnation flame method was developed by Wu and Law [40] and has been widely utilized to investigate the structure, stability, and extinction characteristics of pre-mixed and non-premixed flames [41]. A constant 1-D laminar flame is maintained [42]. The impingement of two similar nozzle-produced flows or the clashing of a flow on a wall creates a stagnation flow field. Pre-mixed fuel/air blend is provided from both nozzles in a premixed configuration, resulting in twin premixed flames as illustrated in Figure 2.6. The stabilized flames in a twin-flame

arrangement have no downward conduction heat transfer due to flame harmony when all that is lost is a tiny portion of radiant heat loss [43]. It is preferred to the stationary flame method because the flame stretch is the only external effect on flames. This method was used by Safer et al. [44], and Xu et al. [45].

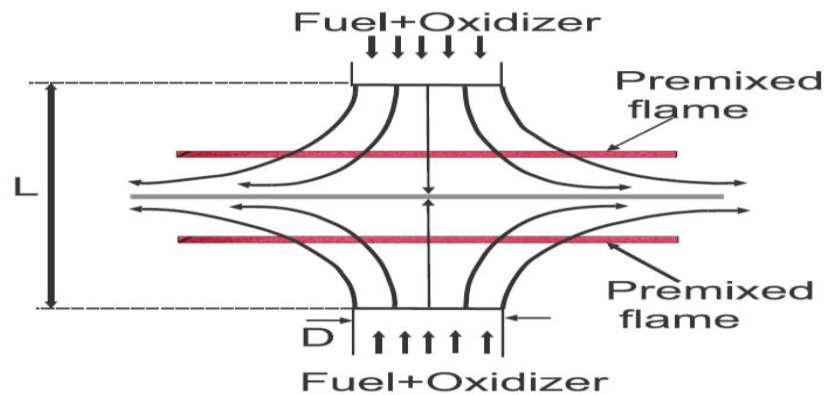


Figure 2.6- Schematic diagram of the Stagnation (counter flow) flame method [14].

2.4.1.6 Nozzle burner method

The method takes into consideration the dispersion of temperature along the flame front to calculate burning velocity directly from flame speed measurements in explosions. The flame speed is proportional to the burning velocity. This technique was used by Kopp et al. [46].

2.4.2 Non-stationary flame

In this classification, the flame spreads across an inactive combustible mixture. Numerous methods can be used to investigate the flame propagation speed of this type of flame. Some of the most used relents are listed here:

2.4.2.1 Tube method

The tube method is a cylindrically shaped tube with one end closed and supplied with a mixture of gases. When the mixture is ignited, it travels in a straight line to the tube's end. This method was used by Almarcha et al. [47], and Fig et al. [48]. It is considered the simplest method for non-stationary flames. However, it has side effects, such as heat loss across the pipe wall.

2.4.2.2. Constant volume bomb method (CVC)

This method is thought to be the most effective for detecting LBV and yielding trustworthy experimental data [14]. The spherical flame method and constant volume bomb are other names for it, as shown in figure (2.7). A premixed flammable mixture contained in a thick-walled container is ignited at the centre under specific conditions [49]. Miriam Reyes et al. [50] used a constant volume combustion bomb for methane/air and hydrogen/air mixtures. The main feature of this technique is that it can reach high pressures and temperatures, similar to the combustion process in reciprocating internal combustion engines.

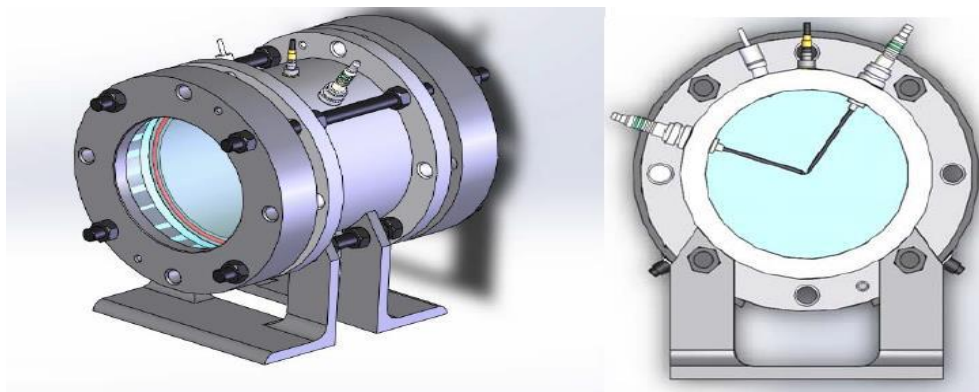


Figure 2.7- Constant volume combustion chamber [14].

A spherical flame propagates across the combustible mixture when the mixture is lit at the chamber's centre (Figure 2.8). In 1906, Hopkinson published the first centre electrical spark igniting experiments for flame propagation within a constant chamber. In 1917 Mache and Flamm proposed a link between the pressure of spherically expanded flames and the amount of mixture consumed[51],[52]. In 1934, Von Elbe and Lewis [53] used a spherical container with no visual access.

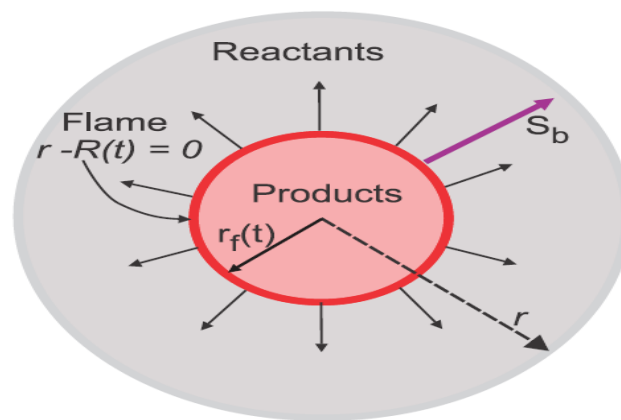


Figure 2.8- Outwards expanding spherical flame [14].

This method is still influenced by flame stretch, flame instability, spark ignition, intruding radiation heat loss, and chamber confinement [19]. As a result, To obtain accurate LBV measurements, the influence of the aforementioned variables on flame propagation must be carefully reduced. During the flame propagation event, an unsteady temporal history is recorded. Burning velocities over a variety of high pressures and high temperatures can be derived based on a single measurement. Yasiry et al.[12] observed that during flame propagation, a greater temperature is quickly attained inside the chamber, no fuel degradation takes place, and the internal structure of the rig is not compromised.

The CVC internal cavity can be designed as a spherical or cylindrical shape with various diameters. Zinong Zuoa et al. [54] investigated CH₄-DM-air mixture at 350 mm, a spherical vessel's inner diameter. The initial pressures were 0.1, 0.3, and 0.5 MPa, and the temperatures were 343, 393, and 443 K. The data demonstrate that when the dissociated methanol (DM) fraction increases, the LBV increase. The addition of CO has a smaller influence on the increase in LBV than the addition of DM.

Zuo et al. [55] used a spherical chamber with a volume of 22.4 L to investigate the effects of dissociated methanol addition on laminar burning velocities and the correlations between LBV and the equivalence ratio at 398 K and 0.1 MPa. At stoichiometric, hydrogen had a stronger influence on increasing LBV than dissociated methanol. The experiments were conducted using a high-speed camera and the Schlieren technique, and the data for the surface of a spherical flame at the initial of propagation was analyzed. Schlieren photos can also be used to analyze the structure of a flame to determine when cellularity and instability occur [56].

Zhiqiang et al. [57] used a stainless steel spherical CVC with internal dimensions of 350 mm. while, Proving the impact of temperature opposite the impact of pressure on blends.

Shu et al. [58] used a spherical shape with a diameter of 250 mm. The speed of laminar flame by the top and bottom flammability equivalence ratio limitations are widened as the methane percentage in the fuel mixture increases and the combustibility concentration limits fall consistently. Furthermore, pressure has a significant effect on upper limits but a negligible effect on lower limits.

Bao et al. [59] carried out their research in a sphere-shaped tank with an inner diameter of 350 mm. For various equivalency ratios and starting temperatures, the LBV of cyclopentanone was computed. At an equivalency ratio of about 1.2, the maximum LBV of cyclopentanone can be observed.

Shuangming Wei et al. [60] used a standard 20 L spherical combustion chamber to find that the laminar flame speeds of hydrogen/dimethyl-ether/methane/air mixtures increase significantly with the hydrogen enrichment ratio and that the laminar flame speeds at fuel-rich conditions were more sensitive to hydrogen enrichment than those at fuel-lean conditions.

Duva et al. [61] used a stainless steel cylindrical chamber with a 304 mm diameter. At 0.1 MPa, 473 K, an explicit correlation was proposed to calculate the LBV for methane/air blends diluted with carbon dioxide, Nitrogen, and water, as well as a blend of 9.50% CO₂/ 71.49% N₂ / 19.01% H₂O. As a result of its greater thermal diffusion effect compared to N₂ and H₂O, carbon dioxide dilution causes the greatest reduction in flame speed.

Lu-Qing et al. [62] used a stainless steel cylindrical container with internal dimensions of 210 mm in length and 210 mm in diameter to research the impact of nitrogen on the LBV of H₂/N₂O/air blends & CH₄/N₂O/air blends. Their results showed that the explosion pressure of N₂O and LBV was reduced at added nitrogen

Sai C. Yelishala et al. [63] used a stainless steel cylindrical container with internal dimensions of 135 mm in length and 135 mm in diameter to research the impact of carbon dioxide on the LBV of propane/air blends. It has been demonstrated that the

LBV of these combinations increases as gas temperature rises and decreases with the addition of carbon dioxide. Additionally, it was demonstrated that the LBV reduces as pressure rises.

A cylindrical hollow with an inner diameter of 180 mm and a length of 210 mm was used by Xin Lu et al. [64] to investigate the effects of dilution on the H_2/O_2 flame with various diluents, such as CO_2 , N_2 , Ar, and He. The critical radii and Markstein lengths decrease with dilution ratios, according to the results.

Another study was conducted on methane-air mixtures by Teknologi et al. [65] with a 29.3-litre cylindrical chamber. According to the findings, flame speed and stretch rate may be computed using flame radii obtained from a flame area study. The highest burning rate occurs at an equivalency ratio of (1.1) with a magnitude of 0.366 m/s.

Nathan Hinton et al. [52] explained that the constant volume method is less accurate than the constant pressure method. This approach requires several assumptions to calculate LBV. Another investigation by Cangsu et al. [66] studied the spherical propagating flame of biofuels in a constant chamber at equivalency ratios from 0.7 to 1.4, pressures ranging from 1 to 4 bar, and temperatures ranging from 358 K to 418 K. Except for the cases where flame cellularity occurred, their data revealed that the difference in LBV between the constant pressure method (CPM) and the constant volume method (CVM) approaches was within 15%.

Figure (2.9) explain the differences in LBV values measured using various methods for stoichiometric CH_4 /air mixes over the last few decades. After applying stretch modifications to the measuring data, it was discovered that the evaluated LBV

was approaching the amount of 36 cm/s due mainly to advances in the understanding of various theoretical aspects, such include the effects of flame stretch, heat loss, and improved measurement methods [35].

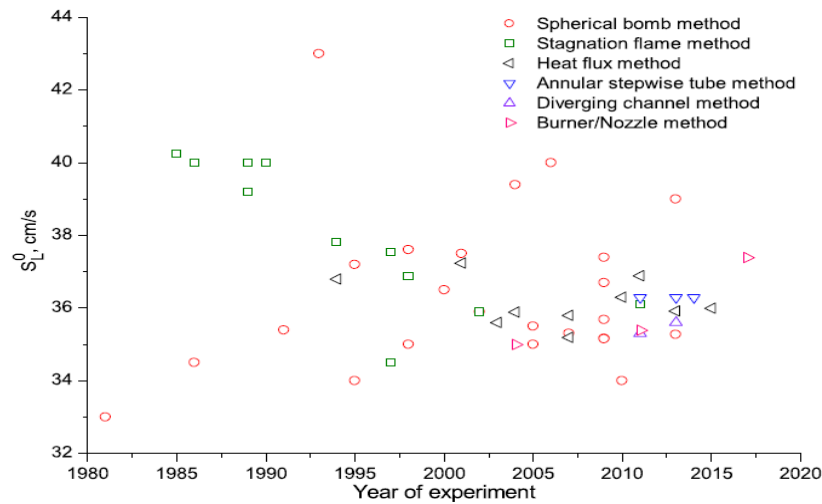


Figure 2.9- The LBV of methane/air blends with various assessment methods [35].

2.5 Measurement techniques for Burning Velocity and Laminar Flame Speed

The reaction zone is frequently referred to as a flame front or reaction wave. Rapid reactions take place in this area, and light is typically released from it [67]. To quantify flame speed by identifying the flame wave along a specified space, a specialized technique is required. As a result, numerous researchers put forth a lot of effort to develop various methodologies to gauge burning velocity and flame speed.

The methods employed for flame speed are described below:-

- 1- **Thermocouple technique:** in this method, the flame moves through several thermocouples as it moves through the combustion vessel. Because the flame front has the highest temperature of all the burned and unburned gases, the

thermocouples can detect the flame front. This technique was used by Saleh and AL-Fattal [68], and Salih and Chaichan [69].

- 2- **Ionized probe technique:** Since the ionization level at the flame front is extremely high, the flame front will be found using this method. Since the levels of ionization remain high behind the flame front, this approach is unable to anticipate where it will be.

The techniques employed to determine burning velocity are:

- **Density ratio method:** The burning velocity was determined this way using equation (2.3):

$$S_u = S_l \frac{\rho_b}{\rho_u} \quad \dots(2.3)$$

Where ρ_u is that of the unburned gases, and ρ_b is the density of the burned gases. Yasiry and Shahad [12], Okafor et al. [70], Grune et al. [71], and Abdulraheem et al.[72] used this method.

- **Pressure measurement method:** it is used in combustion to calculate burning velocity using a constant volume approach, where the pressure changes with the radius of the flame front. using equation (2.4):

$$S_u \propto \frac{d_p}{d_{r_f}} \quad \dots(2.4)$$

Omari and Tartakovsky [73], Hinton et al. [52], and Xu et al. [66] used this method.

3- **Optical technique:** There are various kinds of optical technology. which are:

- Shadow zone photograph: Even though it is a straightforward strategy, it is the least desirable because it is seen as unreliable. Grune et al. [71], Park et al. [74], and Wang et al [75] all used this method.
- Schlieren photograph: it is the technique that is most commonly used in burning investigations since it is more accurate than other techniques. Rozenchan[76], Yasiry and Shahad [12], Farha Khan et al. [77], Zhiqiang et al. [57], and Duva et al. [61] used this technique.
- Visible zone photograph: it is a less precise technique than the other due to the difficulty in accurately defining the viewable region. Sreenivasan et al. [68] used this technique.

2.6 Factors Influencing Flame Speed and Laminar Burning Velocity

Many parameters have an impact on flame speed and burning velocity. Zheng [78] identified the impact of several sources of error, such as initial pressure, initial temperature, equivalency ratio, etc., on laminar flame speed measurement, especially for off-stoichiometric mixtures. The impact of different variables is examined in the following sections.

2.6.1. Initial Pressure

In 1916, Ubbelohde demonstrated the first proof of the impact of pressure on burning velocity by employing the pressure dependency power-law that was used for the pressure range of (1 to 4 bar) [79]:

$$S_u = S_{u,rrf} \left(\frac{P_i}{P_{i,rrf}} \right)^{\beta p} \quad \dots(2.5)$$

Another association was proposed by Smith and Agnew in 1957 [79]:

$$S_u = S_{u,rrf} \text{Exp} \left[b \left(1 - \left(\frac{P}{P_0} \right) X \right) \right] \quad \dots(2.6)$$

Andrews et al. [80] suggested the following correlation:

$$S_u = \frac{43}{\sqrt{p}} \quad \dots(2.7)$$

Kanoshima et al. [81] conducted their tests on ammonia/air mixtures in a cylindrical chamber with an inner diameter of 410 mm and a length of 270 mm. They discovered that the pressure exponent (βP) in equation (2.8) was closer to zero while the temperature exponent (αT) was higher than that of CH₄/air flames.

$$S_u = S_{u,rrf} \left(\frac{T_i}{T_{i,rrf}} \right)^{\alpha T} \left(\frac{P_i}{P_{i,rrf}} \right)^{\beta T} \quad \dots (2.8)$$

Where $T_{i,rrf} = 298$ K and $P_{i,rrf} = 1$ bar denotes the reference conditions, respectively. X. J. GU et al. [92] investigated based on changing initial temperature and initial pressure with an equivalence ratio. Variation's influence on initial pressure was investigated. Flame instability is observed in mixtures under high pressure

Q. Zhou et al. [82] estimated the impact of fuel composition and initial pressure fluctuations on the features of premixed H₂/CO/ CH₄ flames by the spherical expanding flame method. As the initial pressure increases, the laminar flame speed decreases, owing to the increasing unburned blend density and lower H and OH radical

concentrations under the equivalency ratio of 0.6 to 1.5, with initial temperatures of 303 K and pressures of 0.1–0.5 MPa.

Okafor et al. [83] studied increased mixture pressure of ammonia/methane/air mixtures with a 210 mm inner diameter of cylindrical CVC. The result was that the unstretched LBV dropped to an equivalence ratio of 0.7 to 1.3.

Halter et al. [84] studied the influence of pressure and hydrogen addition on premixed methane/air laminar flames using a combustion chamber with a spherical shape, for pressures ranging from 0.1 to 0.5 MPa, with equivalency ratios ranging from 0.7 to 1.2. The LBV for all mixes decreased when the pressure was increased the mole fraction of hydrogen in the methane/hydrogen combination varied from 0 to 0.2. While the laminar flame speed decreased monotonically as the initial pressure was raised around the stoichiometric to CH₄/air blend [85].

Hu et al. [86] investigated the influence of hydrogen flames at elevated pressures in constant volume combustion vessels. The findings show that the LBV reduces as the initial pressure increases. Another study was conducted on premixed CH₄/CO₂/air flames by Farha Khan et al. [77] increased pressure and various dilution ratios. The results were that at higher pressure, the chemical effect is less important than at ambient pressure and that elementary reactions are more pressure-sensitive than the dilution effect, as shown in figure 2.10.

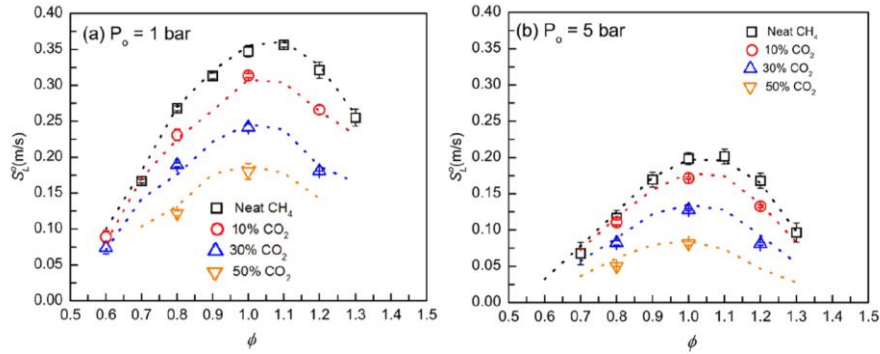


Figure 2.10- Influence of initial pressure and dilution on CH₄/air mixture [77].

Xin Lu et al. [64] studied the influence of several diluents on the H₂/O₂ flame: He, N₂, Ar, and CO₂. The LBV was non-monotonic with pressure when the diluting ratio was low. When initial pressure is raised, critical radius and Markstein lengths are reduced.

Yu Liu and colleagues [87] investigated the influence of increasing the initial pressure from (0.1 to 0.3) MPa at an equivalency ratio of 0.7 to 1.4 on the LBV using a constant volume chamber. The LBV of CH₄/RP-3/air mixture achieves its maximum in a slightly rich blend at 1.1, and the peak LBV of CH₄/RP-3/air mixture increases as the initial pressure decreases.

Baloo et al. [88] investigated the influence of pressure on the laminar burning velocity of methane/iso-octane as an alternative fuel. Based on an initial pressure from 0.1 to 0.5 MPa, and an addition of 70% and 95% methane to iso-octane, As a result, as pressure increases, the LBV decreases.

Willyanto Anggono et al. [89] studied the impact of carbon dioxide content on the LBV of methane/air blends at various pressures. The findings show that the LBV of

methane-air mixtures decreased as the carbon dioxide level and mixture pressure increased.

Okafor et al. [90] studied the influence of initial pressure and ammonia content on the LBV of a CH₄/air blend. Using the constant volume bomb method at initial pressures from 0.1 to 0.50 MPa. The LBV decreased with an ammonia concentration increase in the fuel and blend pressure.

2.6.2 Initial Temperature

It is an important factor in determining burning velocity. Increasing the temperature of the unburned gas causes the LBV to increase. Haiyan Wang et al. [91] investigated temperature influences on the front of the spherical stretched flame and the laminar combustion velocity of the CH₄/air mixture balloon flame. A high-temperature source boosted flame speed, whereas an electric spark diminished it.

Another study by Yu Liu et al. [87] investigated the impact of raising the initial temperature from 450 to 480 K on the LBV. As a result, the maximum LBV of the CH₄/RP-3/air blend grows as the initial temperature does. Zhong et al. [92] investigated the LBVs of methane/iso-octane blends at 1 MPa and 900 K. When the temperature rises and the pressure drops, the LBV rises.

Tang et al. [93] looked at the LBVs of propane/hydrogen/air blends with spherically growing flames at elevated pressures and temperatures, as well as varying hydrogen percentages. The results reveal that when the hydrogen fraction and initial temperature increase, the unstretched flame propagation speed and unstretched LBV increase, but they decrease as the initial pressure increases, as shown in Figure (2.11).

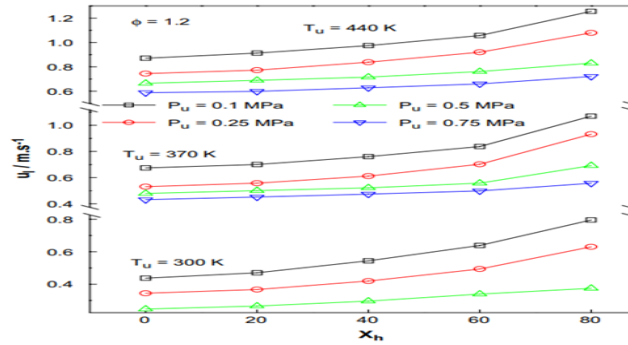


Figure 2.11- The LBV of C₃H₈/H₂/Air blend Vs with Changing P_i and T_i [93].

Finally, Yu Liu et al. [94] studied the influence of temp, initial pressure, and microalgae oil addition on the LBV of microalgae oil/RP-3 aviation kerosene in a constant volume chamber (CVC). The LBV rises as the starting temperature and microalgae oil concentration rise but falls as the initial pressure rises.

2.6.3 Fuel type

A maximum fraction of the combustible mixture is made up of air. As a result, the S_u is somewhat influenced by the fuel's molecular weight. The effect of the fuel's combustion enthalpy is far more significant since it affects the temperature of the adiabatic flame, which has the greatest influence on burning velocity. The oxidation kinetics reactions have importance as well. So that different burning velocities for specific fuels can be accomplished while maintaining adiabatic flame temperatures [12].

The S_u for hydrocarbon fuels typically decreases as the molecular fuels' carbon atom count rises [95]. For various fuels belonging to the alkanes family (methane, propane, LPG, and butane), Saleh and AL-Fattal [68] researched laminar burning

velocity and demonstrated that it is inversely related to the number of carbon atoms in fuel, as shown in the figure (2.12).

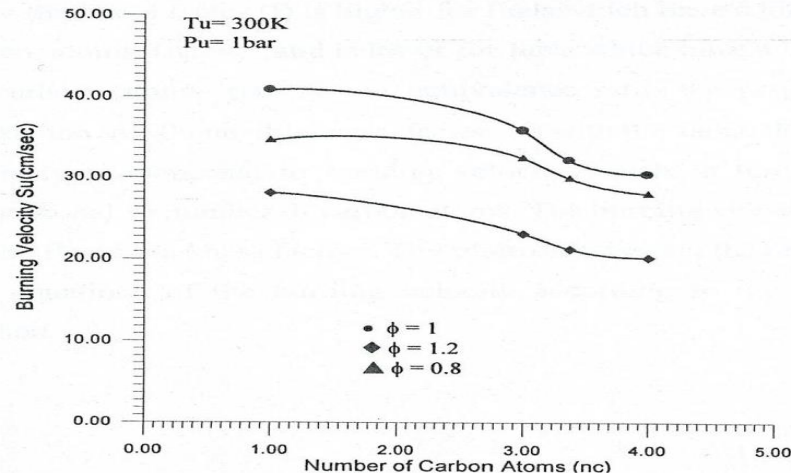


Figure 2.12: Variation of S_u with carbon's number atoms in fuel molecule [68].

2.6.4 Thermal Diffusivity and Specific Heat

The effects of thermal diffusion and reaction rates on combustion rates and burning velocity were examined in a series of experiments. Li et al. [96] studied the influences of diffusional-thermal and hydrodynamic instabilities on flame destabilization, which are enhanced by hydrogen addition. As the initial pressure rises, the diffusional-thermal instability has a minor impact on flame destabilization, but the hydrodynamic instability's effects increase.

Mammadbaghir Baghirzade et al. [97] studied the influence of replacing nitrogen with a noble gas (argon or krypton) as the working fluid to observe how it affected flame stability and dynamics in premixed methane combustion. Because noble gases have a higher specific heat ratio, they improve the thermal efficiency of internal combustion engines, and, due to the lack of nitrogen in the working fluid, they may also

dramatically reduce NO_x emissions. Finally, there is a higher and steeper increase in LBV (300K–475K). Zhihua Wang et al. [98] proved that the thermal expansion of the burner head should not be disregarded, especially when the burner plate temperature is high.

2.6.5 Equivalence ratio (ϕ)

The ratio of real to stoichiometric fuel-air is known as the mixture strength or equivalency ratio (ϕ) as shown in equation 2.9 [99]. It is commonly assumed that a mixture with a maximum flame temperature also has a maximum burning velocity by Barnard et al. [100]. Extremely lean and extremely rich blends are unable to create a propagatable flame because there is not enough fuel or oxidant to keep a deflagration wave steady. As a result, there are flammability upper and lower limits [99].

$$\phi = \frac{\left(\frac{F}{A}\right)_{\text{act}}}{\left(\frac{F}{A}\right)_{\text{stoic}}} \quad \dots 2.9$$

Beeckmann et al. [101] evaluated the LBVs tests of Ethanol, methanol, n-propanol, and n-butanol using a spherical combustion vessel at an initial pressure of 1 MPa and a temperature of 373 K . It demonstrates that the higher LBV at a stoichiometric combination ($\phi=1$) than lean or rich blends, with the exception of methanol, where the blend has a higher flame speed at the rich blend ($\phi=1.3$).

Yanga et al. [102] studied the effect of the equivalency ratio (ϕ) on flame evolution and pressure, which can range from 0.6 to 1.8. The equivalence ratio has a significant impact on the pressure and flame propagation. Another study by Sun et al. [103] investigated the impact of the equivalence ratio on flame instability and flame

speed (gasoline combined with ethanol of 30 percent liquid content). The flame accelerates due to the flame's instability.

2.6.6 Diluents

Many studies investigated the impact of inert additions like (CO₂, Ar, He and H₂O) and hydrogen on the burning velocities of combustible blends.

For energy supply systems, hybrid fuels like hydrogen and methane are gaining popularity. The fundamental reason is that adding hydrogen to a methane-air combination is a useful tool for extending flammability limits, increasing LBV, and lowering carbon dioxide emissions [104]. The LBV of hydrocarbon fuels typically reduces as the number of carbon atoms in a molecular fuel rises, so for some alkane fuels like butane, propane, methane, and liquefied petroleum gas (LPG), the relationship between the number of carbon atoms in a fuel and its burning velocity is inverse [14].

However, using expanding flames for independent hydrogen characterisation is difficult because as pressure rises, instabilities emerge, increasing flame surface area and, as a result, influencing flame speed[105].

Zuhaib Akram et al. [106] studied the addition of hydrogen to LBV. The increase in hydrogen increased the LBV of n-heptane at all operating conditions.

Khan et al. [107] studied the addition of hydrogen to improve the combustion chemistry of all NG blends, resulting in a higher LBV at an initial temperature (T_i)= 300 ± 3 K, initial pressure (P_i) = 0.1 MPa and equivalence ratio of 0.6- 1.4.

As the hydrogen mole fraction rises to 20%, the velocity rises with it due to the thermal diffusivity to hydrogen highest from methane [108, 109]. Erjiang Hu et al. [110] discovered three regimes depending on the hydrogen content of the fuel blend. The methane-dominated combustion regime, in which the hydrogen fraction is less than 60%, the transition regime, in which the hydrogen fraction ranges from 60% to 80%, and the methane-inhibited hydrogen combustion regime, in which the hydrogen fraction is greater than 80%. As shown in Figure 2.13, the LBV increases linearly with the increase in hydrogen fraction in both the methane-dominated and methane-inhibited hydrogen combustion regimes.

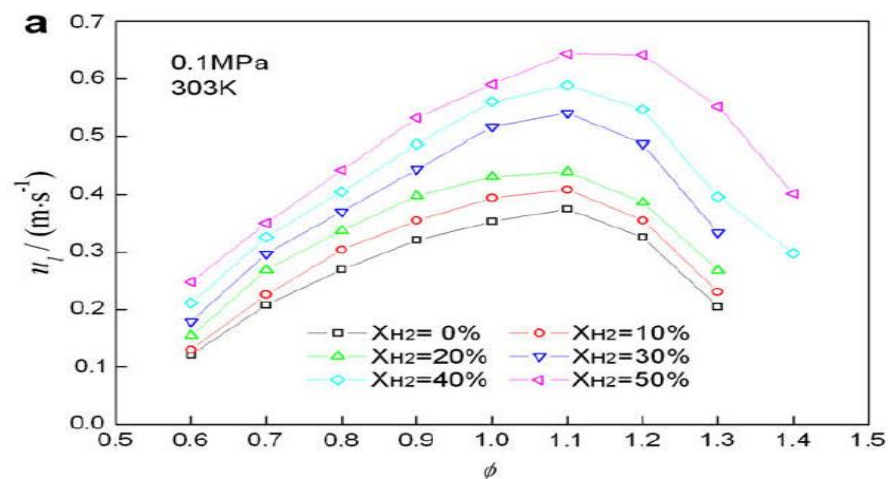


Figure 2.13- Unstretched LBV for $\text{CH}_4/\text{H}_2/\text{air}$ mixture versus equivalence ratio [110].

Vincenzo and Jacopo [111] investigated the effect of hydrogen on the LBV for CH_4/air blend. The addition of hydrogen increased the LBV of these blends.

Daniel [112] studied the influence of hydrogen addition on premixed methane/air laminar flames using a combustion chamber with a cylindrical shape, at pressures of 0.1 MPa, with equivalence ratios ranging from 0.75-1.25 and an initial

temperature of 303 K. As hydrogen is added to the methane/air blend by 1–7%, the LBV is increased slightly.

Shuangming et al. [60] discovered that the hydrogen enrichment ratio increases the LBVs of hydrogen/dimethyl-ether/methane/air blends and that The LBVs are more sensitive to hydrogen enrichment under fuel-rich conditions than under fuel-lean situations.

Xie et al. [113] investigated the carbon monoxide ratio rise in CH₄/CO blended fuels. The LBV rises first, then falls for CH₄/CO/O₂/CO₂ mixes at ambient pressure and a stoichiometric equivalence ratio.

Yelishala et al. [63] studied the influence of carbon dioxide on the LBV of propane/air blends. At a variety of carbon dioxide concentrations of (0–80) % by volume, equivalence ratios of (0.7–1.2). The addition of carbon dioxide reduced the LBV of these mixtures, whereas the increase in gas temperature increased it. It was also discovered that the LBV reduces as pressure rises.

Willyanto et al. [114] investigated the increase in the carbon dioxide dilution ratio was increased to CH₄/air blends at ambient temperature and an equivalence ratio of 0.8 to 1.2. The result was a reduction in the LBV of all blends.

Wei et al. [115] evaluated the effects of carbon dioxide or H₂O on the LBV for CH₄/air blend. By increasing the thickness of the flame and lowering the thermal expansion ratio, carbon dioxide or/and H₂O lessens the intensity of hydrodynamic instability, lowering the laminar burning velocity.

Zhoua et al. [116] studied the impact of diluents (N_2/CO_2) on the LBV and flame instability of a premixed blend of $H_2/CO/CH_4/air$. The results demonstrate that the laminar flame speed reduces as the N_2 and carbon dioxide dilution levels rise.

Berk et al. [61] studied the addition of 71.49 %, 19.01 %, and 9.50 % to the methane by cylindrical CVC. The result was that the pressure rose and the LBV was reduced at Stycometric.

Similarly, the impact of N_2 was studied [64, 117,]. It has been shown that each of these diluents, to varying degrees, suppresses combustion and slows LBV.

2.6.7 Fuel blends

Fuels frequently have a complex chemical admixture. Knowing the S_u of a mixture made up of two or more components with known burning velocities is helpful. The following equation was reportedly proposed by Payman and Wheeler to estimate the S_u of gasoline that had many components [12].

$$S_{u,mix} = \sum x_i * S_{u_i} \quad ..(2.10)$$

Where x_i is the volume fraction of one fuel component and its oxidant for the whole mixture.

$$x_i = \frac{\text{volume of (fuel i + corresponding oxidant)}}{\text{volume of (total fuels + total oxidants)}} \quad \dots (2.11)$$

The simplest mixing rule was this one. According to this, the S_u of the mixture is equal to the component burn rates weighted by the ratio of their individual volume ratios.

The laminar burning velocity of premixed hydrogen/methane/air and hydrogen/natural gas/air flames was predicted by Mitu et al. [118] using Le-rule Chatelier's for mixing fuels (equation 2.12) The findings demonstrated that, in all blends and testing settings, the laminar burning velocity increased as the hydrogen proportion rose. At moderate hydrogen fractions, it fluctuated linearly; but, as hydrogen fraction rises, it begins to vary more sharply.

$$S_{u,\text{blend}}(\phi) = \frac{1}{\sum_{j=1}^n \frac{X_j}{S_{u,j}(\phi)}} \quad \dots(2.12)$$

Where n is the total number of fuels in the blend. X_j is the percentage of j fuel in the blending fuel, and $S_{u,j}(\phi)$ is the laminar burning velocity of j fuel at an equivalence ratio.

2.7 Factors affecting Flame Speed Measuring Accuracy in CVC Method

2.7.1 Ignition energy

A shock wave emerged by a slower thermic wave induced by ignition energy enhances the flame speed by raising the mixture temperature. The spark ignition aids in the formation of a small flame nucleus and has an early impact on flame expansion by Bradley et al. [119]. As a result, avoiding small flame kernels when extracting LBV can dramatically lessen this effect.

Bradley et al. [119, 120] suggested that the ignition energy may affect the propagation of a centrally propagated flame when the flame radius is smaller than 8

mm. Mammadbaghir B. et al. [97] used flame radii of between 8 mm and 17.5 mm for the flame speed measurement at internal radii of wall 140 mm.

Jun Ho al. [121] used flame radii of between 10 mm and 29 mm for the flame speed measurement at an internal radius of 220 mm. Mengni Zhou et al. [122] studied the effect of ignition energy on LBVs for $\text{CH}_4/\text{He}/\text{N}_2/\text{O}_2$ blend at varied ignition energies. The data show that increasing ignition energy improves initial flame propagation speed and broadens the range of flame trajectory influenced by ignition energy, but the rate of development of speed and range slows as ignition energy increases, as shown in figure (2.15). Ngo [123] showed that with an increasing carbon number, the fuel/air equivalence ratio at which the minimum ignition energy occurs increases.

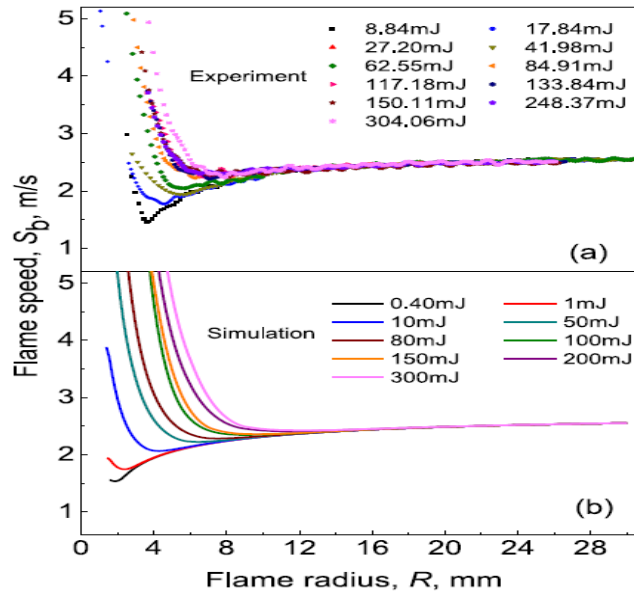


Figure 2.14- Flame Speed vs. Radius for Various Ignition Energies [122].

2.7.2 Flame instabilities

Thermal-diffusive and hydrodynamic instabilities have been shown to accelerate flame propagation speed in constant volume bomb studies [78]. The constant pressure method has the advantage over the constant volume method in that it visualizes the flame as it spreads, making it possible to spot any instability that might arise on the flame front as it does so. To ensure that the flame propagation speed is free from the effects of instability, the upper flame radius should be carefully selected.

When a mixture has a sub-unity Lewis number or a negative Markstein length, a thermo-diffusive flame front cellular instability forms, whereas a hydrodynamic instability often forms when the ratio of the flame thickness to the flame radius drops (for example, at high pressure) [78].

According to Xie et al. [124], thermal-diffusional and hydrodynamic instabilities result in the development of a smooth flame front that becomes a cellular flame surface, greatly increasing the pace of flame propagation. As a result, processing a tiny flame radius with smooth surfaces can be used to eliminate the influence of flame instabilities on the determination of S_u .

2.7.3 Buoyancy

The flame is subject to buoyancy effects because of the significant density differential between the burned and unburned gases [125], which allows the flame to float up and distort its initial spherical flame plane while causing a necessary flow in the surrounding reactants.

Mei et al. [126] demonstrated how oxygen enrichment increases the speed of spherically expanding flames, which reduces the effect of buoyancy on the laminar flame speed of NH_3 , as seen in figure (2.15).

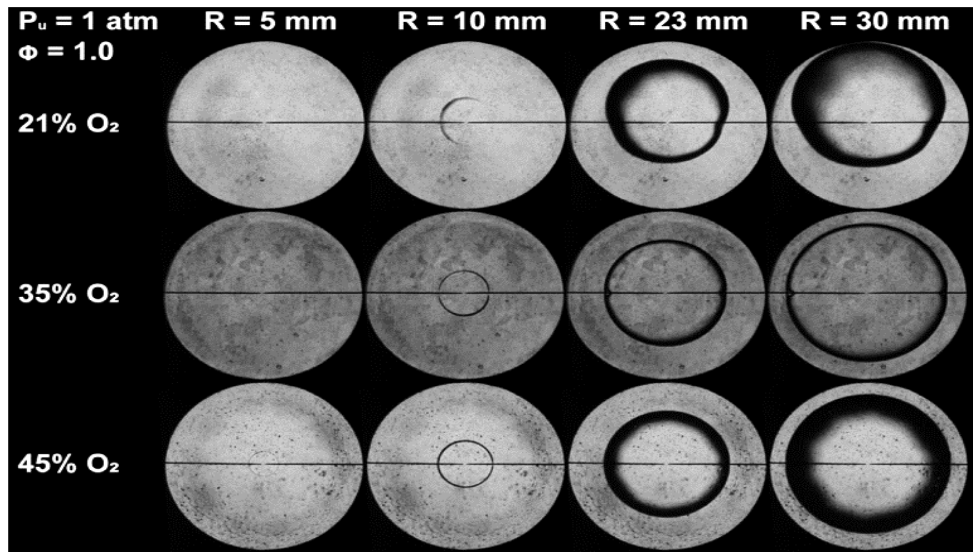


Figure 2.15- Schlieren images of $\text{NH}_3/\text{O}_2/\text{N}_2$ flames at $\phi=1$, $P_i = 1$ atm [126].

2.7.4 Nonlinearity of the stretch rate-flame speed relationship

The flame stretch rate is the rate of area variation per unit area of a flame surface element. Since there isn't a one-dimensional flame, it's important to analyze how stretching affects the burning rate to assess the effects of non-one-dimensionality.

According to Kelley and Law [125], the nonlinear extrapolations enable precise calculation of the Markstein length and laminar flame speed. These techniques produce outcomes that are comparable to those of flat flame burners, where the flame is not stretched. Additionally, they concluded that severe mixture non-equidiffusion and/or

high stretch rates (large values of the Lewis number ($Le = \frac{\alpha_{th}}{D}$)) increase the difference between the linear and nonlinear extrapolation approaches.

Vagelopoulos et al. [127] showed the difference between the linear and nonlinear extrapolation reduces when the Karlovitz number ($Ka = \frac{S}{S_u}$) is low enough ($Ka \sim 0.1$). The linear extrapolation may somewhat underestimate the flame speed for low stretch levels, according to Tien and Matalon [128]. The extent of the extrapolation discrepancy, according to Jayachandran et al. [129], increases for mixes with Le 1.0 and/or significant discrepancies in the fuel and O_2 diffusivities.

2.8 Summary

The laminar burning velocities (S_u) and unstretched flame speeds (S_l) for various fuels and beginning conditions have previously been examined. It was discovered that there was a dearth of research into the effect of CVC geometry on these two parameters. Table (2.1) summarizes the findings of a few cited studies based on their sources.

A new experimental setup is created and tested in this work. It consists of a cylindrical, constant volume combustion chamber that is ignited from the centre. S_l and S_u are investigated under a variety of situations and fuels and the influence of pressure on mixtures, which are not included in the referenced studies. At various equivalency ratios (0.8, 1.0, and 1.2), tests are conducted for various fuels (methane, methane/hydrogen blends (10–30% by volume), initial pressures (0.1MPa), and initial temperatures (303 K). The following aspects will be covered in the research:

1. Investigate the effects of fuel type, beginning pressure, equivalency ratio, and methane/hydrogen and methane/carbon dioxide blending ratio on flame speed and laminar burning velocity.
2. Use Tracker 5.15 and ANSYS-CHEMKIN to conduct a full theoretical investigation employing various mechanisms.
3. Theoretical validation of the experimental LBV for methane.

Table 2.1- Summary of some prior research.

No	Investigator	year	Type of fuel	Initial condition	Dimensions of the chamber	Conclusion
1	Salih and Chaichan[69]	2014	propane	$\phi = 0.5-1.5$ T= 300-350 K P=0.05-0.15Mpa	Cylindrical CVC V=25 L D= 270 mm L= 435mm	The burning velocity decreased when the initial pressure increased.
2	Yasiry and Shahad [12]	2016	LPG+ Hydrogen	$\phi = 0.8-1.3$ T= 308 K P=0.1-0.3Mpa	Cylindrical CVC V=7 L D= 190 mm L= 250mm	S_u was calculated using correlations that were derived for various LPG-hydrogen mixtures and beginning pressures.
3	Khan et al.[107]	2018	Natural gas	T= 300 \pm 3 K P= 0.1 MPa $\Phi = 0.6-1.4$	Cylindrical CVC V=40 L D= 381 mm L= 381mm	The addition of hydrogen improves the combustion chemistry of all NG blends, resulting in a higher LBV.
4	Li et al. [96]	2018	Methane	T=298 K P=0.05,0.1, 0.15 and 0.2 MPa $\Phi = 0.8,1,1.4$	Spherical CVC V=14L D= 300 mm	With hydrogen addition, the maximum explosion pressure rise rate increases greatly, the explosion time decreases significantly and increase the laminar burning velocity.
5	Quan Zhoua et al. [116]	2019	H ₂ /CO/ CH ₄	T=303 \pm 3 K P=0.1–0.5 MPa $\Phi = 0.6-1.5$	Cylindrical CVC V=5 L D= 180mm L= 210 mm	The carbon dioxide dilution has a stronger dilution, thermal, and chemical effect than nitrogen dilution and hence can reduce the laminar flame speed of the H ₂ /CO/CH ₄ /air mixture significantly.
6	Willyanto A. et al.[89]	2019	Methane	T= 298 K. P=0.1 and 0.3 MPa $\Phi = 1$	Cylindrical CVC V= 23 L. D= 270 mm L= 410 mm	The LBV of methane-air mixtures dropped when carbon dioxide content and mixture pressure increased.
7	Sai C. Yelishala et al.[63]	2019	Propane	T= 298–420 K P= 0.05–0.6	Cylindrical CVC V=2 L	The LBV is increase with rising gas temperatures while decreasing with the addition of carbon dioxide

				MPa $\Phi=0.7-1.2$	D= 13.5 cm L= 13.5 cm	and/or with pressure rises.
8	Ekenechukwu et al. [83]	2019	Ammonia	T=298 \pm 3 K P=0.10 - 0.50 MPa $\Phi= 0.7 - 1.3$	Cylindrical CVC V=9 L D=210 mm L= 270 mm	With a decrease in methane content in the fuel and increased mixture pressure, the unstretched LBV dropped.
9	Yongliang et al. [113]	2019	Methane	T= 373 \pm 3 K. P=0.1 MPa $\Phi=1$	Cylindrical CVC V=5 L D= 180 mm L= 210 mm	The CO ratio in CH ₄ /CO blended fuels rise. The laminar flame speed rises first, then falls for CH ₄ /CO/O ₂ / CO ₂ mixes.
10	Willyanto et al. [114]	2020	CH ₄ / CO ₂ /air blends	T=298 K P=0.5 MPa $\Phi=0.8 - 1.2$	Cylindrical CVC V=23 L D= 270 mm L= 410 mm	The results revealed that increasing the carbon dioxide dilution ratio reduced the LBV of all blends
11	Lu-Qing et al. [62]	2020	H ₂ /N ₂ O/air blends & CH ₄ /N ₂ O/ air blends	T=305 K P=0.1 MPa $\Phi=0.6-1.8$	Cylindrical CVC V=7 L D= 210mm L= 210mm	The maximal explosive pressures of hydrogen and methane blends are found to be equal to 0.8 and 1.0, respectively.
12	Xin Lu et al. [64]	2020	Hydrogen	T= 298 \pm 2 K P=0.1-0.4 MPa $\Phi=0.7,1$ and 1. 3.	Cylindrical CVC V=5 L D= 180 mm L= 210 mm	The fastest LBV is found in the He diluted blend, whereas the slowest LBV is found in carbon dioxide diluted combinations.
13	Zhiqiang et al. [57]	2020	Methane	T= 323-423 K P= 0.1-0.3 MPa $\Phi= 0.9, 1.0,$ and 1.1	Spherical CVC V= 22.4L D= 350 mm	When the equivalency ratio and fraction of carbon dioxide are constant, initial temperature and pressure coupling have an analogous effect on flame propagation speed, i.e., flame propagation speed can be kept virtually constant when the beginning temperature and pressure are raised simultaneously.
14	Shuangming et al. [115]	2020	methane	P= 0.2 to- 0.6 MPa. T= 298 \pm 3 K $\Phi=1$	Cylindrical CVC V=24.1L D= 270 mm	By thickening the flame and lowering the thermal expansion ratio, which lowers the LBV, CO ₂ or/and H ₂ O lessen the severity of

					L=400 mm	hydrodynamic instability.
15	Berk et al. [61]	2020	Methane	T= 473 K P=0.1 MPa $\Phi= 0.8, 1.0$ and 1.2	Cylindrical CVC V=23 L D=304.8 mm L=304.8 mm	When the mixes are separately diluted with N ₂ , H ₂ O, and CO ₂ , the carbon dioxide dilution results in the biggest decrease in LBV.
16	S. Mani Sarathy et al.[56]	2020	formic acid	T= 473 K. P= 0.1 MPa $\Phi=0.8-1.3$	Spherical CVC V= 4.2 L D= 200 mm	It can greatly increase flame speeds by adding hydrogen.
17	Zuhaib Akram et al. [106]	2020	n-heptane	T= 393-473K P=0.1 MPa $\Phi=0.8-1.6.$	Spherical CVC V= 33.5 L D= 400 mm	The increase in hydrogen increased the LBV of n-heptane.
18	Berk et al. [20]	2020	Methane	T= 373–473 K P= 0.1–0.5 MPa $\Phi= 1.0$	Cylindrical CVC V=23 D=304.8 mm L=304.8 mm	When 71.49 % of N ₂ , 19.01 % of H ₂ O, and 9.50 % of CO ₂ are introduced, the LBV falls by 27-33 % and 17-25 %, respectively, as pressure rises from 1 bar to 3 bar and 3 bar to 5 bar.
19	Farha Khan et al. [77]	2021	Methane	P= 0.1 and 0.5 MPa T=300K $\Phi= 1$	Spherical CVC V= 18.8 L D=330 mm	The LBV of these CH ₄ /CO ₂ /air mixtures fall as the carbon dioxide dilution ratio is increased, and the influence of the pressure is greater than the dilution effect.
20	Yu Liu et al. [87]	2021	CH ₄ /RP-3/air blend	T=450 and 480 K P= 0.1 and 0.3 MPa $\Phi= 0.7 - 1.4$	Cylindrical CVC V=1.1 L D=90mm L=180 mm	The LBV reaches its maximum at a rich mixture ($\Phi= 1.1$), and as the initial pressure decreases, the peak LBV increases.
21	Shuangming et al. [60]	2021	dimethyl-ether/ methane	T =285 K P= 0.1 MPa $\Phi=0.6–1.6$	Spherical CVC V=20 L D=336 mm	The laminar flame speed was increased when the hydrogen was added.
22	Mammadbaghir et al. [97]	2021	Methane	T= 298 K P=0.1 MPa $\Phi=0.8,1$ and 1.2	Spherical CVC V= 1.4 L D=140 mm	The LBV is faster in either Ar or Kr than in N ₂ . Increasing initial pressures result in decreasing flame speeds.
23	Tao Shu et al. [58]	2021	Ammonia	T= 298 K P=0.1,0.5 MPa	Spherical CVC V=8 L	The methane volume fraction has a linear relationship with the laminar flame speeds.

				$\Phi=0.6-1.4$	D=250 mm	
24	Abdulraheem et al.[72]	2022	propane	T= 348,373, and 398 K P=0.1 MPa $\Phi=0.6-1.4$	Cylindrical CVC V=28 L D=300 mm L=400mm	Investigated the unstretched flame speed of premixed propane-methanol/air flames. According to the findings, raising the methanol blending ratio and starting temperature increased unstretched flame speed.
25	current work	2022	Methane	T=303±3 K P=0.1,0.15, 0.2 MPa $\Phi= 0.8,1$ and 1.2	Cylindrical CVC V=28 L D=300 mm L=400mm	With the addition of hydrogen or carbon monoxide, the maximum explosive pressure rise rate rises dramatically, the explosion time drops drastically, and the LBV increases tremendously. The carbon dioxide dilution ratio decreased all mixtures' laminar burning velocity.

Chapter Three

Experimental Setup

CHAPTER THREE

EXPERIMENTAL SETUP

3.1 INTRODUCTION

The numerical process undertaken for analyzing experimental results, and the design, building, and execution of the proposed testing program are all covered in this chapter. Numerical modelling with Tracker 5.1.5 and ANSYS-CHEMKIN was used to simulate the laminar burning velocities, adiabatic flame temperatures and density ratios. However, using an experimental rig at the University of Babylon to detect laminar flame speed and then compute the burning velocity of various fuel types and mixtures.

3.2 1-D Analysis

CHEMKIN-Pro program can calculate a wide range of thermodynamic characteristics and processes reliably and quickly. CHEMKIN-Pro relies on Reaction Design's Model Fuel Library, which is the most comprehensive and well-compiled library developed by the Model Fuel Consortium. The un-stretched adiabatic laminar burning velocity was computed numerically using ANSYS-CHEMKIN-PRO, a one-dimensional freely propagating laminar flame model, and the findings were compared to those obtained experimentally.

GRI-Mech 3.0 is a mechanism developed by the Gas Research Institute to simulate methane and natural gas combustion. Despite being among the most well-known single-carbon reactions, it also comprises combustion processes for alternate fuels, such as the intricate hydrogen combustion reaction mechanism [34]. The GRI-

Mech 3.0 mechanism is made up of 53 species and 325 reaction steps, each with its own set of rate coefficient expressions and thermochemical characteristics.

3.3 Analysis Assumptions

The LBV can be determined from the schlieren pictures acquired during each test using a set of computations. Many assumptions must be made to use data from the bomb [107, 116], which comprises,

1. At first, the unburned mixtures are at rest.
2. The gas temperature and pressure are initially steady and uniform ($T_i=303$ K), with P_i ranging from (0.1-0.2 MPa) with a 0.5 bar increment.
3. During combustion, pressure across the flame is believed to be constant and uniform.
4. The air contains O_2 and N_2 are present, and their volumetric ratio is 21:79.
5. Gases conserve their whole mass and volume.
6. The influence of ignition energy is ignored, and the mixture is ignited from the centre.
7. The flame front spherically grows and remains smooth.
8. There is no heat transmission in the process since it is adiabatic.
9. The flame front has an endlessly thin thickness.
10. Isentropic compression is used to compress the unburned gas.
11. Chemical equilibrium occurs right behind the flame front.
12. The unburned gas undergoes no chemical reactions.
13. The adiabatic flame temperature is used to calculate burnt gas properties.

3.4 Calculation of Equivalence Ratio

CHEMKIN-Pro program was built to estimate the injection pressures of mixtures for methane, syngas fuel, and air. According to the blend of methane, the equivalency ratio employed, and other chemical features of reactance and product. The equivalent partial pressure levels were the approach used to manage the fuel-to-oxidiser ratio. The following is a simplified derivation of the numerical process. The overall goal is to compute the requisite partial pressure values based on a certain total pressure (P_t) as well as the air-fuel ratio (AFR), defined as (m_a) as mass the percentage of air and (m_f) as the total mass of the fuel mixture [13]:

$$AFR_{act} = \frac{m_a}{m_f} \quad \dots(3.1)$$

The sum of the partial pressures exerted by all of the constituent non-reactive gases makes up the total pressure exerted by the mixture, based on the partial pressure law of Dalton [112], so

$$P_t = P_A + P_B + P_C + \dots \quad \dots (3.2)$$

According to Dalton's Law of Partial Pressures, the molar ratio of the fuel and air is equal to the ratio of their partial pressures (X_i):

$$X_i = \frac{P_i}{P_t} = \frac{n_i}{n_t} \quad \dots\dots (3.3)$$

So from Eqn. 3.3 gives:

$$P_i = X_i * P_t = \frac{n_i}{n_t} P_t \quad \dots\dots (3.4)$$

The mixture used to calculate the air-fuel ratio has fuel and oxidizer components, resulting in a total pressure of

$$P_t = P_a + P_f \quad \dots (3.5)$$

From Eqn.3.3 and Eqn.3.4 at Eqn.3.5 gives the partial pressures of the oxidizer and the fuel:

$$P_f = P_t \left(\frac{n_f}{n_f + n_a} \right) \quad \dots (3.6)$$

$$P_a = P_t \left(\frac{n_a}{n_f + n_a} \right) \quad \dots (3.7)$$

The preceding solutions are given in terms of total needed pressure and equivalency ratio. The air-fuel ratios are normalized to an equivalency ratio to the present work in this thesis [13], as in Eqn.3.8:

$$\phi = \frac{AFR_{stoich}}{AFR_{act}} \quad \dots (3.8)$$

Through the main fuel injection valve, a predetermined amount of gas fuel is pumped into the combustion chamber. To guarantee complete fuel mixing, wait at least five minutes. The ideal gas law ($PV=mRT$) is used to determine the required volume of the fuel based on its vapour partial pressure.

3.5 Adiabatic Flame Temperature

This study uses the first law of thermodynamics, for steady flow processes. The absolute enthalpy of the reactance in the initial position ($T=T_i$, $P=P_i$) equals the absolute enthalpy of the product in the end state ($T=T_{ad}$, $P=P_i$) when a mixture burns adiabatically at constant pressure[19].

$$h_{react}(T_i, p) = h_{prod}(T_{ad}, p) \quad \dots (3.9)$$

$$H_{reactance} = \sum_{react} N_i \bar{h}_i = H_{product} = \sum_{prod} N_i \bar{h}_i \quad \dots (3.10)$$

$$H_{product} = \sum_{product} N_i \left[h_{f,i}^o + cp_i(T_{ad} - 298) \right] \quad \dots (3.11)$$

The adiabatic flame temperature is calculated using equations (3.10) and (3.11). In the data collected from ANSYS-CHEMKIN-PRO, the enthalpy of production of each reactant and product is reported.

The molar specific heat (kJ/kmol.K) for each product species is calculated using the equation:

$$\bar{Cp}_i/R = a + bT + cT^2 + dT^3 + eT^4 \quad \dots (3.12)$$

T is the average temperature, and a,b,c,d and e are constants derived from the curve fit coefficient for thermo-dynamic properties in each mechanism's thermodynamic properties data.

3.6 Density Ratio Calculations

The density ratio is defined as the ratio of the density of the burned mixture to the density of the unburned mixture. It was estimated by assuming the burned gases were in adiabatic equilibrium.

For the initial and final states, the ideal gas equation of state has been used:

$$P_i = \rho_u RT_i \quad \dots (3.13)$$

$$R = \frac{R_o}{m_w} \quad \dots (3.14)$$

R is the constant of a specific gas. Then, based on equations (3.13 and 3.14),

$$(\rho_u)_i = P \times m_{w,i} / R_o T \quad \dots (3.15)$$

The following equation, derived from Dalton's law, is used to calculate the unburned gas density (ρ_u):

$$\rho_u = X_{air} \cdot \rho_{air} + X_{fuel} \cdot \rho_{fuel} \quad \dots (3.16)$$

where x represents each component's mole fraction. The burnt mixture density at T_{ad} can also be calculated with this equation. Pressure, initial and ultimate temperatures, fuel type, and equivalence ratio are all factors that influence the density ratio. In this investigation, the CHEMKIN-Pro program was used to calculate the density ratios.

The LBV is calculated using the density ratio approach, which is dependent on mass conservation across the flame front. It is one of the most widely used techniques in this field. The S_u is calculated by multiplying the unstretched laminar flame speed (S_l) by the density ratio.

3.7 Stretched flame speed analysis

Schlieren photography, which shows the density gradient inside CC and afterwards identifies the location of the flame edge, allows for the quick quantification of the flame radius. Using the unburned gas front radius estimated from the photograph, the (S_n) and (S_u) are calculated directly in this work. The following method for determining the stretched flame speed (S_n) is proposed by Yasiry and Shahad [12].

$$S_n = \frac{dr}{dt} \quad \dots (3.17)$$

Tracker 5.1.5 program is used to retrieve data on the variation of the flame radius over time. The slope of a line segment with two adjacent radii against time is the

instantaneous S_n . Table 1 lists the Tracker software's configuration information (3.1), to follow the progression of the flame front.

Table 3.1- Tracker Software Settings for Measuring Flame Speed.

Clip Setting	
Start frame	Variable
Step size	4 (frame)
End frame	Variable
Start time	Variable
Frame rate	3600 f/s
Frame dt	2.78E-4 s

3.8 Flame Stretched Rate and Markstein Length

The stretch rate is defined for every position on the flame front [114]:

$$\alpha = \frac{d(\ln A)}{dt} = \frac{1}{A} \frac{dA}{dt} \quad \dots (3.18)$$

The flame stretch rate for an outwards propagating spherical flame can be calculated as follows:

$$\alpha = \frac{1}{A} \frac{dA}{dt} = \frac{2}{r_u} \frac{dr_u}{dt} = \frac{2}{r_u} S_n \quad \dots (3.19)$$

The unstretched flame speed (S_l) and Markstein length (L_b) were calculated in this work using the linear extrapolation approach (equation 3.20). It's the most popular and straightforward form of extrapolation.

$$S_l - S_n = L_b \alpha \quad \dots (3.20)$$

Furthermore, the flame stretch rate (α) for a spherical expanding flame can be calculated using equation (3.19). Because the flame curvature and flow strain induce this stretch, producing one-dimensional, adiabatic, planar flames is impossible. The flame speed and the LBV can be considerably affected by stretch.

3.9 Laminar Burning Velocity

The total volume of the burned gases is taken to be roughly 5% of the volume of the CC at the start of flame propagation. The flame develops isobarically, and the S_u is related to S_l by mass conservation across the flame front.

$$\rho_b A S_l = \rho_u A S_u \quad \dots (3.21)$$

The flame front area is A , and the unburned and burned gas densities are ρ_u and ρ_b , respectively. Equation (3.21) [90] can be used to calculate the unstretched laminar burning velocity.

$$S_u = S_l \frac{\rho_b}{\rho_u} \quad \dots (3.22)$$

3.10 The Experimental Rig's Components

The design, building, and execution of the proposed testing rig are all covered in this section, as shown in Fig. 3.1. The rig's purpose is to detect laminar flame speed and then compute the burning velocity of various fuel types and blends. The impact of the

blending ratio, equivalency ratio, and initial pressure operating parameters is investigated. The flame speed is measured using the constant volume combustion chamber method and the schlieren photography technique. Figure (3.2) depicts the entire setup of the equipment. It is made up of the following components:

1. Combustion chamber unit.
2. Ignition system and control unit.
3. Gaseous injection unit.
4. Electrical control board.
5. Photographing.

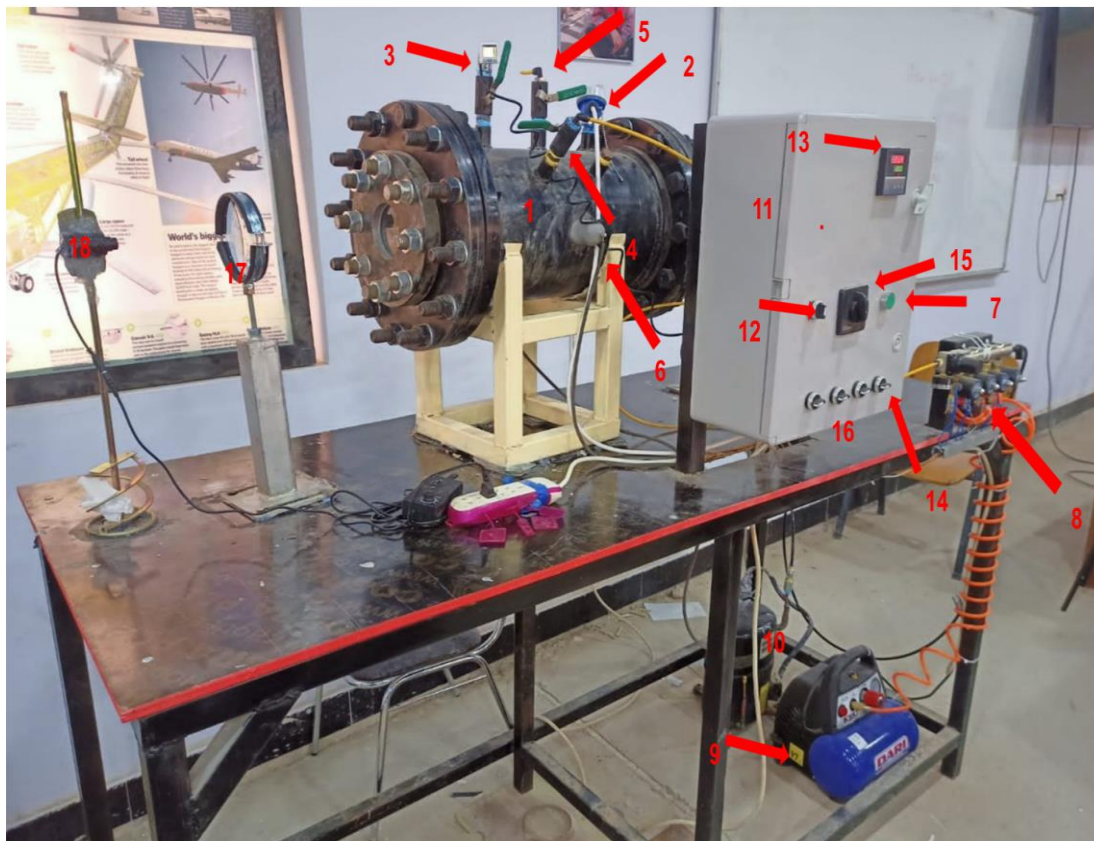


Figure 3.1- Photography for the experimental rig used in the study.

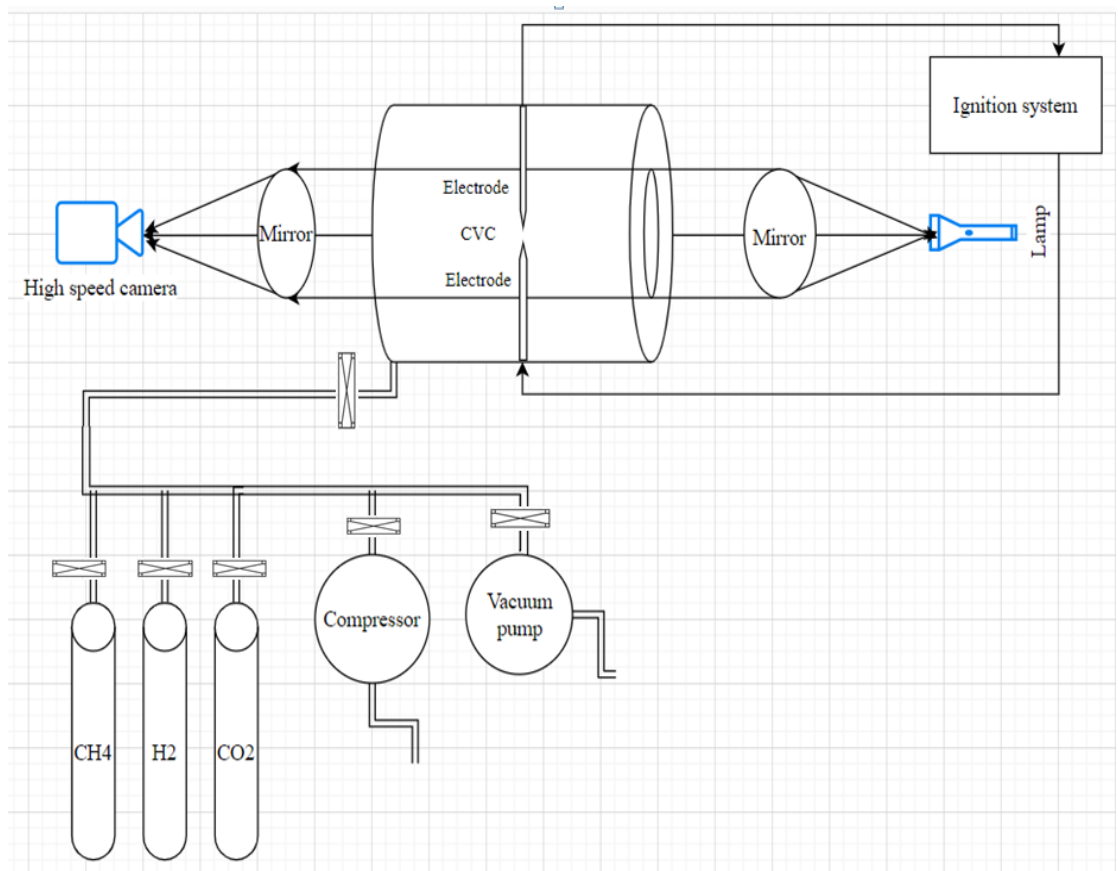


Figure 3.2- Schematic layout for the experimental setup.

Each of the units mentioned above consists of many components:

- Constant Volume Unit:-
 - (1) Combustion chamber, (2) Thermocouple,
 - (3) Pressure transmitter, (4) Inlet valve, and (5) Exhaust valve.
- Ignition System Unit:- (6) Sparking ignition electrodes, and (7) Ignition switch
- Gas injection unit (8) The manifold (9) Air compressor,
- (10) Vacuum System
- Electrical Control Board Unit. (11) Electrical board, (12) Main power switch,
- (13) temperature controller, (14) Compressor switch, (15) Vacuum switch, (16) Gaseous fuels Pushbuttons,(7) Ignition switch.

- Photographing Unit. (17)Convex lens, (18) Source of Light

Each of the units mentioned above consists of many components:

- Constant Volume Unit:-
 - (1) Combustion chamber, (2) Thermocouple,
 - (3) Pressure transmitter, (4) Inlet valve, and (5) Exhaust valve.
- Ignition System Unit:- (6) Sparking ignition electrodes, and (7) Ignition switch
- Gas injection unit (8) The manifold (9) Air compressor,
 - (10)Vacuum System
- Electrical Control Board Unit. (11) Electrical board, (12) Main power switch, (13) temperature controller, (14) Compressor switch, (15) Vacuum switch, (16) Gaseous fuels Pushbuttons,(7) Ignition switch.
- Photographing Unit. (17)Convex lens, (18) Source of Light

3.11 Constant Volume Unit

3.11.1 Combustion chamber

The CVC was made of carbon steel and was designed to provide a long enough experimental time frame in the pressure-unaffected area of flame expansion. As the flame propagates, reactant pressure builds, influencing the observed flame speed more and more. Duva et al. [61] recommend that the maximum usable flame radius for a cylindrical bomb be around 25% of the overall chamber dimension.

The combustion chamber in this investigation is a cylindrical type with a 250 mm inner diameter, 510 mm length, 10 mm wall thickness, and a total volume of 25 L. The system was constructed with a huge safety factor of five, and this value may be

greatly improved for additional testing by adjusting the size or quantity of bolts used to withstand the high combustion pressure and temperature. Two flanges with a diameter of 400 mm are utilized to close both ends of the cylinder, which are made of carbon steel and have a 20 mm thick side. These flanges are connected to the CC by 12 bolts (B7) and 12 nuts (2H) on each side.

The CVC created in this study has a maximum useful flame radius of 3.75 cm. To allow a perpendicular line of sight across the centre of the room, two opposed ports were constructed. Quartz windows with a diameter of 9 cm are housed in these apertures, enabling visual access to the maximum usable flame radius. The chamber was hydrostatically tested before an over-pressure valve was installed in the exhaust line, and it was designed to sustain an internal pressure rise of 6 MPa. Two pressure-resistant high transparency glass windows with a net diameter of 90 mm and a thickness of 20 mm are placed and fastened on both sides of the combustion chamber by two 20 mm thick side flanges with a diameter of 230 mm, allowing optical access to the combustion process.

The cylinder has seven sockets with a diameter of 1/2 in, two of which are co-linear and used to insert and fix the ignition electrodes that are attached to the ignition system. The other is utilized for introducing gaseous fuel and air, scavenging exhaust gases, and inserting thermocouples, pressure transmitters, and spare parts. To support its considerable weight, the combustion vessel is mounted on a sturdy carbon steel platform, as shown in Figure (3.3).



Figure 3.3 - Photography for the carbon-steel CC unit.

3.11.2 Temperature measurement and control

Use one type (pt-100) thermocouple used to measure the bomb temperature, Note that all experiments we will perform are at normal room temperature at 300 k, A screen was also used to display the temperature on the control panel and keep the desired temperature, as shown in figure (3.4).



(a)



(b)

Figure 3.4- a) Digital temperature controller, b) Temperature sensor.

3.11.3 Pressure transmitter

The vacuum, starting, and combustion pressures inside the CC are measured using a pressure sensor (DPA-Mpa) with a range of -0.1 to +1 MPa. This sensor reads data in a variety of units, including bar, mbar, Pa, kPa, MPa, mm HG, mm H₂O, Psi, and so on. In the present work, it is set to kpa, as shown in figure (3.5).



Figure 3.5- Pressure transmitter, DPA-Mpa.

3.11.4 Gasket

Two pairs of thermal asbestos gaskets of 3 mm thickness are used for each of the big flanges and the other pair for each of the optical flanges to achieve the requisite sealing for the combustion chamber and to ensure that no leakage occurs either in a vacuum or in combustion high pressure, as shown in figure (3.6).



Figure 3.6- Gasket

3.12 Ignition System Unit

To produce the powerful spark required to ignite the mixture and to control the timing and power delivered, an electronic circuit is designed and used to supply the required power to the two electrodes. The ignition system consists of a 220 V AC electrical source which is supplying the electricity to a rotary variable transformer to provide the required voltage for ignition, and the output is connected to an ignition burner transformer (10 kV maximum voltage) to supply the two electrodes with high tension voltage to generate the required powerful spark. Fine stainless steel electrodes with a diameter of 1.5 mm were inserted in the chamber to have minimum effect on flame propagation.

The high-speed camera and logging devices were also connected to the pulse generator, allowing video and data recording to be sequenced to the point of igniting. The usage of an auto-ignition coil was used to ignite the discharge. Willyanto et al. [114] and Jun et al. [121] used a similar technique to construct the system.

A spark is generated in the centre of the combustion chamber using two opposing, co-linear electrodes. To improve the electric field at the gap, the spark gap is fixed to 1 mm and the electrode tips are sharpened. (See Fig. 3.7).

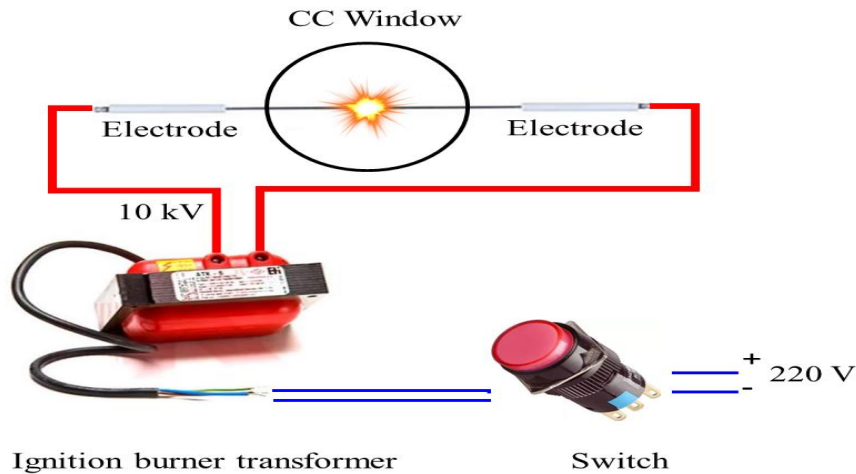


Figure 3.7- Schematic diagram of an electronic circuit for the ignition unit.

3.13 Gas injection unit

3.13.1 The manifold

The fuel and oxidiser were separately fed into the combustion chamber by the manifold. The manifold has three different types of valves, as shown below:

- a. Ball valve (1/4 in) linked to Vacuum pump.
- b. Needle valve control (1/4 in), which is attached to the combustion chamber and allows the admission process to be precisely controlled.
- c. Four solenoid valves, 24 V DC (closed to open), powered by an electrical transformer (220v AC to 24v DC), one of which is connected to the air compressor and the other three to methane, hydrogen storage tanks, and spare. This sort of valve is used to electronically admit air and gaseous fuel to help with precise injection. Fuel valves

were linked to all specified cylinders using 1/6-inch tubing and connected to a manifold. This allowed for the use of several feeds in a single chamber port during a test. The fuel unit as showed fig.(3.8)



Figure 3.8- The gas manifold.

3.13.2 Fuel tank

The required fuel is supplied to the manifolds via a pressure-lowering valve, as illustrated in figure 3.9, which reduces and regulates the rate of flow of the fuel gas from tank value to a pressure between 0 and 3 bar.



Figure 3.9- Pressure organizer valve.

3.13.3 Air compressor

A compressor (type DARI, 1.5 HP, 8 bar) supplies the air for the combustion chamber at the requisite pressure, as shown in figure (3.10).



Figure 3.10- Air compressor.

3.13.4 Vacuum System

The CVC contents were evacuated between tests using a vacuum pump at a nominal rate of $0.3 \text{ m}^3 \cdot \text{h}$. It is designed to connect the vacuum pump to the same line as the injection system of the combustion chamber, and therefore, to avoid the large number of connections that cause or avoid many suspicious areas if any leakage occurs. After each test, the combustion chamber is cleaned of its combustion products.

3.14 Electrical Control Board Unit

It's a 40x30x15 cm electrical board with the following components see in fig.

(3.11):

1. Temperature displayer: Used to measure with this instrument temperature inside the combustion chamber.
2. Power supply selector switch. supplying the board with electricity.
3. Vacuum selector switch: a device that is used to turn the vacuum compressor
4. Fuel selector switch: Two selection switches were employed to regulate the solenoid valves for gaseous fuels, with one remaining as a spare.
5. Ignition and camera push button: used to start the ignition and the camera for started capturing the whole process of combustion.

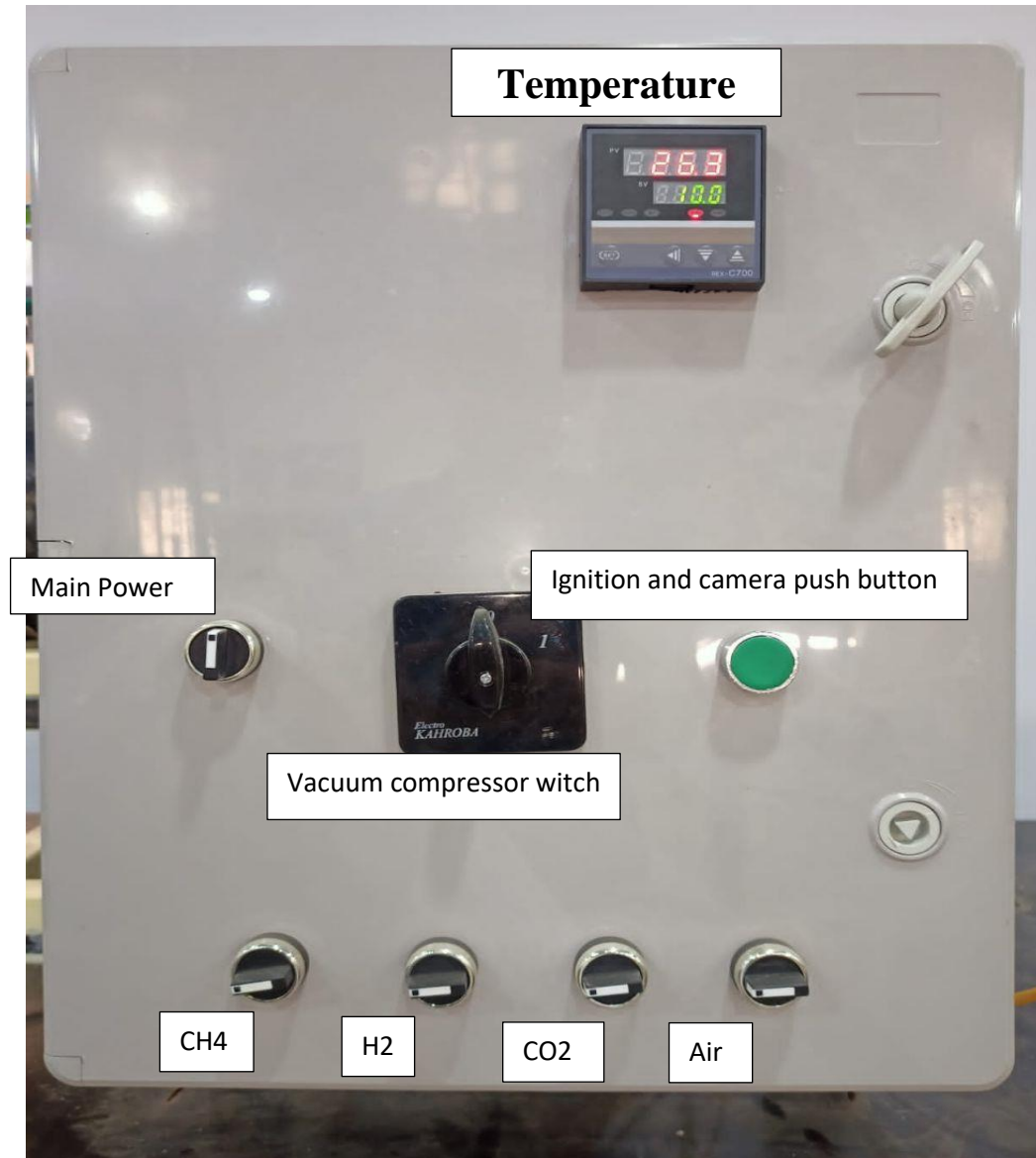


Figure 3.11- Electrical control board unit.

3.15 Photographing Unit

A schlieren technique is used to visualize the process of flame propagation with a high-speed camera (AOS -Q PRI) using a light source and plano-convex lenses as shown in figure (3.12).

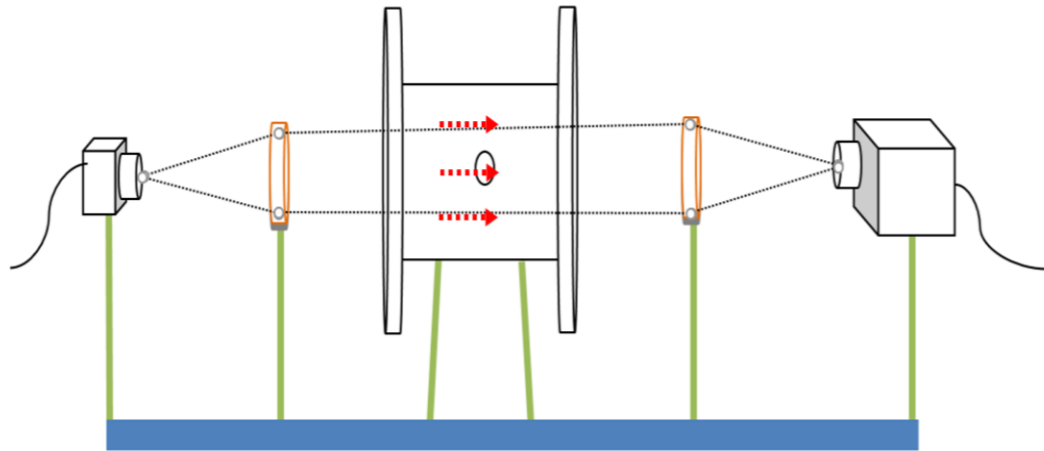


Figure 3.12- Schematic diagram of Photographing Unit.

3.15.1 Optical path

Collimate a filament light source through two of the polar opposite viewing windows. The area that the light beam traverses as it travels through the chamber's centre and it's filled with gases is the working area under investigation. When a high-speed camera captures the beam after it has been imperfectly focused by the mirror. This process results in gradients of light intensity, which are influenced by variations in refractive index brought on by changes in working gas density. As a result, any borders that get darkened or brightened due to combustion are isotherms that indicate a significant change in density and are therefore taken to be the flame front boundary [12].

A lens concentrates the light, which is then collected by a charge-coupled element in a high-speed camera called a Photron. The chosen filming rate was adjusted to record as many useful frames (effective data points) as possible, depending on the fuel under examination. To minimize overly big video files, the filming pace was reduced for slower flames. As a result, the image size, shutter speed, and, as a result, the

power and intensity of the light in the system, all limit the increase in frame rate, as shown in figure 3.2.

The optical lenses are kept in place by plastic and iron collars, and placed over iron stands by screws, as illustrated in figure (3.13).



Figure 3.13: Convex lens.

3.15.2 Camera and Source of Light

In this study, the flame propagation is captured using a portable high-speed camera (AOS - Q-PRI), which has a resolution of 3 Mega Pixel and 16,000 FPS as shown in figure (3.14). 3600 FPS is the setting that was used in the test. The necessary light rays are produced by a lamp powered by 12V DC.



Figure 3.14- High-speed camera (AOS -Q PRI).

3.16 Calibration

The high-speed camera (AOS - Q-PRI), pressure and temperature measuring equipment are calibrated to ensure that all the data collected from the measuring devices are accurate.

Thermocouple and pressure transmitter calibration is performed at the Central Organization for Standardization as indicated in figure (3.15.a & b), whereas the high-speed camera calibration is performed by the manufacturing business as shown in the appendix.

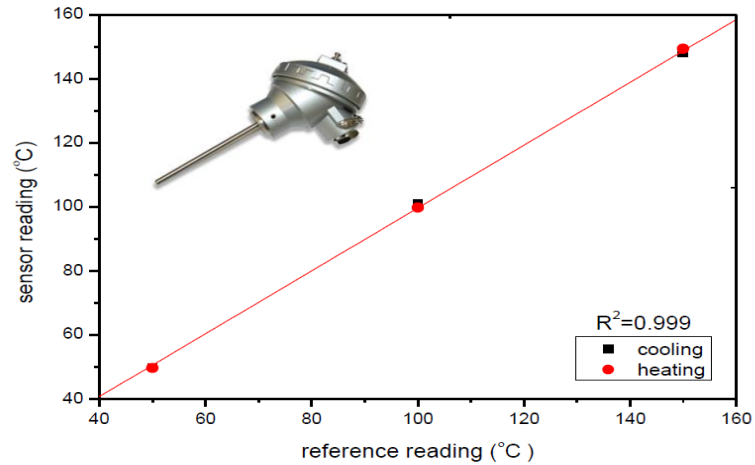


Figure 3.15.a: Thermocouple calibration.

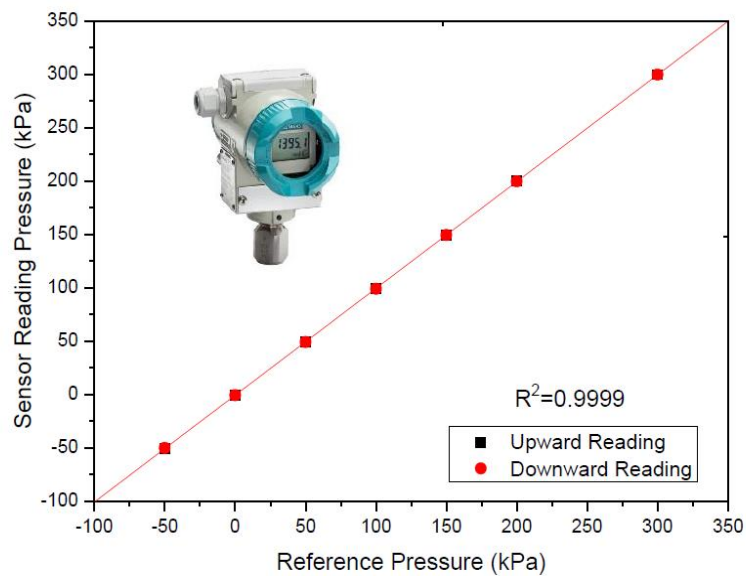


Figure 3.15.b: Pressure gauge calibration.

3.17 Methods of Experimentation and Data Collection

This section begins with a description of the experimental procedure used, followed by more precise details about the methodology.

1. The vacuum pump was then opened, displacing the contents of the CVC. To remove the combustion byproducts from the prior test, the CVC was twice emptied between each test. The goal was to reduce errors caused by an imprecise vacuum.
2. After reaching the appropriate starting evacuated pressure, the needed amount of Fuel was slowly injected by tiny needle valve control, giving the vacuum gauge time to settle down at a given value as the gas adjusted to chamber temperature.
3. The reactants in the vessel have now been blended together. This would result in a well-mixed mixture of the reactants. Allowed for another 3 minutes to dissipate any remaining turbulence.
4. The camera was prepared to record before ignition. In the ignition program on the control board, the chosen trigger mechanism was indicated as a push button 10 msec. The system would record constantly in a loop, with the final trigger point used to indicate the centre frame. The original rationale for this decision was to ensure that no frames from the point of ignition were missed.
5. The pulse generator was activated, and the reactants ignited, following a final check to ensure that all safety standards were followed and that all isolation valves and gas cylinders were closed.
6. In preparation for the following test, the chamber's contents are evaporating. Video files, dilution ratios, and pressure data were saved and reproduced.

Chapter Four

Results and Discussion

CHAPTER FOUR**Results and Discussion****4.1 INTRODUCTION**

This chapter is split into two sections. The numerical results are provided and discussed in the first section, while the experimental results are presented in the second part.

The flame propagation speed and LBV for methane/hydrogen/and air mixtures are measured in a constant volume combustion chamber. The spark is ignited at the centre of the experiment, and the flame starts and spreads outwards. Schlieren technique is used to study the flame using a high-speed camera. Initial pressures (0.1MPa) at 303 ± 3 K, equivalence ratios (0.8, 1.0, and 1.2), and hydrogen content (0-30)%.

In the numerical section, the ANSYS-CHEMKIN Program is used to compute the un-stretched adiabatic laminar burning velocity for methane/syngas/air blends at various initial pressures, equivalency ratios, and initial temperatures of 303 k. Experimental and published results are used to validate the numerical results.

4.2 Program Validation

The CHEMKIN program is used to calculate the physical properties of reactance and expected product, as well as adiabatic flame temperature and initial admitting pressure for each reactance mixture (mole and mass analysis for reactance and expected

product, densities, specific heat, thermal conductivity, and thermal diffusivity for the unburnt and burnt mixture). The system can run on pure hydrocarbons (CH_4 , C_2H_6 , C_3H_8 , C_4H_{10} , C_5H_{12}), a CH_4/H_2 blend, or another syngas mixture of multi-hydrocarbons combined with hydrogen. The program's outputs are validated by comparing them to other studies, as shown published in Figure (4.1).

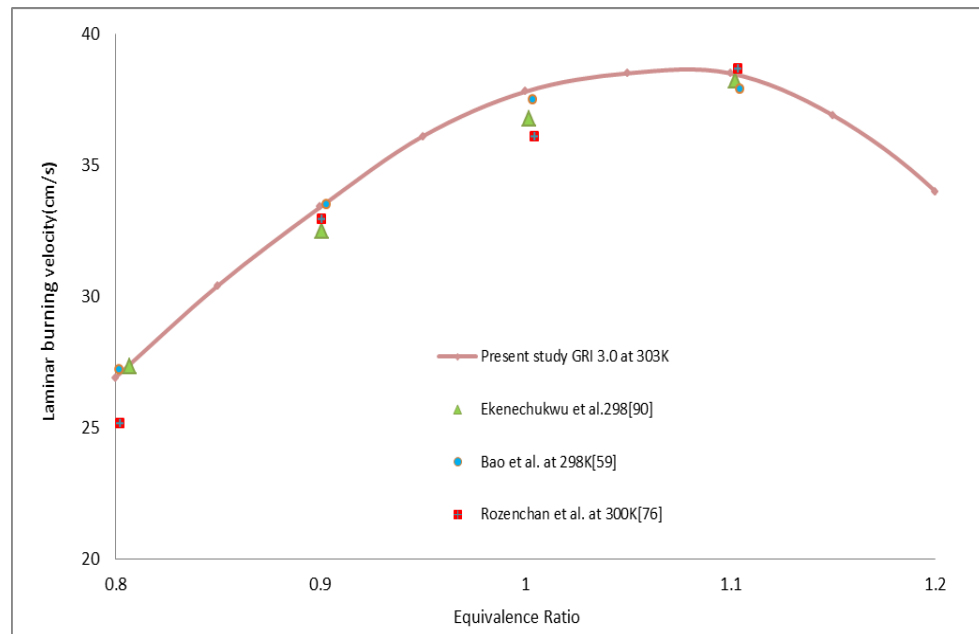


Figure 4.1- Experimental and simulation data for LBV of methane at $P_1=0.1\text{MPa}$ compared to published results.

Equation (4.1) is used to calculate the error based on average findings, as illustrated in figure (4.2):

$$error(\%) = \left| \frac{S_{u,av} - S_{u,prog}}{\left(\frac{S_{u,av} + S_{u,prog}}{2} \right)} \right| * 100\% \quad ..(4.1)$$

Where $S_{u,prog}$ is the estimated burning velocity and $S_{u,av}$ is the average burning velocity for the other codes. Figure (4.2) indicates that the highest error occurs at the stoichiometric combination of 5.2% when comparing the ANSYS-CHEMKIN Program result with those of Wang et al.[59], and Zou et al.[120] due to the errors in flame temperature. This is brought on by disregarding dissociation. Each physical property in the product experiences an increase in error as the equivalency ratio rises. The mistake of properties in the lean combination is proper due to its reliance on the initial state.

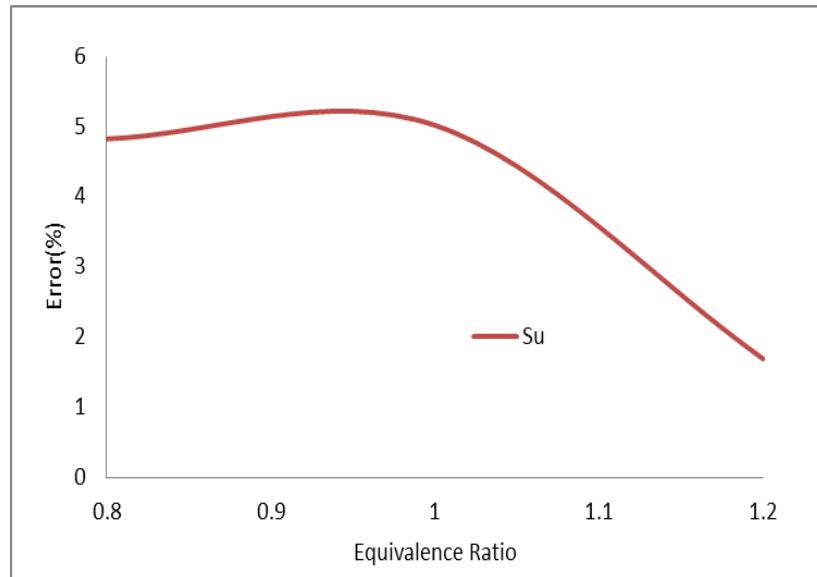


Figure (4.2)- Error of burning velocity of methane for current study with different equivalence ratio

4.3 Adiabatic Flame Temperature

The thermodynamic parameters of the combustible mixture are represented by the adiabatic flame temperature. The heat release capacities of the unburned mixture are indicated by adiabatic flame temperature, which is related to a variety of chemical phenomena such as flame propagation speed, flame extinction, flammability limits, and so on. The ANSYS-CHEMKIN programs were used to determine the adiabatic flame temperature. The adiabatic flame temperatures of methane (using the GRI. 3.0 mechanism) and blends were validated by comparing the results to those of other researchers, as shown in figure (4.3).

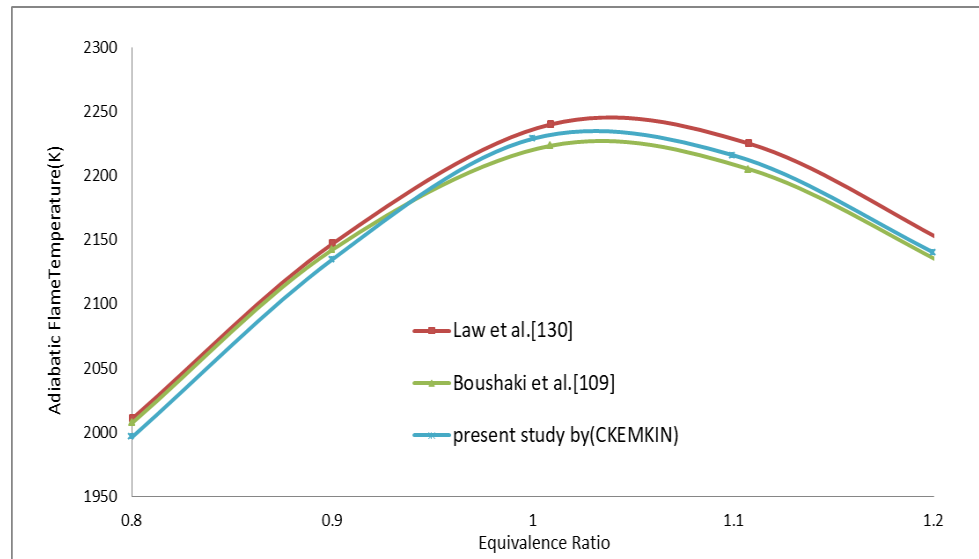


Figure 4.3- A comparison of adiabatic flame temperature with earlier methane tests under normal settings at $T_i = 303 \pm 3$ k and $P_i = 0.1$ MPa.

The CHEMKIN program was relied on to analyze the numerical results. Due to the type of polynomial equations utilized in the software and the GRI-Mech 3.0

mechanism being made up of 53 species and 325 reaction steps, each with its own set of rate coefficient expressions and thermochemical characteristics.

The adiabatic flame temperature of methane-syngas-air mixes with various initial pressures is shown in Table 4.1 and Figures (4.4). With the addition of hydrogen, the adiabatic flame temperature increases. This is because the heating value of the combustible mixture increases when hydrogen is added because hydrogen has a larger heating value than methane, resulting in increased heat release and thus a higher adiabatic flame temperature.

It's also worth noting that as the methane ratio rises, the pace at which the adiabatic flame temperature drops rises. Furthermore, the amount of methane in the blended gas drops as the carbon dioxide level rises, lowering overall heat release and lowering the adiabatic flame temperature. Chan et al. [30] and Halter [84] both concur on this behaviour. Additionally, it is shown that under stoichiometric conditions, the adiabatic temperature is maximized. Simply put, the presence of oxygen for lean mixtures and both carbon monoxide and hydrogen for rich mixtures serve as diluents that absorb heat and serve as heat sinks, resulting in a decrease in the temperature of the adiabatic flame.

\emptyset	$T_{ad,0\%H_2}$	$T_{ad,10\%H_2}$	$T_{ad,20\%H_2}$	$T_{ad,30\%H_2}$
0.8	1996.43	1997.284	1999.08	2002.119
1	2228.914	2231.029	2235.614	2239.409
1.2	2139.894	2149.466	2157.572	2164.149

(a)

\emptyset	$T_{ad,0\%H_2}$	$T_{ad,10\%H_2}$	$T_{ad,20\%H_2}$	$T_{ad,30\%H_2}$
0.8	1996.729	1998.337	2001.385	2004.751
1	2235.193	2237.193	2241.593	2245.52
1.2	2142.23	2151.246	2158.287	2165.286

(b)

\emptyset	$T_{ad,0\%H_2}$	$T_{ad,10\%H_2}$	$T_{ad,20\%H_2}$	$T_{ad,30\%H_2}$
0.8	1996.919	1998.515	2001.768	2005.197
1	2240.705	2242.402	2246.564	2251.178
1.2	2144.514	2152.458	2158.808	2166.1

(c)

Table 4.1- Adiabatic flame temperature versus equivalence ratio for $CH_4/H_2/air$ mixtures at $T_i=303\pm 3K$ with different initial pressures. (a) $P_i=0.1MPa$ (b) $P_i=0.2MPa$ (c) $P_i=0.3MPa$.

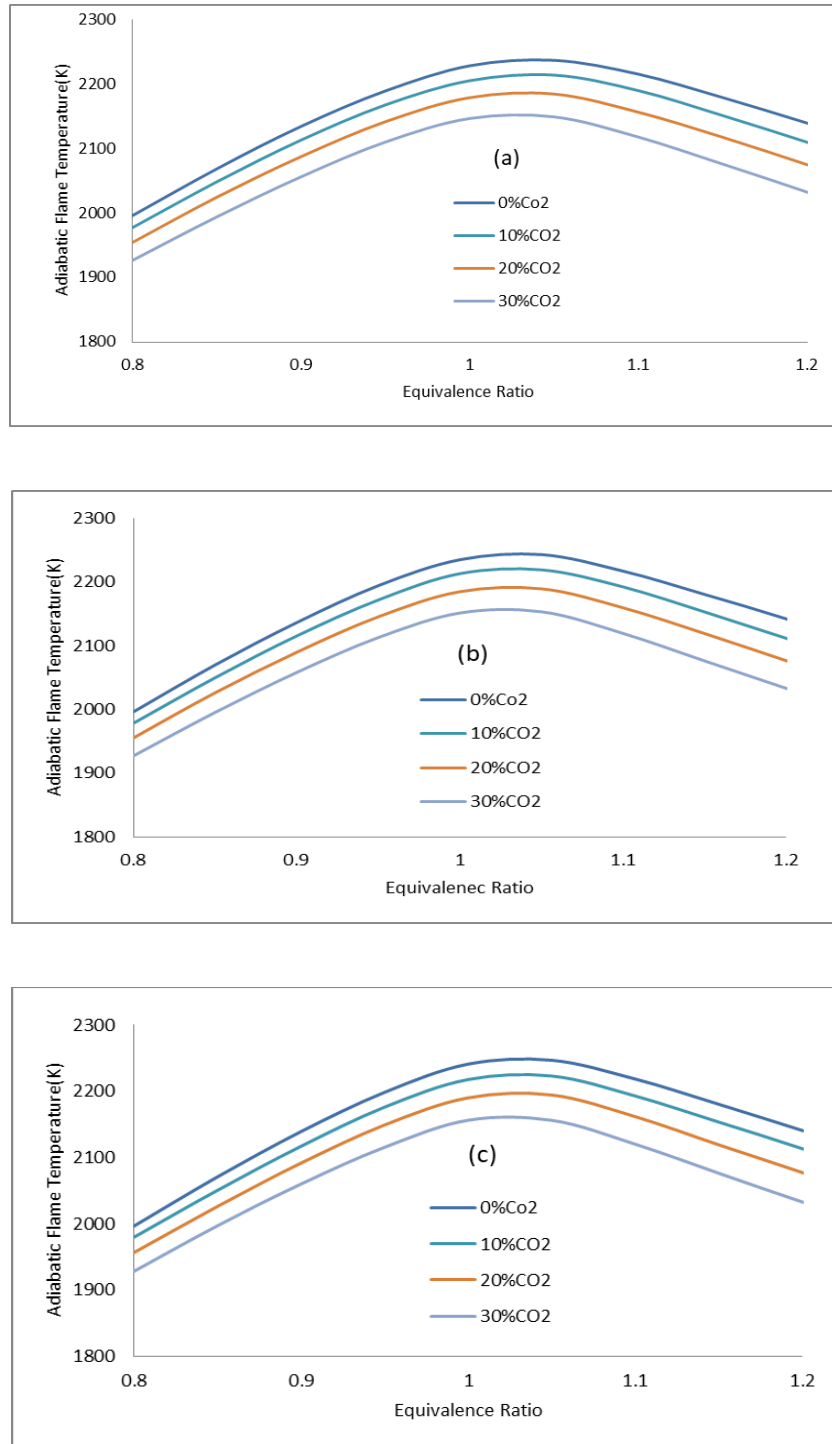


Figure 4.4- Adiabatic flame temperature versus equivalence ratio for $\text{CH}_4/\text{CO}_2/\text{air}$ mixtures at $T_i = 303 \pm 3\text{K}$ with different initial pressures. (a) $P_i = 0.1\text{MPa}$ (b) $P_i = 0.2\text{MPa}$ (c) $P_i = 0.3\text{MPa}$.

Table 4.2 shows how the adiabatic flame temperature of methane varies with initial pressure for various equivalence ratios. The adiabatic flame temperature rises with increasing starting pressure. The cause of this tendency is an increase in mixture density, which leads to long-term chain branching processes, particularly at the stoichiometric ratio, which is the most important owing to complete combustion. Boushaki et al. [109] and Ueda et al. [108] both concur on this behaviour. It's also worth noting that at stoichiometric conditions, the adiabatic temperature is at its highest.

Equivalence ratio	$P_i = 0.1MPa$	$P_i = 0.15MPa$	$P_i = 0.2MPa$
0.8	$T_{ad} = 1996.43$	$T_{ad} = 1996.729$	$T_{ad} = 1996.919$
1	$T_{ad} = 2228.914$	$T_{ad} = 2235.193$	$T_{ad} = 2240.705$
1.2	$T_{ad} = 2139.894$	$T_{ad} = 2142.23$	$T_{ad} = 2144.514$

Table 4.2- Adiabatic flame temperature vs equivalence ratio for methane with various initial pressures at $T_i = 303 \pm 3$ K.

4.4 Experimental Results

The experimental analyses of CH_4 /air mixtures and Methane/hydrogen/air mixtures at 303 ± 3 K and 0.1 MPa is used in this section. The given output after computationally processing the test video file (recorded at 3,600 fps) is a succession of rising pixel counts, which are then scaled to give a propagating Schlieren flame radius (r), as it will be seen later. To reduce the impact of ignition energy discharge during the early stages of propagation, data up to a 6-mm radius is ignored. Bradley et al. [119] suggested adding another safety factor to the 8 mm requirement.

The numerical technique for analyzing experimental results is described in this chapter, which uses methane and methane/hydrogen to compare the obtained values to data from similar research publications. The results of both linear and optical techniques are compared. The experimental and analytical uncertainties are then investigated in further detail.

4.4.1 Repeatability Test

The experimental apparatus was created specifically for this study. To compare experimental results with those of other studies, the repeatability of one case study and the use of alternate fuel is used. These tests are done to ensure that the rig is accurate. The mixture is created inside the CVC as previously indicated. In the mixing process, the partial pressure blending method is used.

A pre-set combination is formed at initial pressure, initial temperature, fixed equivalency ratio, and blend ratio. The same mixture is used for four successive combustion experiments. The findings of these four tests were remarkably consistent. Figure (4.5) shows the results. The repeatability is acceptable.

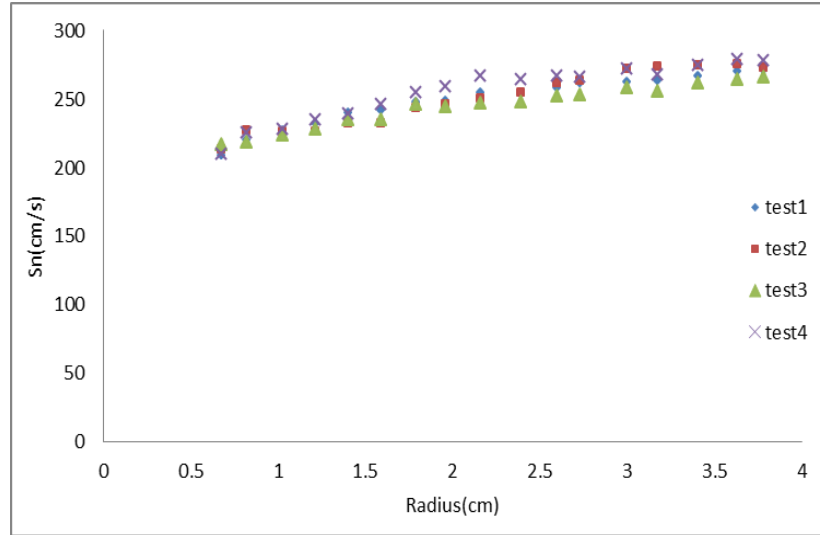


Figure 4.5- Schlieren Radius vs. stretched Flame Speed for four consecutive methane/air mixture experiments at $T_i=303\pm 3\text{K}$ and $P_i= 0.1\text{MPa}$.

Also, to validate the current measurement system, the results of burning mixtures at atmospheric pressure and $T_i = 303\text{ K}$ with varied equivalency ratios from 0.8 to 1.2 of methane and other characteristics are compared with data from other studies, as shown in figure (4.1). The comparison demonstrates good agreement, indicating that the experimental technique and measurement methodologies are highly accurate.

4.4.2 Ignition energy

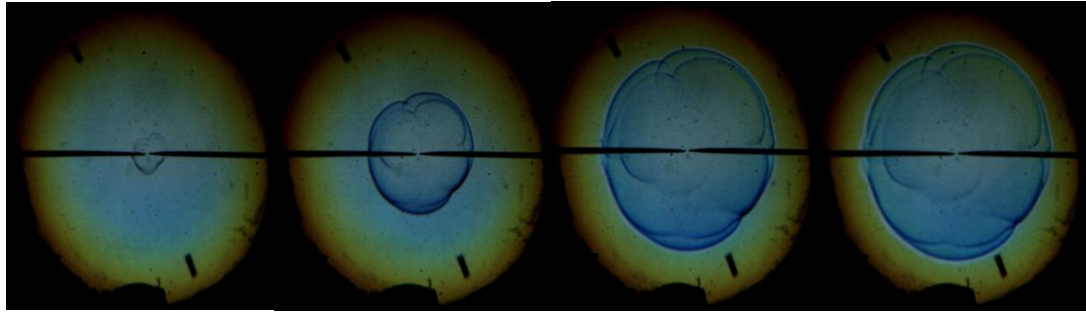
All these experiments on methane/air and hydrogen blends were carried out at $303\pm 3\text{ K}$ and 0.1 MPa for varied equivalency ratios. The minimum ignition energies of molecules lighter than air (hydrogen and methane) occur in lean mixtures due to increased diffusivities. Ngo [123] had earlier seen a similar pattern.

4.4.3 Flame Speed Analysis

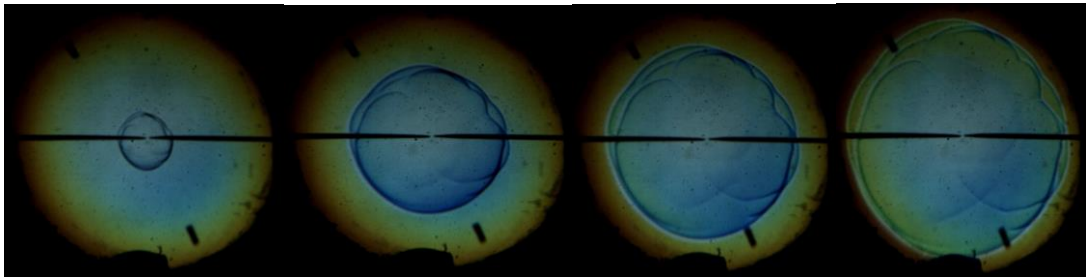
This section contains the findings of the expanding spherical flame studies. After the spark, ignition occurs at the chamber's centre, the flame spreads spherically across the mixture.

Figure 4.6 depicts a series of frames of a growing spherical flame with a stoichiometric methane/air mixture as a typical scenario of flame propagation. The Schlieren flame photos reveal a disk that grows in diameter over time. The spatial flame speed is calculated as the rate of change in flame size utilizing the flame image analysis.

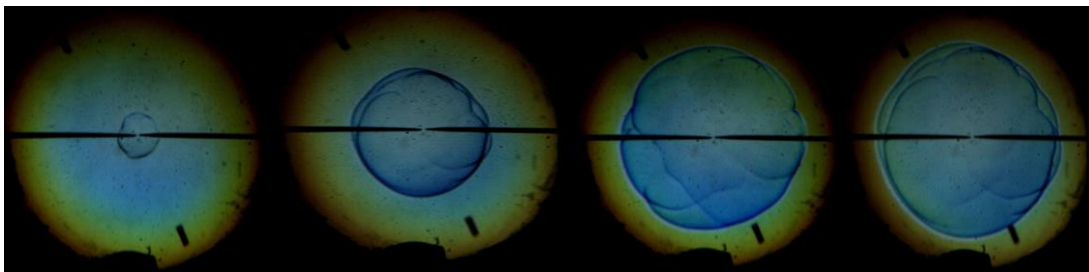
$$\phi = 0.8$$



$$\phi = 1$$



$$\phi = 1.2$$



5ms

10ms

15ms

20ms

Figure 4.6- Flame propagation photographs for methane at $T_i = 303 \pm 3$ K, $P_i = 0.1$ MPa, and various equivalence ratios.

The radius of the growing flame as a function of time for each run is determined from the images by using Tracker software. On the other hand, Figure 4.7 provides a plot of the experimental values of flame radius over time for the methane fuel at equivalency ratios of 0.8, 1, and 1.2 at initial temperatures and pressures of $303\pm 3\text{K}$ and 0.1MPa , respectively. These data show that increasing the amount of methane fuel improves flame propagation speed and, thus, the flame radius at a given instant. Previous studies [65], and [78] found a similar pattern. In addition, the time for any specific radius is greater at 1.2 compared to 0.8, due to the flame speed being greater, as will be shown later.

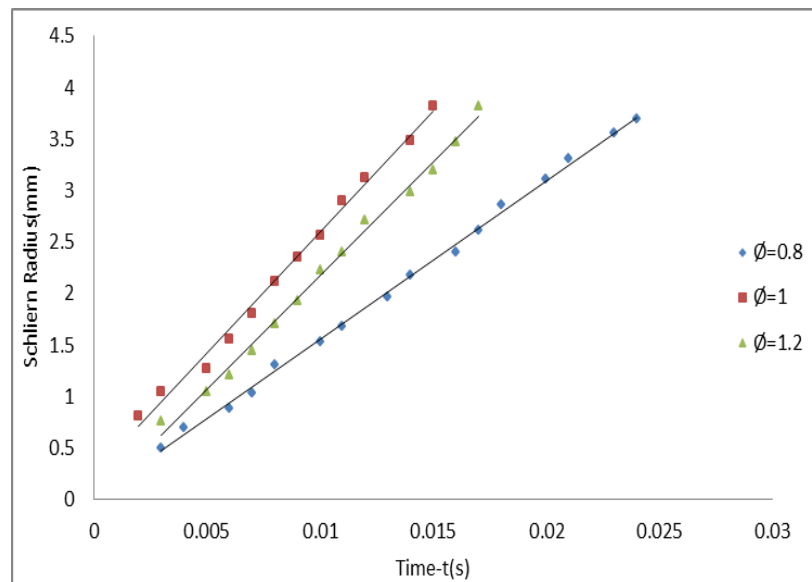


Figure 4.7- Methane flame radius at stoichiometry as a function of time for various conditions at $T_i=303\pm 3\text{K}$ and $P_i= 0.1\text{MPa}$.

The data was obtained from the experiment recordings using Tracker 5.1.5 software, which was used to extract information on the variation of the flame radius over time to track the flame front's progression. The slope of the line segment

comprising two neighbouring radii against time is the instantaneous stretched flame speed (S_n).

$$S_n = dr/dt \quad \dots (4.2)$$

The flame speed is computed by averaging four radiuses (one for each direction) against time because of the irregularity of the flame front form. A disadvantage of Tracker software's averaging technique is that locations around the lower radii are particularly sensitive to slight deviations as compared to the end points. The effect becomes apparent at large radii as a result of the electrode thickness and increased combustion pressure volume. The greatest measured radius will have a larger uncertainty than usual. This increases the number of errors caused by a lack of clarity in the photos on the film, which could be caused by multiple factors. The rubber gasket between the window and the flange of the combustion bomb degrades in the presence of flame temperatures, as does the matching of the lenses at the optimal focal length and the location of the focal length position in the test media.

4.4.4 Stretched Laminar Flame Speed

Stretched flame speed has been measured experimentally in CVC. The influence of hydrogen blending and equivalency ratio at various initial pressures on flame speed has been investigated.

The data utilized in the analysis is restricted to a flame radius of between 8 and 38 mm. The first region is the initiation region, where the ignition energy may influence the propagation of a centrally lit flame in the early stages of flame development when the flame radius is smaller than 8 mm. Bradley et al. [120] pointed out that the ignition

energy would increase the flame speed for fuel/air mixes with a flame radius of less than (5mm). This study also discovered the S_n decreases as the flame radius increases from 5 to 8 mm, depending on the equivalency ratio and hydrogen concentration. Because of the interference of undeveloped flame, the flame speed determined previously in this location cannot be utilized to establish the laminar flame speed.

The completely evolved zone is the second, where S_n would be nearly constant. Berk Can et al. [61] proposed that the flame radius range be less than one-quarter the radius of the combustion bomb for the computation to be realistic. The combustion bomb utilized in this study has an interior radius of (150mm). Because the flame speed for a fully developed flame is generally high and approximately stable, as well as the consideration of isobaric combustion, we used a flame radius of (38 mm) to compare with the other parameters in this study.

When the flame radius exceeds (38mm) in the third area, the strain in the flow field significantly reduces flame speed, as well as the effect of combustion pressure. The first and third regions are not to be considered. In general, as the spherical flame radius grows, the flame propagation speed increases. Previous research has discovered this behaviour [65,57].

In summary, the following data are plotted for each blend and set of conditions: Figure (4.8) shows S_n versus radius for methane/air mixtures with different stoichiometry.

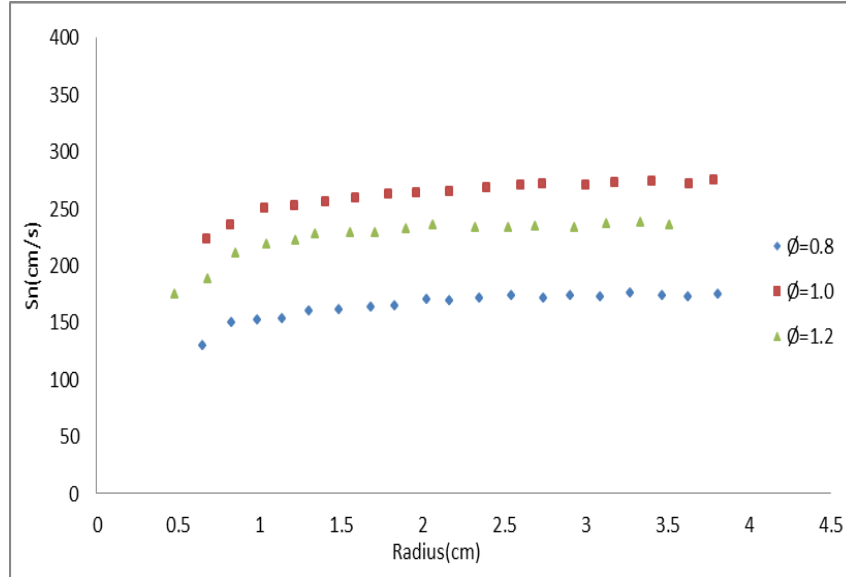


Figure 4.8- S_n variation with a flame radius for methane at $T_i = 303 \pm 3$ K and $P_i = 0.1$ MPa for various equivalence ratios.

4.4.4.1 Influence of stoichiometry

The experimental flame speed against stoichiometry limits for methane and methane/hydrogen blending ratios at atmospheric pressure is shown in figure (4.9). The flame speed was increased as the combinations progressed from lean to stoichiometric, and then declined as rich mixtures approached. While blending ratios of 10%–30% are observed, the flame speed at ($\phi=1.2$) is greater than that at ($\phi=0.8$).

Figure (4.10) shows the experimental flame speed against flame radius data for methane with varied hydrogen concentrations and stoichiometry at atmospheric pressure. It demonstrates that the stoichiometric combination has a faster flame speed than lean or rich mixes for any hydrogen blend. There is enough oxygen in the lean and stoichiometric mixture to completely burn the fuel, releasing all of the heat. When a stoichiometric combination flame has enough oxygen to consume the fuels and no

surplus air, the flame temperature and speed should theoretically be at their maximum. However, through proper mixing processes, the highest temperature is maintained at an equivalency ratio of (1.10-1.15), and the result is maximum flame speed. Because of incomplete combustion and dissociation, the flame temperature and thus flame speed drop on the rich side.

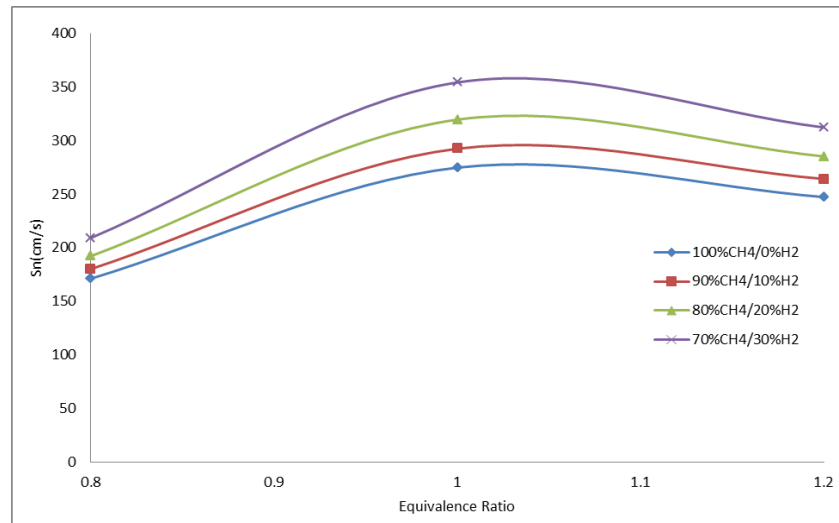


Figure 4.9- Variation of S_n with Equivalence Ratios for Methane with Various Hydrogen Percentages at (2cm) Radius, $T_i = 303 \pm 3$ K and Atmosphere Pressure.

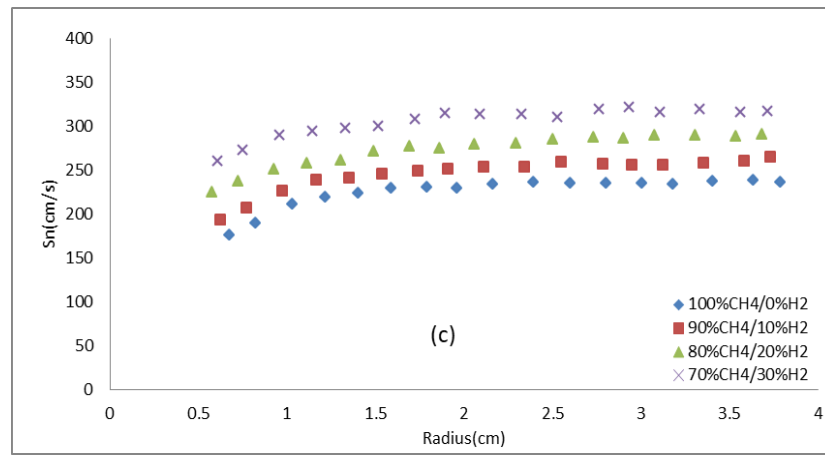
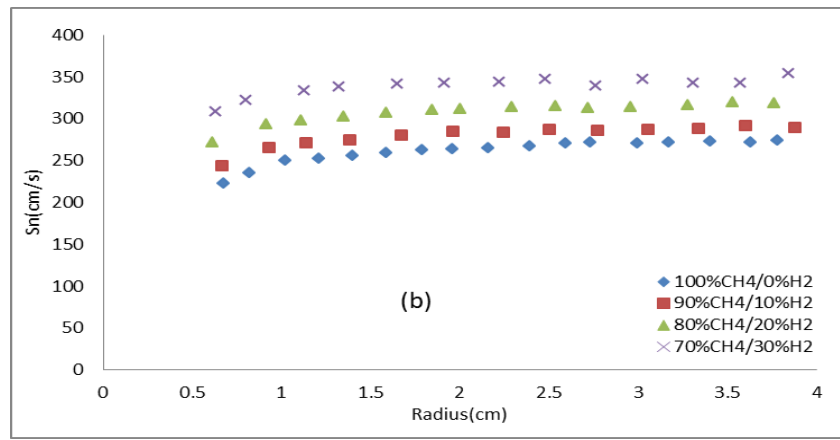
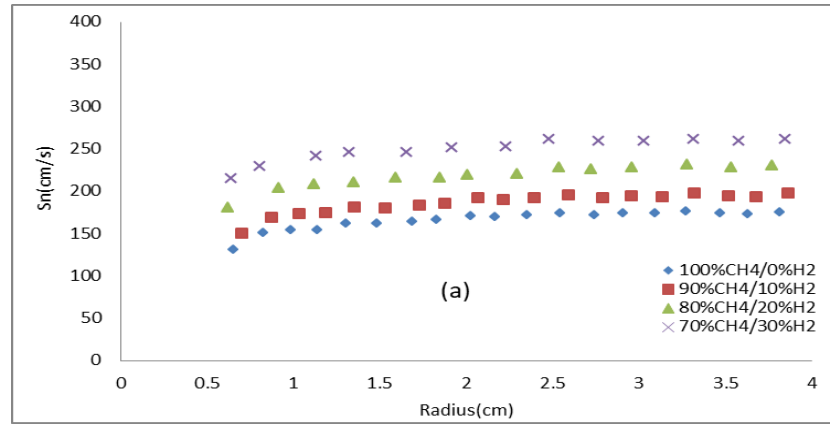


Figure 4.10- S_n Variation with a flame radius for methane at $T_i = 303 \pm 3$ K and $P_i = 0.1$ MPa with various hydrogen percentages and stoichiometry : (a) $\varnothing = 0.8$ (b) $\varnothing = 1$ and (c) $\varnothing = 1.2$.

4.4.4.2 Influence of hydrogen blending ratio

The experimental flame speed against radius data for several hydrogen mixtures is shown in Figure (4.11). The results have a key factor to consider as the hydrogen blends increase. First, the flame propagation speed increases because the flame temperature of hydrogen is greater than methane, so the flame speed increases.

The fluctuation of S_n with hydrogen blends under atmosphere Pressure as shown in figure (4.12). It illustrates that for initial pressures, the flame speed rises as the hydrogen increases in the mixtures.

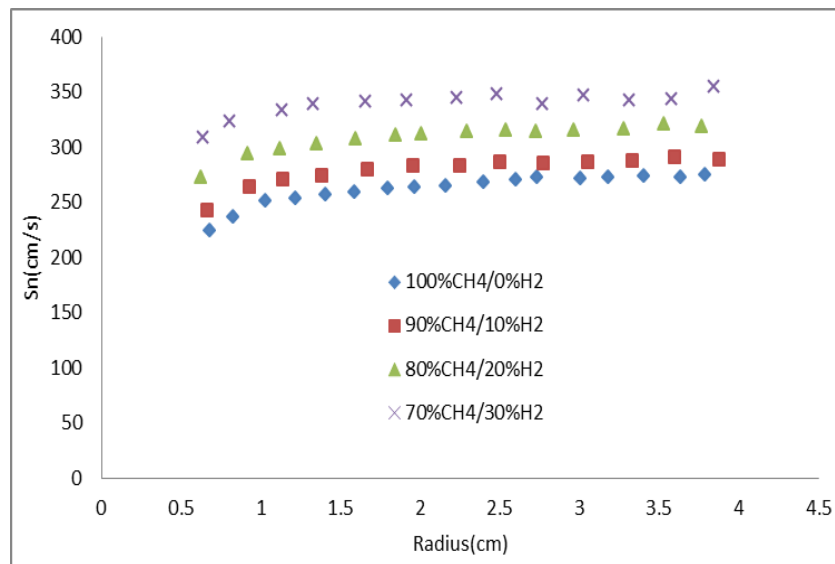


Figure 4.11- S_n Variation with Flame Radius for Methane with Different Hydrogen Mixtures for Stoichiometric Mixture ($\phi=1$) at Atmospheric Pressure.

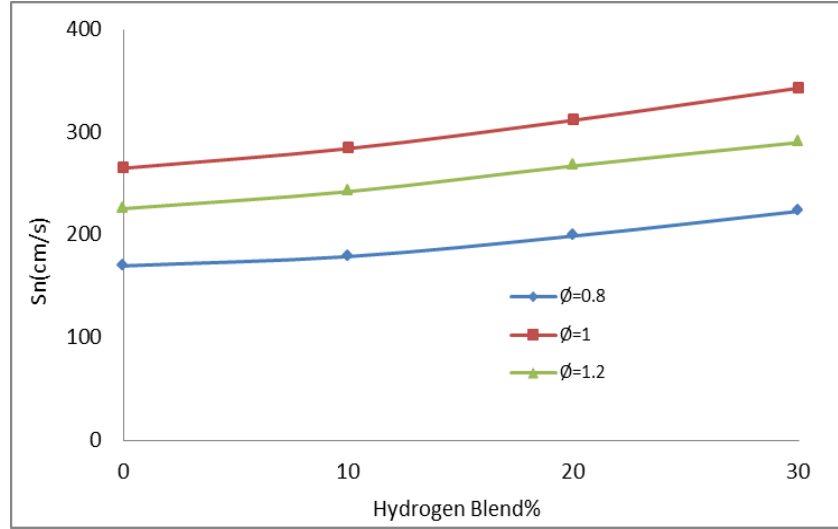


Figure 4.12- S_n Variation with Hydrogen Percent for various Equivalence Ratio at a radius of 2 cm, at $T_i = 303 \pm 3$ K and 0.1MPa initial pressures.

4.4.5 Stretch Rate and Un-stretched Flame Speed

The stretch rate of a flame front surface is too high in the early stages of flame propagation when the flame radius is small because the relationship is directly proportional to flame speed and inversely related to a flame radius. A linear association between the stretched flame propagation speed and the flame stretch rate is proven by deleting data impacted by the ignition energy and electrodes during the early stages of flame formation, as well as data with a large radius when the pressure is increased.

The linear extrapolation employs the relationship described in Eqn. 3.20 ($S_l - S_n = L_b \alpha$) in attributing a linear trend to the data and extrapolating to values of zero stretch rate. Thus, by regressing a linear fit to the plotted data and obtaining the requisite coefficients, the method is straightforward to be used. Figure (4.13) depicts the previously provided data with the linear connection overlay and forecasted to zero

stretch circumstances. As a result of this sample test, a stoichiometric unstretched flame speed of 289.02 cm.s^{-1} will be obtained. The adiabatic density ratio of products to reactants, as shown in Eqn. 3.22, must be applied to obtain a value for the S_u .

The GRI-Mech 3.0 database was designed to model methane combustion and was used to calculate the relative densities in this test. The stretch rate influence lessens as the flame propagates because the stretch rate is inversely related to the radius. As the flame radius increases, the flame shape becomes less curved, and it appears as a planar, one-dimensional, and hence un-stretched flame. Because of the substantial curvature associated with a small spherical surface, the stretch rate (α) exhibits excessive values during the early phases of flame propagation. Flame stretch influences flame speed; it may be properly estimated when the stretch is minimal, i.e. when $r \rightarrow \infty$.

In the plot of S_n against the unstretched flame propagation speed, S_l , is determined as the intercept value of S_n at $\alpha = 0$, Obtained through applying Eqns. 3.18 and 3.19. This is significant because it yields the value of S_u from equation (3.20) [164]. In a tiny stretch rate, the strain in the flow field causes a severe fall in stretched flame speed, whereas the cellular flame causes a strong increase in stretched flame speed [307]. Only a flame radius between 8 and 38 mm is considered in the computation due to the influences of spark, cellular flame, and flow field strain.

The impact of the stretch influence on flame propagation varies depending on the conditions (fuel kinds, equivalency ratios, etc.), as shown in the figures (4.14, 4.15). With an increasing stretch rate, the stretched flame propagation speed shows a declining trend. This means that, given a stretch rate, the slope of S_n is always negative.

However, can be used Linear methodology to attain a representative flame speed uninfluenced by a stretch.

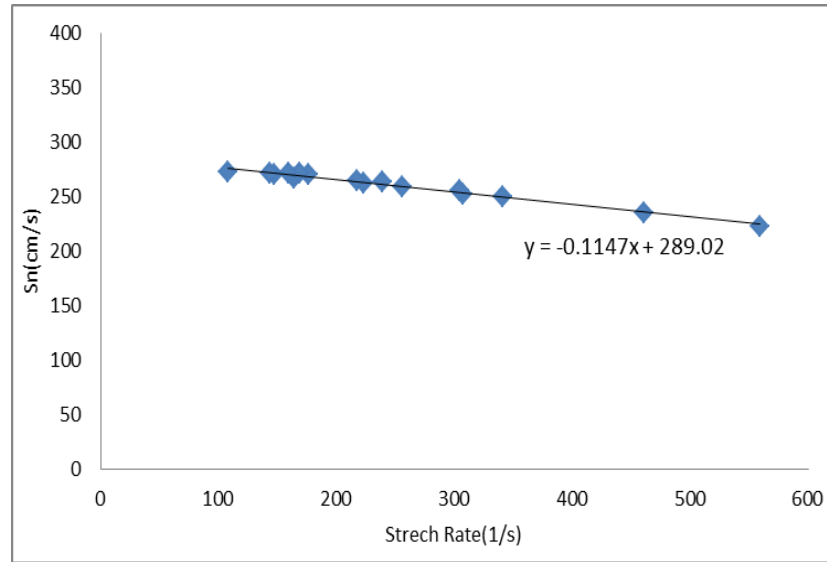


Figure 4.13- S_n stoichiometric CH_4/air values against at $T_i = 303 \pm 3$ K and $P_i = 0.1$ MPa with a linear relationship (Eq. 3.34).

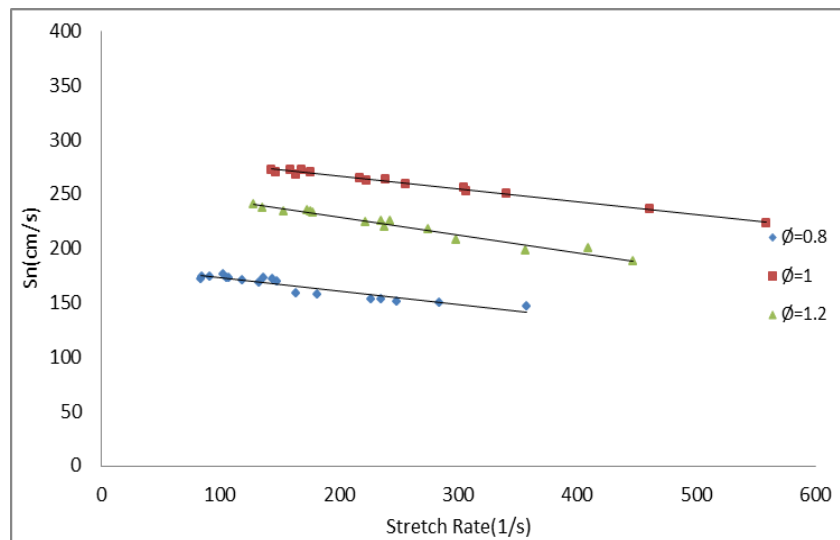


Figure 4.14- Stretched flame speed vs. stretch rate for methane at $T_i = \pm 303$ K and $P_i = 0.1$ MPa for various equivalence ratios.

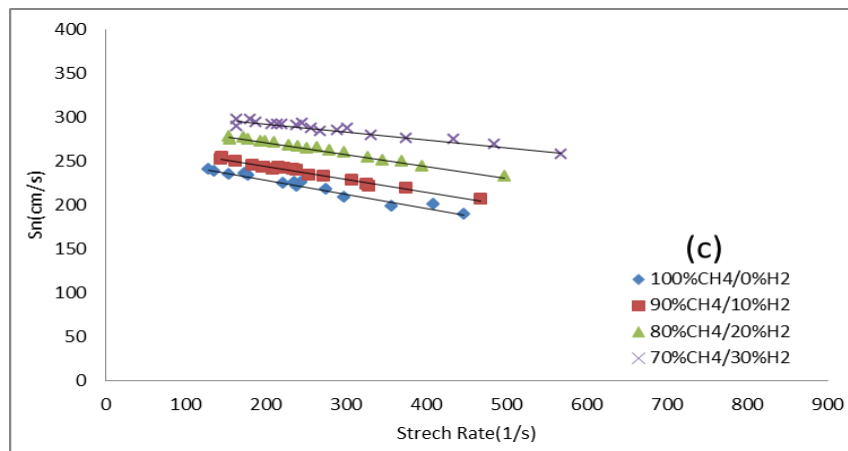
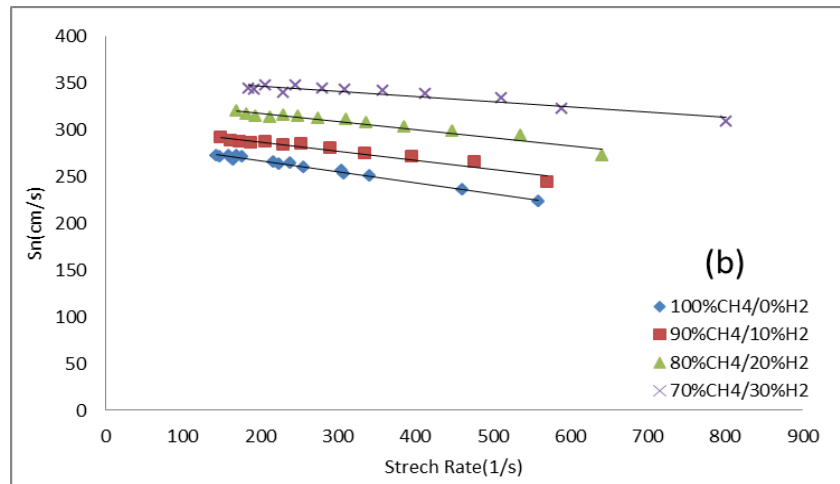
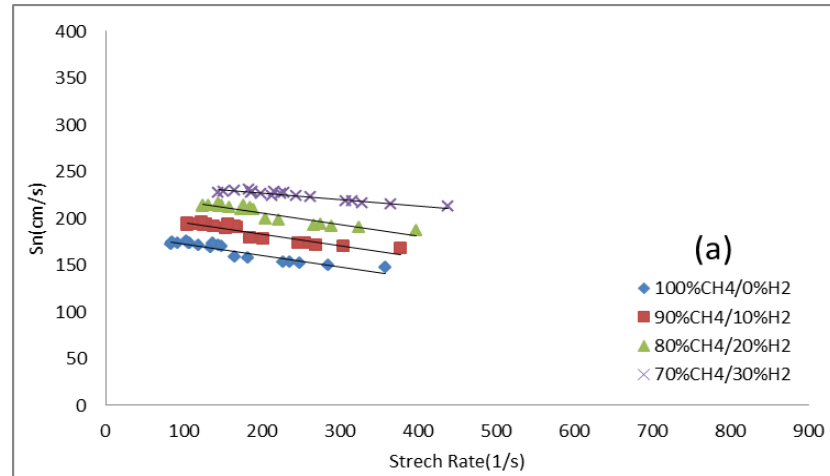


Figure 4.15- Stretched flame speed vs. stretch rate for methane at $T_i = 303 \pm 3$ K and

$P_i = 0.1$ MPa for various equivalence ratios: (a) $\phi = 0.8$ (b) $\phi = 1$ (c) $\phi = 1.2$.

4.4.5.1 Influence of Stoichiometry

The flame stretched rate versus stretched flame speed for methane/air mixtures at different stoichiometries for various hydrogen blends is shown in figures (4.12-4.14). The stretched flame propagation rates rise as the stretch rate increases for any stoichiometry, and the gradients of S_n -lines. In a stoichiometric mixture, S_l reaches its maximum value. This is because all of the reactance is completely burned, resulting in a higher adiabatic temperature. This affects the density ratio between reactance and products, causing the stoichiometric speed to be the maximum.

The unstretched flame propagation speed with equivalency ratio for different hydrogen mixtures is shown in Figure (4.16). The graph of S_l versus equivalency ratio for all hydrogen, mixes follow a similar trend, with the highest value of the equivalence ratio of (1.0). The unstretched flame propagation speed for the lean mixture increases as the equivalence ratio rises. The ratio in the rich mixture side drops as the equivalence ratio increases and the adiabatic temperature of the mixture decreases.

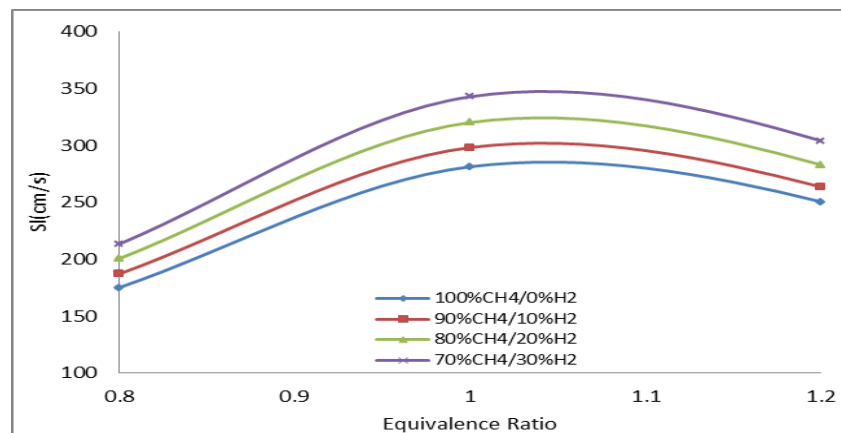


Figure 4.16- Unstretched flame propagation speed versus equivalence ratios for methane/hydrogen/air mixtures at an initial pressure of 0.1MPa at different H_2 blends.

4.4.5.2 Influence of hydrogen blending ratio

The stretched rate vs. stretched flame speed for methane/hydrogen blends at atmospheric pressure with various hydrogen blends versus equivalency ratios is shown in figure (4.15). The findings showed that when the hydrogen mixture increased, the stretch rate also increased, leading to greater stretched flame propagation speeds.

Figure (4.17) shows how the unstretched flame propagation speed increases as the hydrogen mixtures increase from 0% to 30% for both the lean and rich flames. The maximum unstretched flame propagation speed was the stoichiometric mixtures. Due to the influence of adiabatic temperature for hydrogen, S_l for a rich mixture is higher than S_l for a lean mixture for a given hydrogen blend. S_n increases as the hydrogen mixtures increase, implying that flame propagation is proportional to the stretch effect. Furthermore, the amount of S_l rises considerably when the hydrogen mix rises.

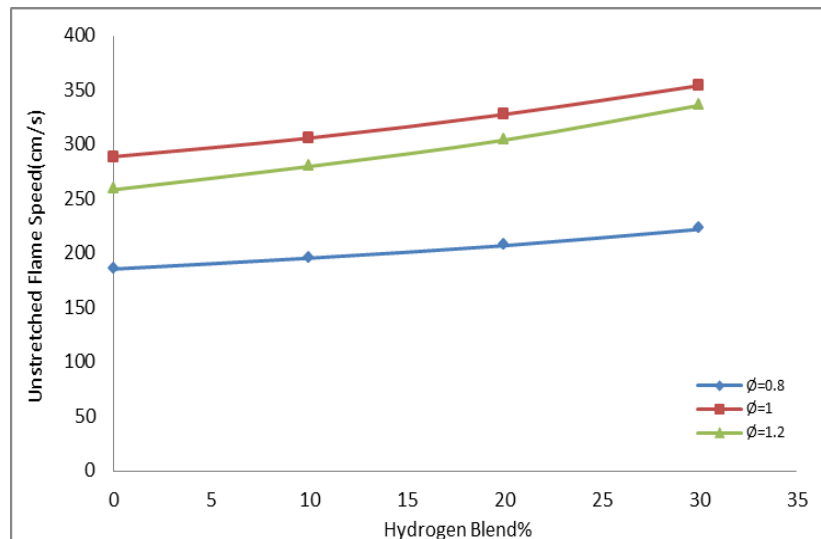


Figure 4.17- Flame propagation speed vs. hydrogen blend for different equivalence ratios at $T_i = 303 \pm 3$ K and $P_i = 0.1$ MPa.

4.4.6 Laminar Burning Velocity

It was necessary to first achieve values of adiabatic density ratio for the complete dataset to convert the optically observed unstretched flame speed to a comparable value of S_u . In CHEMKIN-PRO, these were derived using the GRI-Mech 3.0, reaction mechanism. GRI-Mech 3.0 has 325 reactions and 53 chemical species, and it has been utilized in many of the investigations benchmarked for experimental comparability. The model's oxidiser was a straightforward 79/21-N₂/oxygen air mixture.

It is the most basic Physico-chemical data used to evaluate the flame propagation process, and it contains data on the fuel's reactivity, exothermicity, and diffusivity. The LBV is also utilized to verify chemical kinetic pathways, as well as to estimate turbulent burning velocities and perform flame structure analysis. It is determined by the combustible mixture's initial temperature and pressure, as well as the fuel type and equivalence ratio.

The LBV is tightly related to thermal, diffusive, and kinetic parameters, according to Yasiry and Shahad [12]. The adiabatic temperature (T_{ad}) is used to indicate the contribution of the thermal effect, while thermal diffusivity is used to represent the diffusion effect. Laminar flame speed improvement is favoured by a higher adiabatic temperature and high diffusion. Furthermore, the kinetic effect is thought to play a key role in the change of LBV.

Figure (4.18) shows the S_u versus hydrogen fraction in fuel mixtures at equivalence ratios (0.8, 1.0, and 1.2) and atmospheric pressure. They have the same

trend due to hydrogen addition. This indicates that large linear effects exist in chemical kinetics, as evidenced by the measurements of unstretched laminar burning velocity at all equivalence ratios with various blends, as shown in Figure (4.22).

The hybrid flame propagation can be determined based on the hydrogen mole percentage in the fuel blends. It is the methane-dominated combustion regime when the hydrogen percentage is less than 60%. With the addition of hydrogen, a linear and/or slight rise in LBV is shown. This behaviour has been discovered previously [111,106].

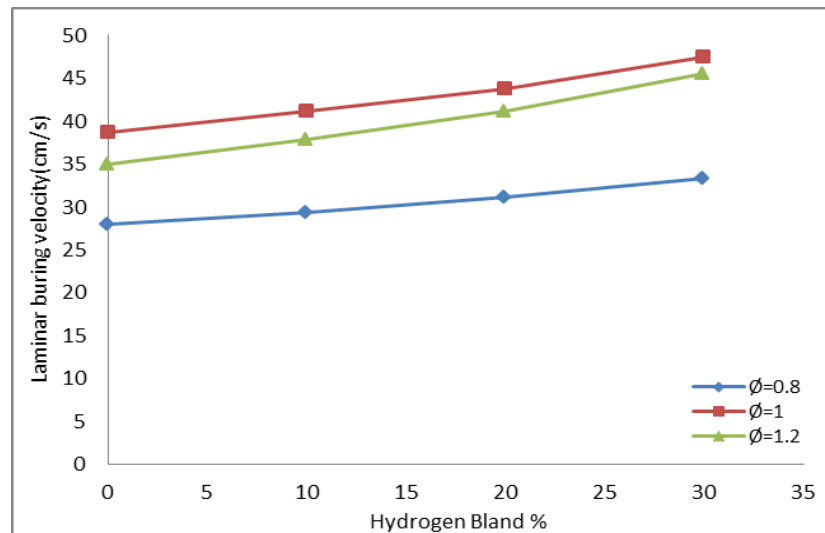


Figure 4.18- Burning velocity vs. hydrogen fraction at various equivalency ratios, $T_i=303\pm 3$ K and $P_i=0.1$ MPa.

4.4.6.1 Influence of Stoichiometry

The LBV versus equivalency ratio for various hydrogen blends is shown in Figure (4.19) at atmospheric pressure. The adiabatic flame temperature and density ratio determine the burning velocity according to equation (3.4). These considerations cause the burning velocity to increase on the lean side when the flame speed increases despite

the increasing adiabatic flame temperature. Because of the dip in adiabatic flame temperature on the rich side, the flame speed will slow down. It can be shown that when the equivalence ratio on the weak side of the mixture grows, the burning velocity increases until it reaches its maximum value at roughly an equivalence ratio of (1.1). Following that, when the equivalency ratio for the hydrogen blend increases, it starts to drop on the rich side of the combination. These graphs indicate that the sites of maximum burning velocity and maximum flame temperature are not always the same. Other factors that influence flame speed include diffusivity, specific heat, and chemical structure [88].

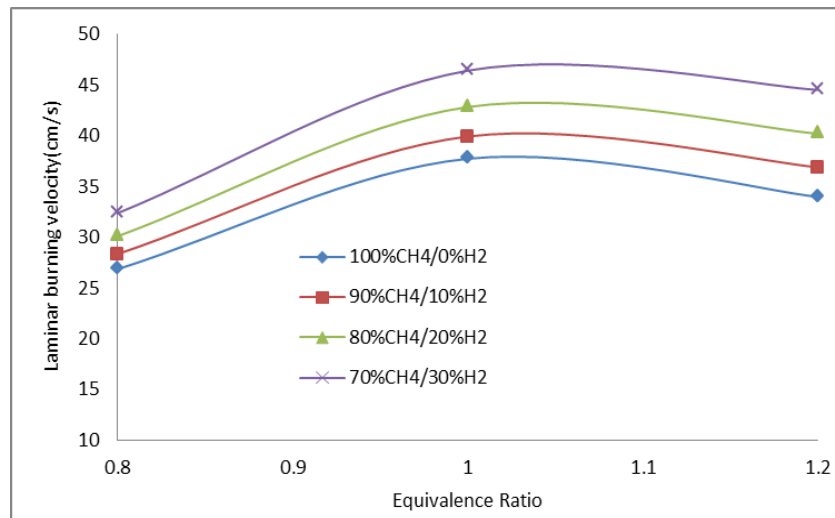


Figure 4.19- Equivalence Ratio vs. LBV for Different Hydrogen Blends at $T_i = 303 \pm 3$ K and $P_i = 0.1$ MPa.

4.4.6.2 Influence of hydrogen blending ratio

The LBV of methane increases as hydrogen addition increases, as shown in figures (4.21-4.22). In addition, as the hydrogen content rises, so does the increase in

LBV. Under the stoichiometric condition, the LBV of 70 % methane and 30 % hydrogen is (46.3 cm/s), which is significantly lower than the LBV of pure hydrogen (220 cm/s)[110]. Methane is the dominant gas in hydrocarbon mixtures containing 10 per cent to 30 per cent hydrogen. The 30% methane in the fuel mixture, on the other hand, decreases the LBV of hydrogen to less than a quarter of that of pure hydrogen. This trend suggests that even a small proportion of methane has a significant decelerating effect on the LBV of the hydrogen combination. Zhou et al. [82], and Moccia et al. [111] also showed similar effects of other syngas on methane.

The rise in hydrogen content in fuel mixtures increases diffusional-thermal instability, while hydrodynamic instability is unaffected. The adiabatic flame temperature is not the most important influencing factor for mixes with varying hydrogen fractions, but the high thermal diffusivity of hydrogen increases the LBV. With rising hydrogen content and an equivalency ratio, The LBVs increase (0.8-1.0). This is mostly owing to hydrogen strong reactivity, which results in a high rate of H and OH radical generation.

4.5 Simulation of Laminar Burning Velocity

In this study, CHEMKIN-PRO of ANSYS is used to model the adiabatic LBV of methane/syngas/air mixture at various initial pressures (0.1,0.15, and 0.2MPa), initial temperatures of $303\pm 3k$, and equivalency ratios from (0.8-1.2). CHEMKIN is a powerful software application for modelling and solving complex chemical reactions. It's commonly used to model combustion, catalysis, chemical vapour deposition,

plasma, and other chemical reactions. The three main software programs that makeup CHEMKIN are gas phase kinetics, surface kinetics, and transfer processes.

The 0 and 1-dimensional combustion models are utilized in this part to further investigate the methane laminar combustion process. Among the output data are adiabatic temperature, LBV, molar distribution of many key radicals, flow rate sensitivity of intermediary reactions, and reaction routes. The experimental LBV achieved in the current study was used to validate the simulation results. For determining the LBV, adiabatic flame temperatures, and the density ratios of alcohol fuels and GRI 3.0 for methane/syngas/air mixes were employed in the numerical section.

4.5.1 Comparison of Laminar Burning Velocity

The statistics show that GRI 3.0 can successfully depict the changing trend of many laminar combustion parameters under various operating situations, but it cannot precisely anticipate the result data.

The LBV relative equivalence ratio for methane with various mechanisms (experimental and numerical) at $303\pm 3\text{k}$ and 0.1MPa initial pressure and published studies, as shown in Figure (4.1).

4.5.2 Adiabatic flame temperature for different Syngas Blends

The data suggest that increasing the hydrogen concentration from 0 to 30% improved S_u . The S_u grew at a faster rate as hydrogen content increased. The high-calorie value of the mixed gas rises as the hydrogen concentration rises. Figure (4.20) shows the temperature of the adiabatic flame as a function of hydrogen concentration.

The adiabatic flame temperature is calculated using the equilibrium gas model and the GRI 3.0 full thermal data. The rise in hydrogen concentration increased the adiabatic flame temperature because hydrogen increased the combustion heat release. Through reactions, raising hydrogen increased the H and OH radicals, speeding up the combustion rate.

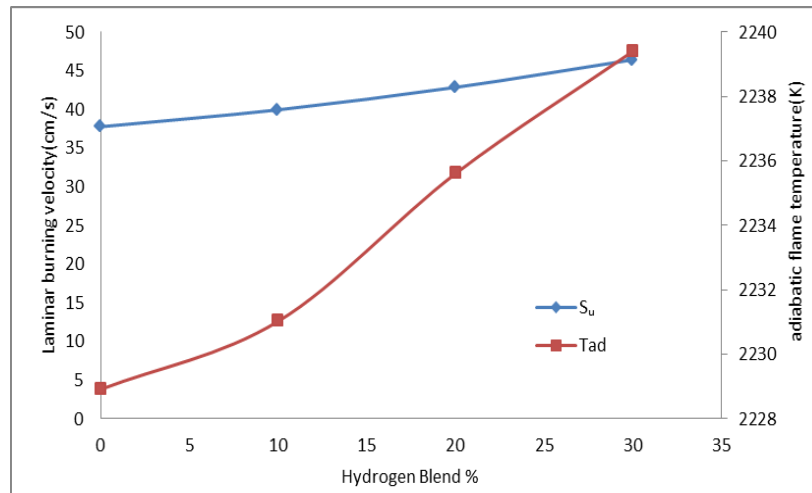


Figure 4.20- S_u versus H_2 concentrations and adiabatic flame temperature at $\phi=1$, $T_i=303\pm 3\text{K}$ and $P_i = 0.1\text{MPa}$.

The effects of carbon dioxide concentrations on S_u are shown in Figure (4.21). The laminar flame speed slows as carbon dioxide concentrations rise. This is because carbon dioxide is a non-combustible gas. First, when the carbon dioxide percentage rises, the amount of CH_4 drops, lowering the total heat released by the blended gas. Second, the diluting influence of carbon dioxide minimizes the chance of free radicals colliding. Third, the thermal property of the increased carbon dioxide resulted in a lower adiabatic flame temperature. As a result, the flame temperature of the carbon dioxide -dilution gas blend is lower. The carbon dioxide decreases the likelihood of

active molecules colliding. As a result of the aforementioned factors, the carbon dioxide reduce of S_u .

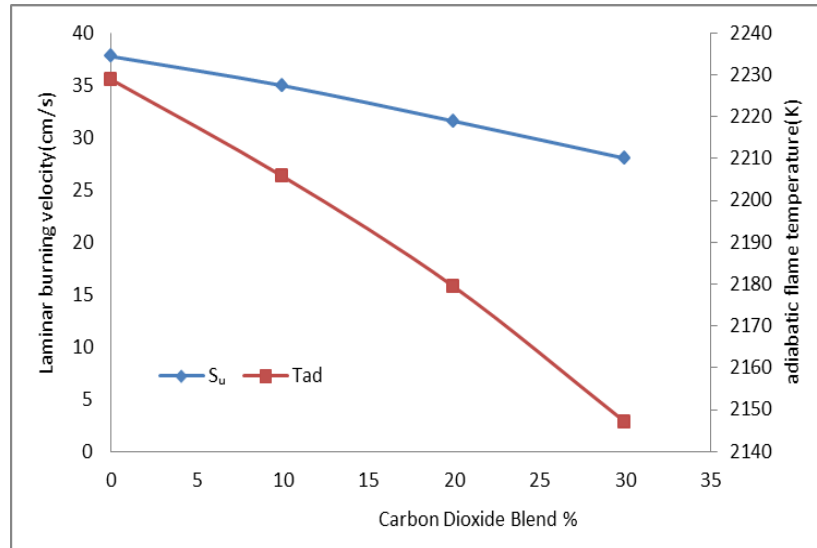


Figure 4.21- S_n versus CO_2 concentrations and adiabatic flame temperature at $\phi=1$, $T_i=303\pm 3k$ and P_i 0.1MPa.

4.5.3 Influence of initial Pressure

The LBV vs. equivalency ratio for all types of blends (CH_4/H_2 , CH_4/CO_2) at varied beginning pressures is shown in figures (4.22-4.23). The results show that as the initial pressure is increased, the LBV falls for all fuel types and stoichiometry, which is qualitatively consistent with previously observed behaviour [104]. This is due to the fuel mixture's thermal diffusivity decreasing as the starting pressure rises [82]. It was also discovered that when the pressure rises, the rate of S_u decreases, as illustrated in figures (4.24-4.25), which show the LBV against the added hydrogen or carbon dioxide to methane for various initial pressure types.

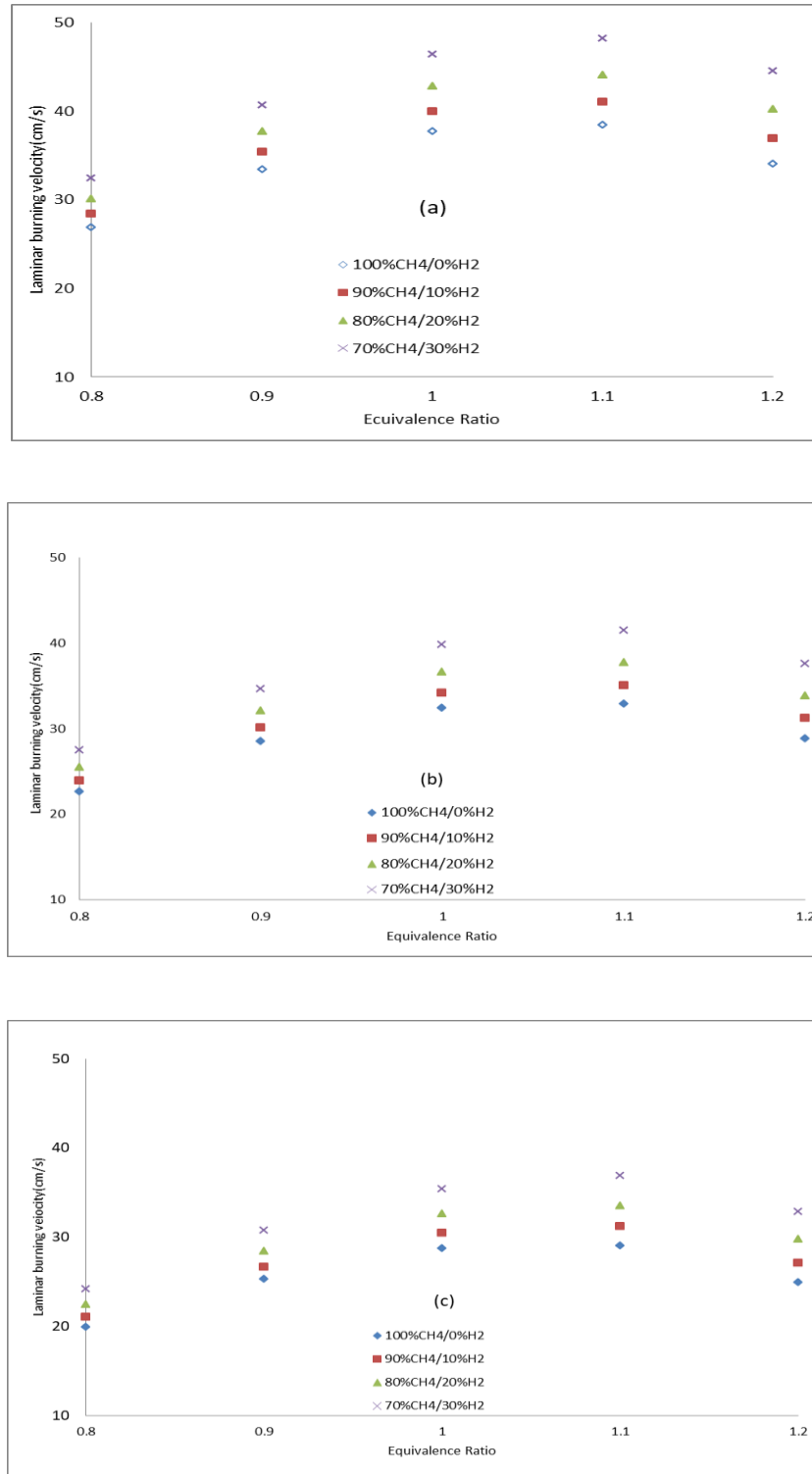


Figure 4.22- S_u versus equivalence ratio concentrations at $303\pm 3k$ and (a) $P_i = 0.1MPa$, (b) $P_i = 0.15MPa$ and (c) $P_i = 0.2MPa$.

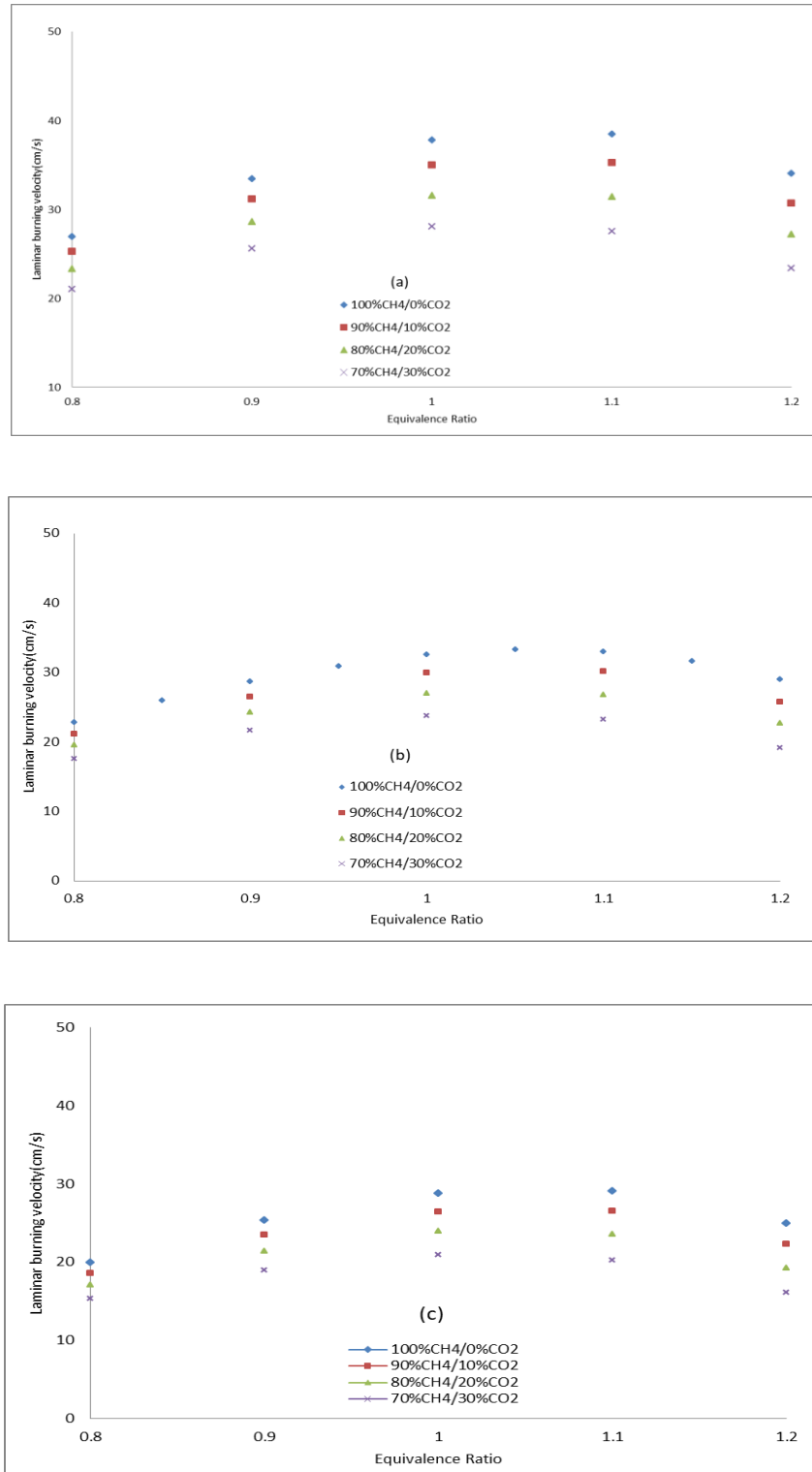


Figure 4.23- S_u versus equivalence ratio concentrations at 303 ± 3 K and (a) $P_i = 0.1$ MPa, (b) $P_i = 0.15$ MPa and (c) $P_i = 0.2$ MPa.

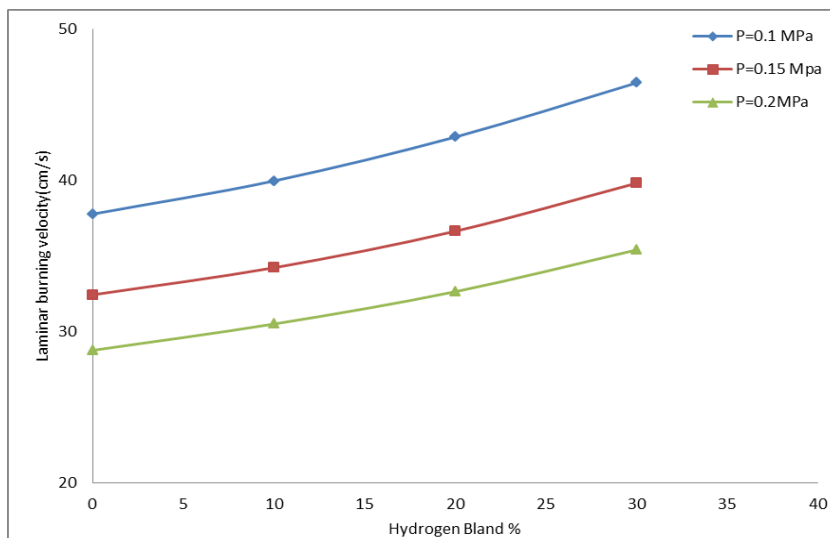


Figure 4.24- LBV vs. Hydrogen Blend at Stoichiometric Mixture for Different Initial Pressures.

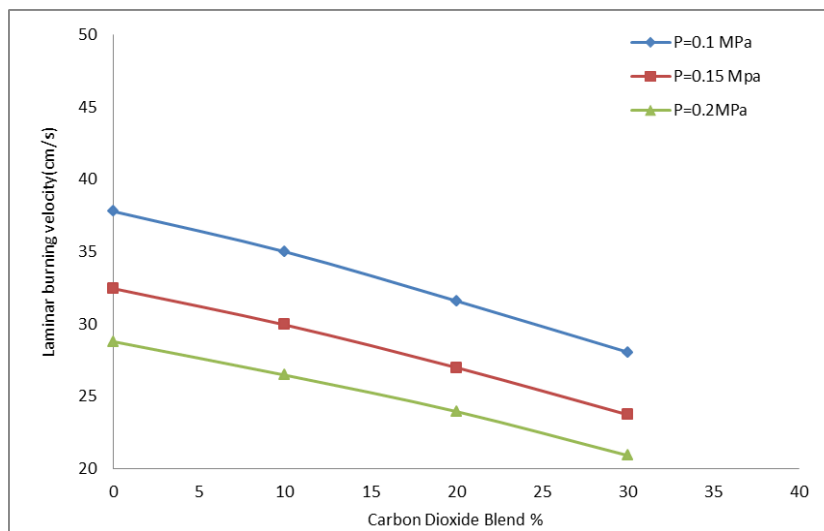


Figure 4.25- LBV vs. Carbon dioxide Blend at Stoichiometric Mixture for Different Initial Pressures.

4.6 Correlation of Laminar Burning Velocity

Based on the experimental results of the current study, the hydrogen blends and equivalency ratios are related to the laminar burning velocities for the binary fuel/air combination is correlated by the mixing rule of Le Chatelier [118]:

$$S_{u, blend}(\phi) = \frac{1}{\sum_{j=1}^n \frac{x_j}{S_{u,j}(\phi)}} \quad \dots(4.3)$$

Where $S_{u,j}$ is the reference laminar burning velocity as stated, which is determined by fitting data to the second-order polynomial function represented in the following equation.

$$S_{u,j} = A + B\phi + C\phi^2 \quad \dots (4.4)$$

Where A, B, and C are constants has been obtained experimentally. The reference temperature and reference pressure for this study was set at 303 ± 3 K and 0.1 Mpa, respectively. Laminar burning velocities for methane are referenced by the formulae below: -

$$S_{u, methane} = -176.56 + 413.58\phi - 198.74\phi^2 \quad \dots (4.5)$$

$$S_{u, hydrogen} = 49.0123 + 287.25\phi - 120.28\phi^2 \quad \dots(4.6)$$

Laminar burning velocities increase exponentially with the increase of hydrogen blends and they increase in lean mixtures while decreasing with the rich mixtures.

Chapter Five
Conclusion
And
Suggestions

CHAPTER FIVE**CONCLUSIONS AND SUGGESTIONS****5.1 Conclusions**

In particular, the methane/syngas/air combinations are the focus of this thesis's discussion of numerical models for estimating burning velocities. Experiments were carried out to investigate the LBV of methane at different hydrogen blends (10%, 20%, and 30%) at a temperature of 303 ± 3 K and an initial pressure of 0.1 MPa. The numerical model for premixed combustion heavily depends on thermal diffusivity and chemical time scale depending on fuel concentration, initial temperature, and initial pressure, among other factors, in predicting laminar burning velocity. The following conclusions have been obtained from the current study's findings:

- 1- The equivalence ratio has an eminent impact on the LBV of the methane/air mixture and methane /syngas/air mixture.
- 2-The numerical method was used to find the LBV for methane/syngas/air mixtures at initial pressures of 0.1, 0.15, and 0.2 MPa and concentrations from 0 to 30%.
- 3- The flame propagation speed increases progressively as the spherical flame radius grows at the conditions studied.
- 4- For all equivalence ratios, adding hydrogen to a methane flame accelerates the LBV. While adding carbon dioxide to methane flame decreases the LBV.
- 5-The highest value of LBV is at the minimum initial pressure, and the LBV falls as the initial pressure rises.

6- The highest un-stretched flame speed and LBV for methane/syngas mixes occurred at stoichiometric ratios.

7-The mechanism GRI 3.0 used in CHEMKIN software give corresponding results of LBV for methane/syngas/air under the experimental test at the same conditions.

8-The addition of hydrogen raises the adiabatic flame temperature and thermal diffusivity of reacting mixtures while decreasing the flame thickness.

9-An empirical correlation describing the influence of equivalency ratio and blending ratio on LBV has been obtained for the methane/air mixture, which agrees well with experimental results.

10- Finally, it is concluded that hydrogen must be added by more than 30% of methane/air mixture volume to exceed the negative effect of doubling the initial pressure and quite the opposite when adding carbon dioxide.

5.2 Suggestions for Future Work

The following recommendations are suggested for future works:

1- The experimental apparatus can be used to investigate the LBV of other types of gaseous and liquid fuels in the future.

2- The development of experimenting with the influence of multi-ignitions upon flame structures by installing multi-ignition devices at various positions inside the CVC and adjusting the time of each spark and the period between them.

3- Expansion of the theoretical portion to simulate the LBV of mixed fuels at various conditions by the CHEMKIN program.

4- Replace the schlieren photography technique with Z-type schlieren photography to improve the capturing mechanism.

5-Increase the diameter of the bomb's glass window to identify cellularity.

REFERENCE

- [1] D. Mishra. (2014). Experimental combustion: an introduction. Crc Press.
- [2] Turner, M. A., Paschal, T. T., Parajuli, P., Kulatilaka, W. D., & Petersen, E. L. (2021). Resolving flame thickness using high-speed chemiluminescence imaging of OH* and CH* in spherically expanding methane–air flames. *Proceedings of the Combustion Institute*, 38(2), 2101–2108. <https://doi.org/10.1016/j.proci.2020.07.112>
- [3] Poinso, T. and Veynante, D. (2005). Theoretical and numerical combustion. Edwards. Philadelphia.
- [4] Glassman, I. & Yetter, R. A. (2008). *Combustion*, Fourth edi. Printed in the United States of America.
- [5] Beeckmann, J., Hesse, R., Schaback, J., Pitsch, H., Varea, E., & Chaumeix, N. (2019). Flame propagation speed and Markstein length of spherically expanding flames: Assessment of extrapolation and measurement techniques. *Proceedings of the Combustion Institute*, 37(2), 1521–1528. <https://doi.org/10.1016/j.proci.2018.08.047>
- [6] Fayad, M. A., & Dhahad, H. A. (2021). Effects of adding aluminum oxide nanoparticles to butanol-diesel blends on performance, particulate matter, and emission characteristics of diesel engine. *Fuel*, 286. <https://doi.org/10.1016/j.fuel.2020.119363>
- [7] Arafin, F., & Belmont, E. (2018). Combustion Flame Speeds and Stability of Associated Natural Gas with High Concentrations of C2-C4 Alkanes. *Energy and Fuels*, 32(11), 11821–11830. <https://doi.org/10.1021/acs.energyfuels.8b01739>
- [8] Turns, S. R. (1996). *An Introduction to Combustion Concepts and Applications*. McGraw-Hill, Inc.
- [9] Fayad, M. A., & Dhahad, H. A. (2021). Effects of adding aluminum oxide nanoparticles to butanol-diesel blends on performance, particulate matter, and emission characteristics of diesel engine. *Fuel*, 286. <https://doi.org/10.1016/j.fuel.2020.119363>
- [10] Liu, Y., & Ma, L. (2016). Impacts of low oil price on China and the world natural gas industry chain. *Natural Gas Industry B*, 3(5), 493–503. <https://doi.org/10.1016/j.ngib.2017.02.010>
- [11] Percheron, G., Brechignac, F., Soucaille, P. et al. Carbon dioxide desorption from fermentation broth by use of oxygen vectors. *Bioprocess Engineering* **12**, 11–16 (1995). <https://doi.org/10.1007/BF01112987>

- [12] Yasiry, A. S., & Shahad, H. A. K. (2016). An experimental study of the effect of hydrogen blending on burning velocity of LPG at elevated pressure. *International Journal of Hydrogen Energy*, 41(42), 19269–19277. <https://doi.org/10.1016/j.ijhydene.2016.08.097>
- [13] Law, C.K. (2006). *Combustion Physics*. 1st ed. Cambridge University Press.
- [14] Abdulraheem, A. A., Saleh, A. M., & Shahad, H. A. (2021). Measurements and Data Analysis Review of Laminar Burning Velocity and Flame Speed for Biofuel/Air Mixtures. *IOP Conference Series: Materials Science and Engineering*, 1094(1), 012029. <https://doi.org/10.1088/1757-899x/1094/1/012029>
- [15] Sun, C. J., Sung, C. J., He, L., & Law, C. K. (1999). *Dynamics of Weakly Stretched Flames: Quantitative Description and Extraction of Global Flame Parameters*.
- [16] Bunkute, B. (2008). *Burning Velocities of Coal-derived Syngas Mixtures*. Thesis, Cranfield University.
- [17] Swart, d. (2004). *The combined effect of flame stretch and preferential diffusion on the mass burning rate of premixed laminar flames*, Thesis, Eindhoven University of Technology.
- [18] Farhat, A., Kumar, R. E. V., & Samimi-Abianeh, O. (2020). Laminar Burning Velocity Measurement Using the Filtered Broadband Natural Emissions of Species. *Energy and Fuels*, 34(3), 3772–3779. <https://doi.org/10.1021/acs.energyfuels.9b04291>
- [19] Salah, A. M. (2006). *Effect of Pressure upon Laminar Burning Velocity of Paraffinis Gaseous Fuel in Closed Vessel*. Unpublished Ph.D. Thesis, Department of Machines and Equipment - University of Technology, Baghdad.
- [20] Chang, X., Zhang, B., Ng, H. D., & Bai, C. (2020). The effects of pre-ignition turbulence by gas jets on the explosion behavior of methane-oxygen mixtures. *Fuel*, 277. <https://doi.org/10.1016/j.fuel.2020.118190>
- [21] Hagos, F. Y., Rashid, A., Aziz, A., & Sulaiman, S. A. (2013). Study of syngas combustion parameters effect on internal combustion engine. *Asian Journal of Scientific Research*, 6(2), 187–196. <https://doi.org/10.3923/ajsr.2013.187.196>
- [22] Andrade, R. V., Cortabarría Castañeda, L. A., Yepes Maya, D. M., Pedroso Cesar Corrêa Junior, P. S., Mello e Pinto, L. R., Silva Lora, E. E., Vilas Bôas de Sales Oliveira, C. A., & Pinto, B. A. (2020). Assessment of laminar flame velocity of producer gas from biomass gasification using the Bunsen burner method. *International*

Journal of Hydrogen Energy, 45(20), 11559–11568.

<https://doi.org/10.1016/j.ijhydene.2020.02.082>

[23] Wu, S., Lv, Z., Ding, K., Huang, W., Li, G., Hou, Z., Ni, J., Ke, Y., & Huang, H. (2020). The Analyses of 45-Degree Bunsen Burner Test and Oil Burner Test for Cargo Liners. *Journal of Physics: Conference Series*, 1549(4). <https://doi.org/10.1088/1742-6596/1549/4/042066>

[24] Rocha, R. C., Zhong, S., Xu, L., Bai, X. S., Costa, M., Cai, X., Kim, H., Brackmann, C., Li, Z., & Aldein, M. (2021). Structure and laminar flame speed of an ammonia/methane/air premixed flame under varying pressure and equivalence ratio. *Energy and Fuels*, 35(9), 7179–7192. <https://doi.org/10.1021/acs.energyfuels.0c03520>

[25] Lewis, B., & von Elbe, G. (1943). Stability and structure of burner flames. *The Journal of Chemical Physics*, 11(2), 75–93. <https://doi.org/10.1063/1.1723808>

[26] Andrews, G. E., & Bradley, D. (1972). Determination of Burning Velocities: A Critical Review'. In *COMBUSTION AND FLAME* (Vol. 18).

[27] Chung, K. L. (2006). *Combustion physics*. Cambridge University Press, UK: United States of America by Cambridge University Press, New York.

[28] Sileghem, L., Alekseev, V. A., Vancoillie, J., van Geem, K. M., Nilsson, E. J. K., Verhelst, S., & Konnov, A. A. (2013). Laminar burning velocity of gasoline and the gasoline surrogate components iso-octane, n-heptane and toluene. *Fuel*, 112, 355–365. <https://doi.org/10.1016/j.fuel.2013.05.049>

[29] Goswami, M., Bastiaans, R. J. M., Konnov, A. A., & de Goey, L. P. H. (2014). Laminar burning velocity of lean H₂-CO mixtures at elevated pressure using the heat flux method. *International Journal of Hydrogen Energy*, 39(3), 1485–1498. <https://doi.org/10.1016/j.ijhydene.2013.10.164>

[30] Chan, Y. L., Zhu, M. M., Zhang, Z. Z., Liu, P. F., & Zhang, D. K. (2015). The Effect of CO₂ Dilution on the Laminar Burning Velocity of Premixed Methane/Air Flames. *Energy Procedia*, 75, 3048–3053. <https://doi.org/10.1016/j.egypro.2015.07.621>

[31] Walter, G., Wang, H., Kanz, A., Kolbasseff, A., Xu, X., Haidn, O., & Slavinskaya, N. (2020). Experimental error assessment of laminar flame speed measurements for digital chemical kinetics databases. *Fuel*, 266. <https://doi.org/10.1016/j.fuel.2020.117012>

[32] Akram, M., Kishore, V. R., & Kumar, S. (2012). Laminar burning velocity of propane/CO₂/N₂-air mixtures at elevated temperatures. *Energy and Fuels*, 26(9), 5509–5518. <https://doi.org/10.1021/ef301000k>

- [33] Katoch, A., Millán-Merino, A., & Kumar, S. (2018). Measurement of laminar burning velocity of ethanol-air mixtures at elevated temperatures. *Fuel*, 231, 37–44. <https://doi.org/10.1016/j.fuel.2018.05.083>
- [34] Akram, M., & Kumar, S. (2011). Experimental studies on dynamics of methane-air premixed flame in meso-scale diverging channels. *Combustion and Flame*, 158(5), 915–924. <https://doi.org/10.1016/j.combustflame.2011.02.011>
- [35] Konnov, A. A., Mohammad, A., Kishore, V. R., Kim, N. il, Prathap, C., & Kumar, S. (2018). A comprehensive review of measurements and data analysis of laminar burning velocities for various fuel+air mixtures. In *Progress in Energy and Combustion Science* (Vol. 68, pp. 197–267). Elsevier Ltd. <https://doi.org/10.1016/j.pecs.2018.05.003>
- [36] Liu, Z., & Kim, N. il. (2014). An assembled annular stepwise diverging tube for the measurement of laminar burning velocity and quenching distance. *Combustion and Flame*, 161(6), 1499–1506. <https://doi.org/10.1016/j.combustflame.2013.11.020>
- [37] Jung, Y., Lee, M. J., & Kim, N. il. (2016). Direct prediction of laminar burning velocity and quenching distance of hydrogen-air flames using an annular stepwise diverging tube (ASDT). *Combustion and Flame*, 164, 397–399. <https://doi.org/10.1016/j.combustflame.2015.12.005>
- [38] Benim, A. C., & Pfeiffelmann, B. (2019). Prediction of burning velocity and quenching distance of hydrogen flames. *E3S Web of Conferences*, 128. <https://doi.org/10.1051/e3sconf/201912801012>
- [39] Simmons, R. F., & Wolfhard, H. G. (1957). Some Limiting Oxygen Concentrations for Diffusion Flames in Air Diluted with Nitrogen.
- [40] Wu, C. K., & Law, C. K. (1984). ON THE DETERMINATION OF LAMINAR FLAME SPEEDS FROM STRETCHED FLAMES.
- [41] SPALDING, D. B. (1961). Theory of Mixing and Chemical Reaction in the Opposed-Jet Diffusion Flame. *ARS Journal*, 31(6), 763–771. <https://doi.org/10.2514/8.5626>
- [42] Egolfopoulos, F. N., Cho, P., & Law, C. K. (1989). Laminar Flame Speeds of Methane-Air Mixtures Under Reduced and Elevated Pressures. In *COMBUSTION AND FLAME* (Vol. 76).
- [43] Egolfopoulos, F. N., Hansen, N., Ju, Y., Kohse-Höinghaus, K., Law, C. K., & Qi, F. (2014). Advances and challenges in laminar flame experiments and implications for

combustion chemistry. In *Progress in Energy and Combustion Science* (Vol. 43, pp. 36–67). Elsevier Ltd. <https://doi.org/10.1016/j.pecs.2014.04.004>

[44] Safer, M., Tabet, F., Ouadha, A., & Safer, K. (2015). A numerical investigation of structure and emissions of oxygen-enriched syngas flame in counter-flow configuration. *International Journal of Hydrogen Energy*, 40(6), 2890–2898. <https://doi.org/10.1016/j.ijhydene.2014.12.117>

[45] Xu, W., Jiang, Y., Qiu, R., & Ren, X. (2017). Influence of halon replacements on laminar flame speeds and extinction limits of hydrocarbon flames. *Combustion and Flame*, 182, 1–13. <https://doi.org/10.1016/j.combustflame.2017.03.029>

[46] Kopp, M., Coleman, D., Stiller, C., Scheffer, K., Aichinger, J., & Scheppat, B. (2017). Energiepark Mainz: Technical and economic analysis of the worldwide largest Power-to-Gas plant with PEM electrolysis. *International Journal of Hydrogen Energy*, 42(19), 13311–13320. <https://doi.org/10.1016/j.ijhydene.2016.12.145>

[47] Almarcha, C., Denet, B., & Quinard, J. (2015). Premixed flames propagating freely in tubes. *Combustion and Flame*, 162(4), 1225–1233. <https://doi.org/10.1016/j.combustflame.2014.10.010>

[48] Fig, M. K., Bogin, G. E., Brune, J. F., & Grubb, J. W. (2016). Experimental and numerical investigation of methane ignition and flame propagation in cylindrical tubes ranging from 5 to 71 cm - Part I: Effects of scaling from laboratory to large-scale field studies. *Journal of Loss Prevention in the Process Industries*, 41, 241–251. <https://doi.org/10.1016/j.jlp.2016.03.018>

[49] Sikes, T., Mathieu, O., Kulatilaka, W. D., Mannan, M. S., & Petersen, E. L. (2019). Laminar flame speeds of DEMP, DMMP, and TEP added to H₂ - and CH₄ -air mixtures. *Proceedings of the Combustion Institute*, 37(3), 3775–3781. <https://doi.org/10.1016/j.proci.2018.05.042>

[50] Reyes, M., Tinaut, F. v., Horrillo, A., & Lafuente, A. (2018). Experimental characterization of burning velocities of premixed methane-air and hydrogen-air mixtures in a constant volume combustion bomb at moderate pressure and temperature. *Applied Thermal Engineering*, 130, 684–697. <https://doi.org/10.1016/j.applthermaleng.2017.10.165>

[51] Mitu, M., Giurcan, V., Movileanu, C., Razus, D., & Oancea, D. (2021). Propagation of CH₄-N₂O-N₂ flames in a closed spherical vessel. *Processes*, 9(5). <https://doi.org/10.3390/pr9050851>

- [52] Hinton, N., Stone, R., & Cracknell, R. (2018). Laminar burning velocity measurements in constant volume vessels – Reconciliation of flame front imaging and pressure rise methods. *Fuel*, 211, 446–457. <https://doi.org/10.1016/j.fuel.2017.09.031>
- [53] Lewis, B., & von Elbe, G. (1934). Determination of the speed of flames and the temperature distribution in a spherical bomb from time-pressure explosion records. *The Journal of Chemical Physics*, 2(5), 283–290. <https://doi.org/10.1063/1.1749464>
- [54] Zuo, Z., Pei, Y., Qin, J., Xu, H., & Lu, L. (2018). Laminar burning characteristics of premixed methane-dissociated methanol-air mixtures under lean burn conditions. *Applied Thermal Engineering*, 140, 304–312. <https://doi.org/10.1016/j.applthermaleng.2018.05.040>
- [55] Zuo, Z., Pei, Y., Qin, J., Lu, L., & Xu, H. (2018). Impact of dissociated Methanol addition on premixed Toluene reference fuel-air mixtures in a constant-volume chamber. *International Journal of Hydrogen Energy*, 43(13), 6745–6755. <https://doi.org/10.1016/j.ijhydene.2018.02.091>
- [56] Sarathy, S. M., Brequigny, P., Katoch, A., Elbaz, A. M., Roberts, W. L., Dibble, R. W., & Foucher, F. (2020). Laminar Burning Velocities and Kinetic Modeling of a Renewable E-Fuel: Formic Acid and Its Mixtures with H₂ and CO₂. *Energy and Fuels*, 34(6), 7564–7572. <https://doi.org/10.1021/acs.energyfuels.0c00944>
- [57] Han, Z., Zhu, Z., Yu, W., Liang, K., Zuo, Z., Xia, Q., & Zeng, D. (2020). On the equivalent effect of initial temperature and pressure coupling on the flame speed of methane premixed combustion under dilution. *Energy*, 207. <https://doi.org/10.1016/j.energy.2020.118269>
- [58] Shu, T., Xue, Y., Zhou, Z., & Ren, Z. (2021). An experimental study of laminar ammonia/methane/air premixed flames using expanding spherical flames. *Fuel*, 290. <https://doi.org/10.1016/j.fuel.2020.120003>
- [59] Bao, X., Jiang, Y., Xu, H., Wang, C., Lattimore, T., & Tang, L. (2017). Laminar flame characteristics of cyclopentanone at elevated temperatures. *Applied Energy*, 195, 671–680. <https://doi.org/10.1016/j.apenergy.2017.03.031>
- [60] Wei, S., Yu, M., Pei, B., Ma, Z., Li, S., & Kang, Y. (2021). Effect of hydrogen enrichment on the laminar burning characteristics of dimethyl-ether/methane fuel: Experimental and modeling study. *Fuel*, 305. <https://doi.org/10.1016/j.fuel.2021.121475>
- [61] Duva, B. C., Chance, L. E., & Toulson, E. (2020). Dilution effect of different combustion residuals on laminar burning velocities and burned gas Markstein lengths of premixed methane/air mixtures at elevated temperature. *Fuel*, 267. <https://doi.org/10.1016/j.fuel.2020.117153>

- [62] Wang, L. Q., Ma, H. H., & Shen, Z. W. (2020). Explosion characteristics of H₂/N₂O and CH₄/N₂O diluted with N₂. *Fuel*, 260. <https://doi.org/10.1016/j.fuel.2019.116355>
- [63] Yelishala, S. C., Wang, Z., Metghalchi, H., Levendis, Y. A., Kannaiyan, K., & Sadr, R. (2019). Effect of Carbon Dioxide on the Laminar Burning Speed of Propane-Air Mixtures. *Journal of Energy Resources Technology, Transactions of the ASME*, 141(8). <https://doi.org/10.1115/1.4042411>
- [64] Lu, X., Hu, E., Kokjohn, S., Gao, Q., Yin, G., Zeng, K., & Huang, Z. (2020). Experimental and kinetic study of laminar flame characteristics of H₂/O₂/diluent flame under elevated pressure. *International Journal of Hydrogen Energy*, 45(56), 32508–32520. <https://doi.org/10.1016/j.ijhydene.2020.08.142>
- [65] Teknologi, J., Suhaimi, M. S., Saat, A., Wahid, M. A., Sies, M., Malaysia, T., & Bahru, U. J. (2016). FLAME PROPAGATION AND BURNING RATES OF METHANE-AIR MIXTURES USING SCHLIEREN PHOTOGRAPHY (Vol. 78). www.jurnalteknologi.utm.my
- [66] Xu, C., Wang, H., Oppong, F., Li, X., Zhou, K., Zhou, W., Wu, S., & Wang, C. (2020). Determination of laminar burning characteristics of a surrogate for a pyrolysis fuel using constant volume method. *Energy*, 190. <https://doi.org/10.1016/j.energy.2019.116315>
- [67] Kuo, K. (1986). *Principle of combustion*. New York, John Wiley & Sons, Cambridge University Press.
- [68] Saleh, A. M., & AL-Fattal, M. N. (2006). Effect of Initial Pressure Upon Laminar Burning Velocity of Paraffinis Gaseous Fuel in Closed Vessel. Thesis, Department of Machines and Equipment - University of Technology, Baghdad.
- [69] Salih, A. M., & Chaichan, M. T. (2014). The effect of initial pressure and temperature upon the laminar burning velocity and flame stability for propane-air mixtures. In *Global Advanced Research Journal of Engineering, Technology and Innovation* (Vol. 3, Issue 7). <http://garj.org/garjeti/index.htm>
- [70] Okafor, E. C., Naito, Y., Colson, S., Ichikawa, A., Kudo, T., Hayakawa, A., & Kobayashi, H. (2019). Measurement and modelling of the laminar burning velocity of methane-ammonia-air flames at high pressures using a reduced reaction mechanism. *Combustion and Flame*, 204, 162–175. <https://doi.org/10.1016/j.combustflame.2019.03.008>

- [71] Grune, J., Sempert, K., Kuznetsov, M., & Jordan, T. (2021). Experimental investigation of unconfined spherical and cylindrical flame propagation in hydrogen-air mixtures. *International Journal of Hydrogen Energy*, 46(23), 12487–12496. <https://doi.org/10.1016/j.ijhydene.2020.09.062>
- [72] Abdulraheem, A. A. A., Saleh, A. M., & Shahad, H. A. K. (2022). Effect of Propane-Methanol Blending Ratio on the Stretched and Unstretched Flame Speeds at Elevated Initial Temperatures. *FME Transactions*, 50(1), 121–130. <https://doi.org/10.5937/fme2201121A>
- [73] Omari, A., & Tartakovsky, L. (2016). Measurement of the laminar burning velocity using the confined and unconfined spherical flame methods - A comparative analysis. *Combustion and Flame*, 168, 127–137. <https://doi.org/10.1016/j.combustflame.2016.03.012>
- [74] Park, S., Kim, G., Terracciano, A. C., Vasu, S., Allison, T. C., Chang, S., Lim, C., & Jin, Y. (2020). High-pressure ignition and flame propagation measurements of CO₂ diluted natural gas/oxidizer mixtures for advanced rocket and gas turbine combustors. *AIAA Scitech 2020 Forum*, 1 PartF, 1–7. <https://doi.org/10.2514/6.2020-0128>
- [75] Wang, N., Huang, S., Zhang, Z., Li, T., Yi, P., Wu, D., & Chen, G. (2021). Laminar burning characteristics of ammonia/hydrogen/air mixtures with laser ignition. *International Journal of Hydrogen Energy*, 46(62), 31879–31893. <https://doi.org/10.1016/j.ijhydene.2021.07.063>
- [76] Rozenchan, G., Zhu, D. L., Law, C. K., & Tse, S. D. (2002). OUTWARD PROPAGATION, BURNING VELOCITIES, AND CHEMICAL EFFECTS OF METHANE FLAMES UP TO 60 atm. In *Proceedings of the Combustion Institute* (Vol. 29).
- [77] Khan, F., Elbaz, A. M., Saxena, S., Mannaa, O., & Roberts, W. L. (2021). Effect of CO₂ Dilution on Methane/Air Flames at Elevated Pressures: An Experimental and Modeling Study. *Energy and Fuels*, 35(3), 2639–2653. <https://doi.org/10.1021/acs.energyfuels.0c03568>
- [78] Chen, Z. (2015). On the accuracy of laminar flame speeds measured from outwardly propagating spherical flames: Methane/air at normal temperature and pressure. *Combustion and Flame*, 162(6), 2442–2453. <https://doi.org/10.1016/j.combustflame.2015.02.012>
- [79] Christensen, M., Nilsson, E. J. K., & Konnov, A. A. (2015). The temperature dependence of the laminar burning velocities of methyl formate + air flames. *Fuel*, 157, 162–170. <https://doi.org/10.1016/j.fuel.2015.04.072>

- [80] Andrews, G. E., & Bradle, D. (1972). The Burning Velocity of Methane-Air Mixture (Vol. 19).
- [81] Kanoshima, R., Hayakawa, A., Kudo, T., Okafor, E. C., & Colson, S. (2022). Effects of initial mixture temperature and pressure on laminar burning velocity and Markstein length of ammonia/air premixed laminar flames. *Fuel*, 122149. <https://doi.org/10.1016/j.fuel.2021.122149>
- [82] Zhou, Q., Cheung, C. S., Leung, C. W., Li, X., Li, X., & Huang, Z. (2019). Effects of fuel composition and initial pressure on laminar flame speed of H₂/CO/CH₄ bio-syngas. *Fuel*, 238, 149–158. <https://doi.org/10.1016/j.fuel.2018.10.106>
- [83] Okafor, E. C., Naito, Y., Colson, S., Ichikawa, A., Kudo, T., Hayakawa, A., & Kobayashi, H. (2019). Measurement and modelling of the laminar burning velocity of methane-ammonia-air flames at high pressures using a reduced reaction mechanism. *Combustion and Flame*, 204, 162–175. <https://doi.org/10.1016/j.combustflame.2019.03.008>
- [84] Halter, F., Chauveau, C., Djebaili-Chaumeix, N., & Gökalp, I. (2005). Characterization of the effects of pressure and hydrogen concentration on laminar burning velocities of methane-hydrogen-air mixtures. *Proceedings of the Combustion Institute*, 30(1), 201–208. <https://doi.org/10.1016/j.proci.2004.08.195>
- [85] Xuna, L., Xuefeng, L., Guanyu, X., Dong, C., & Cai, D. (n.d.). Investigation of Methane-Air Laminar Flame to Apply in Internal Combustion Engines. <https://hal.archives-ouvertes.fr/hal-01703294v2>
- [86] Hu, E., Huang, Z., He, J., & Miao, H. (2009). Experimental and numerical study on laminar burning velocities and flame instabilities of hydrogen-air mixtures at elevated pressures and temperatures. *International Journal of Hydrogen Energy*, 34(20), 8741–8755. <https://doi.org/10.1016/j.ijhydene.2009.08.044>
- [87] Liu, Y., Wang, J., Gu, W., Ma, H., & Zeng, W. (2021). Effects of CH₄ mixing on the laminar burning velocity and Markstein length of RP-3/air premixed flame. *Fuel*, 289. <https://doi.org/10.1016/j.fuel.2020.119761>
- [88] Baloo, M., Dariani, B. M., Akhlaghi, M., & Aghamirsalim, M. (2016). Effects of pressure and temperature on laminar burning velocity and flame instability of iso-octane/methane fuel blend. *Fuel*, 170, 235–244. <https://doi.org/10.1016/j.fuel.2015.12.039>
- [89] Anggono, W., Hayakawa, A., Okafor, E. C., & Gotama, G. J. (2019). Experimental and numerical investigation of laminar burning velocities of artificial biogas under

various pressure and CO₂ concentration. E3S Web of Conferences, 130.
<https://doi.org/10.1051/e3sconf/201913001037>

[90] Okafor, E. C., Naito, Y., Colson, S., Ichikawa, A., Kudo, T., Hayakawa, A., & Kobayashi, H. (2019). Measurement and modelling of the laminar burning velocity of methane-ammonia-air flames at high pressures using a reduced reaction mechanism. *Combustion and Flame*, 204, 162–175.
<https://doi.org/10.1016/j.combustflame.2019.03.008>

[91] Wang, H., Zhang, L., Zhang, J., Wang, P., Hu, L., & Guo, Z. (2021). Study on the propagation velocity of methane/air pleated flames based on image processing and fractal interpolation. *AIP Advances*, 11(6). <https://doi.org/10.1063/5.0047915>

[92] Zhong, Z., Zhou, J., & Long, J. (2020). Effect of high temperature and pressure on laminar burning velocity and reaction kinetics of methane/iso-octane mixtures. *Energy Sources, Part A: Recovery, Utilization and Environmental Effects*.
<https://doi.org/10.1080/15567036.2020.1818006>

[93] Tang, C., He, J., Huang, Z., Jin, C., Wang, J., Wang, X., & Miao, H. (2008). Measurements of laminar burning velocities and Markstein lengths of propane-hydrogen-air mixtures at elevated pressures and temperatures. *International Journal of Hydrogen Energy*, 33(23), 7274–7285. <https://doi.org/10.1016/j.ijhydene.2008.08.053>

[94] Liu, Y., Gu, W., Wang, J., Ma, H., Dong, N., & Zeng, W. (2022). Laminar burning velocity of microalgae oil/RP-3 premixed flame at elevated initial temperature and pressure. *Fuel*, 309. <https://doi.org/10.1016/j.fuel.2021.122081>

[95] Kenneth, K. K. (2004). *Principles of Combustion*. Second edi. John Wiley and Sons, Inc.

[96] Li, Y., Bi, M., Li, B., Zhou, Y., & Gao, W. (2018). Effects of hydrogen and initial pressure on flame characteristics and explosion pressure of methane/hydrogen fuels. *Fuel*, 233, 269–282. <https://doi.org/10.1016/j.fuel.2018.06.042>

[97] Baghirzade, M., Nasim, M. N., Nawaz, B., Aguilar, J., Shahsavan, M., Morovatiyan, M., & Mack, J. H. (2021). Analysis of premixed laminar combustion of methane with noble gases as a working fluid. *Proceedings of ASME 2021 Internal Combustion Engine Division Fall Technical Conference, ICEF 2021*.
<https://doi.org/10.1115/ICEF2021-67516>

[98] Wang, Z., Han, X., He, Y., Wang, S., Ji, R., Zhu, Y., & Cen, K. (2020). Investigation of flame and burner plate interaction during the heat flux method used for laminar burning velocity measurement. *Fuel*, 266.
<https://doi.org/10.1016/j.fuel.2020.117051>

- [99] Turns, R. S. (2000). *An Introduction to Combustion*. McGraw-Hill.
- [100] Barnard, J.A., & Bradley, J.N. (1985). *Flame and Combustion*, Chapman and Hall, London.
- [101] Beeckmann, J., Cai, L., & Pitsch, H. (2014). Experimental investigation of the laminar burning velocities of methanol, ethanol, n-propanol, and n-butanol at high pressure. *Fuel*, 117(PART A), 340–350. <https://doi.org/10.1016/j.fuel.2013.09.025>
- [102] Yang, J., Guo, J., Wang, C., Wang, X., Li, J., Zhang, S., Duan, Z., & Yang, F. (2020). Effect of equivalence ratio on hydrogen–methane–air deflagration in a duct with an open end. *Fuel*, 280. <https://doi.org/10.1016/j.fuel.2020.118694>
- [103] Sun, C., Li, Y., Liu, Z., He, X., & Liu, F. (2021). Experimental investigation on the effect of equivalence ratio on the development of cellular structure of E30-air mixture. *Experimental Thermal and Fluid Science*, 123. <https://doi.org/10.1016/j.expthermflusci.2020.110330>
- [104] Li, Y., Bi, M., Gao, W., Cong, H., & Li, B. (2021). Self-Acceleration and Self-Similarity of Hydrogen–Methane–Air Flame at Elevated Pressure. *Combustion Science and Technology*, 193(6), 1005–1021. <https://doi.org/10.1080/00102202.2019.1679126>
- [105] Konnov, A. A., Mohammad, A., Kishore, V. R., Kim, N. il, Prathap, C., & Kumar, S. (2018). A comprehensive review of measurements and data analysis of laminar burning velocities for various fuel+air mixtures. In *Progress in Energy and Combustion Science* (Vol. 68, pp. 197–267). Elsevier Ltd. <https://doi.org/10.1016/j.pecs.2018.05.003>
- [106] Akram, M. Z., Liu, F., & Wu, H. (2020). Study on lean burn limits and burning characteristics of n-heptane with effects of hydrogen enrichment. *International Journal of Hydrogen Energy*, 45(46), 25452–25467. <https://doi.org/10.1016/j.ijhydene.2020.06.244>
- [107] Khan, A. R., Ravi, M. R., & Ray, A. (2019). Experimental and chemical kinetic studies of the effect of H₂ enrichment on the laminar burning velocity and flame stability of various multicomponent natural gas blends. *International Journal of Hydrogen Energy*, 44(2), 1192–1212. <https://doi.org/10.1016/j.ijhydene.2018.10.207>
- [108] Ueda, A., Nisida, K., Matsumura, Y., Ichikawa, T., Nakashimada, Y., Endo, T., & Kim, W. (2021). Effects of hydrogen and carbon dioxide on the laminar burning velocities of methane–air mixtures. *Journal of the Energy Institute*, 99, 178–185. <https://doi.org/10.1016/j.joei.2021.09.007>

- [109] Boushaki, T., Dhué, Y., Selle, L., Ferret, B., & Poinso, T. (2012). Effects of hydrogen and steam addition on laminar burning velocity of methane-air premixed flame: Experimental and numerical analysis. *International Journal of Hydrogen Energy*, 37(11), 9412–9422. <https://doi.org/10.1016/j.ijhydene.2012.03.037>
- [110] Hu, E., Huang, Z., He, J., Jin, C., & Zheng, J. (2009). Experimental and numerical study on laminar burning characteristics of premixed methane-hydrogen-air flames. *International Journal of Hydrogen Energy*, 34(11), 4876–4888.
- [111] Moccia, V., & D'Alessio, J. (2013). Burning behaviour of high-pressure CH₄-H₂-air mixtures. *Energies*, 6(1), 97–116. <https://doi.org/10.3390/en6010097>
- [112] Pugh, D. (2013). Combustion characterisation of compositionally dynamic steelworks gases. Thesis, Cardiff University.
- [113] Xie, Y., Lv, N., Li, Q., & Wang, J. (2020). Effects of CO addition on laminar flame characteristics and chemical reactions of H₂ and CH₄ in oxy-fuel (O₂/CO₂) atmosphere. *International Journal of Hydrogen Energy*, 45(39), 20472–20481. <https://doi.org/10.1016/j.ijhydene.2019.10.138>
- [114] Anggono, W., Hayakawa, A., Okafor, E. C., Gotama, G. J., & Wongso, S. (2021). Laminar Burning Velocity and Markstein Length of CH₄/CO₂/Air Premixed Flames at Various Equivalence Ratios and CO₂ Concentrations Under Elevated Pressure. *Combustion Science and Technology*, 193(14), 2369–2388. <https://doi.org/10.1080/00102202.2020.1737032>
- [115] Wei, S., Yu, M., Pei, B., Zhu, Z., & Zhang, Z. (2020). Suppression of CO₂ and H₂O on the cellular instability of premixed methane/air flame. *Fuel*, 264. <https://doi.org/10.1016/j.fuel.2019.116862>
- [116] Zhou, Q., Cheung, C. S., Leung, C. W., Li, X., & Huang, Z. (2019). Effects of diluents on laminar burning characteristics of bio-syngas at elevated pressure. *Fuel*, 248, 8–15. <https://doi.org/10.1016/j.fuel.2019.03.062>
- [117] Zhang, C., Wen, J., Shen, X., & Xiu, G. (2019). Experimental study of hydrogen/air premixed flame propagation in a closed channel with inhibitions for safety consideration. *International Journal of Hydrogen Energy*, 44(40), 22654–22660. <https://doi.org/10.1016/j.ijhydene.2019.04.032>
- [118] Mitu, M., Razus, D., & Schroeder, V. (2021). Laminar burning velocities of hydrogen-blended methane–air and natural gas–air mixtures. calculated from the early stage of p(t) records in a spherical vessel. *energies Article*, vol. 14, p. 7556, 2021.

- [119] Bradley, D. (1996). Burning velocities, Markstein lengths, and flame quenching for spherical methane-air flames: A computational study. *Fuel and Energy Abstracts*, 37(3), 204. [https://doi.org/10.1016/0140-6701\(96\)88849-7](https://doi.org/10.1016/0140-6701(96)88849-7)
- [120] Bradley, D., Hicks, R. A., Lawes, M., Sheppard, C. G. W., & Woolley, R. (1998). The Measurement of Laminar Burning Velocities and Markstein Numbers for Iso-octane-Air and Iso-octane-n-Heptane-Air Mixtures at Elevated Temperatures and Pressures in an Explosion Bomb.
- [121] Song, J. H., Cho, S. H., Lee, K. M., & Park, J. (2020). Measurements of laminar burning velocity and Markstein length in outwardly-propagating spherical SNG-air premixed flames at elevated pressures. *Fuel*, 275.
- [122] Zhou, M., Li, G., Liang, J., Ding, H., & Zhang, Z. (2019). Effect of ignition energy on the uncertainty in the determination of laminar flame speed using outwardly propagating spherical flames. *Proceedings of the Combustion Institute*, 37(2), 1615–1622. <https://doi.org/10.1016/j.proci.2018.07.084>
- [123] Ngo, M. (2009). DETERMINATION OF THE MINIMUM IGNITION ENERGY (MIE) OF PREMIXED PROPANE/AIR.
- [124] Xie, Y., Wang, J., Cai, X., & Huang, Z. (2016). Self-acceleration of cellular flames and laminar flame speed of syngas/air mixtures at elevated pressures. *International Journal of Hydrogen Energy*, 41(40), 18250–18258. <https://doi.org/10.1016/j.ijhydene.2016.07.239>
- [125] Wu, Y. (2017). Experimental investigation of laminar flame speeds of kerosene fuel and second generation biofuels in elevated conditions of pressure and preheat temperature. Normandie Université.
- [126] Mei, B., Zhang, X., Ma, S., Cui, M., Guo, H., Cao, Z., & Li, Y. (2019). Experimental and kinetic modeling investigation on the laminar flame propagation of ammonia under oxygen enrichment and elevated pressure conditions. *Combustion and Flame*, 210, 236–246. <https://doi.org/10.1016/j.combustflame.2019.08.033>
- [127] Vagelopoulos, C. M., Egolfopoulos, F. N., & Law, C. K. (1994). FURTHER CONSIDERATIONS ON THE DETERMINATION OF LAMINAR FLAME SPEEDS WITH THE COUNTERFLOW TWIN-FLAME TECHNIQUE.
- [128] Tien, J. H., & Matalon, M. (1991). On the Burning Velocity of Stretched Flames. In *COMBUSTION AND FLAME* (Vol. 84).
- [129] Jayachandran, J., Zhao, R., & Egolfopoulos, F. N. (2014). Determination of laminar flame speeds using stagnation and spherically expanding flames: Molecular


transport and radiation effects. *Combustion and Flame*, 161(9), 2305–2316.
<https://doi.org/10.1016/j.combustflame.2014.03.009>


[130] Law, C. K., Makino, A., & Lu, T. F. (2006). On the off-stoichiometric peaking of adiabatic flame temperature. *Combustion and Flame*, 145(4), 808–819.

Appendix

Calibration Certificate (A)


A.1 Pressure Transmitter





COSQC
Central Organization For
Standardization and Quality
Control
Calibrated

Cert. No: **PRE/338**
Date: **17/5/2020**
Due to (if applicable):



Calibration Certificate FOR-TC-012

Central Organization for Standardization and Quality Control (COSQC)
Metrology Department/Mass & Pressure Section/Pressure Lab.
P.O. Box13032 Algeria street, Baghdad ,Tel:7765180

E-Mail : cosqc@cosqc.gov.iq
Certificate No: **PRE/ 338 /2019**
Date of issue : **17/ 5 /2019**

Customer	
Name:	احمد عبد الأمير عبد الرحيم
Address:	العراق - بغداد
Item under calibration	
Description:	Pressure Transmitter
Manufacturer:	SIEMENS
Model:	7MF4033-1EA00-1AB7-Z
Serial number:	N1-R924-9430763
Other identification:	Range = 4000 kpa d = 0.01 kpa
Date of reception:	3 / 5 /2020 Order No.=179
Condition of reception	As found
Standard(s) used in the calibration	
Description:	Portable Pressure Calibrator
Manufacturer:	AMETEK
Model:	IP1300CBXXANDG
Serial number:	9894005
Other identification:	Range = 2000 kpa d = 0.001 kpa
Calibration information	
Date of calibration:	17 / 5 /2020
Place of calibration:	Pressure Lab.
Method(s) of	Calibration method are based on (PROC-TC-012)
Calibrated quantity:	Pressure
Results of calibration:	Attached a complete result in Annex 1 of this certificate
Measurement uncertainty:	The reported expanded uncertainty is DKD-6-1:2014the standard Uncertainty multiplied by coverage factor k=2 to give confidence level of 95% .
Metrological traceability:	The traceability of measurement to the SI units issued by the National Standard maintained at central organization for standardization and quality control through calibration certificat issued (UME) of certificate NO. = G2BA-0080
Environmental conditions of calibration:	Temp. (22.5 °C) R. H.(43.4%)
Observations, opinions or Recommendations:	The results are within the tolerance according to DKD-6-1:2014

Approved by

Khulood khalid shukri
Head of Mass & Pressure Section

This certificate is issued in accordance with the laboratory accreditation requirements. It provides traceability of measurement to reo-standards, and to the units of measurement realized at the COSQC or other recognized national standards laboratories. This certificate may not be reproduced other than in full by photographic process. This certificate refers only to the particular item submitted for calibration



Calibration Certificate

FOR-TC-012

Central Organization for Standardization and Quality Control (COSQC)
Metrology Department/Mass & Pressure Section/Pressure Lab.

P.O. Box13032 Algeria street, Baghdad ,Tel:7765180

E-Mail : cosqc@cosqc.gov.iq

Certificate No: PRE/ 338 /2019

Date of issue: 17/ 5 /2019

Annex 1/ Results

APP.Pressure	Reading		Mean Reading	Deviation (M-A)	Error
	Upward	Downward			
kpa	kpa	kpa	kpa	kpa	% of F.S
-50	-51.00	-50.20	-50.600	-0.600	0.015
0	-0.80	-0.80	-0.800	-0.800	0.020
50	49.10	49.00	49.050	-0.950	0.024
100	99.30	98.90	99.100	-0.900	0.022
150	148.80	149.30	149.050	-0.950	0.024
200	199.70	199.50	199.600	-0.400	0.010
300	299.60	299.60	299.600	-0.400	0.010
Max. Expanded Uncertainty =			± 0.466	kpa	

Calibrated by:

Nabeel Lateef

Revised by :

khulood khalid

Approved by:

khulood khalid shukri
 Head of Maas & Pressure Sectio

page 2of 2

This certificate is issued in accordance with the laboratory accreditation requirements. It provides traceability of measurement to recognized national standards, and to the units of measurement realized at the COSQC or other recognized national standards laboratories. This certificate may not be reproduced other than in full by photographic process. This certificate refers only to the particular item submitted for calibration

A.2 Temperature Control with PT100



Calibration Certificate
Central Organization for Standardization and Quality Control (COSQC)
Metrology Department - Physics Section (FOR-TC-012)
 P.O. Box13032 Algaderia street, Baghdad , Tel:7785180 - E-Mail : cosqc@cosqc.gov.iq

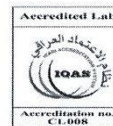
Certificate No.: PHT 283/2020
 Date of issue : 17/05/2020

Customer	
Name:	الجامعة التكنولوجية / ق. ه. الميكانيكية / طالب الدراسات العليا احمد عبد الامير عبد الرحيم
Address:	العراق - بغداد
Item under calibration	
Description:	Temperature Control with PT100
Manufacturer:	Nano Sens
Model:	
Serial number:	
Other identification:	(-40 --- 450) °C Res. 0.1 °C
Date of reception:	Order no. : (127) , Date of Reception : 11/05/2020
Condition of reception:	As Found
Standard(s) used in the calibration	
Description:	Thermometer Readout (Chub) PT100 (secondary standard)
Manufacturer:	Fluke / USA Fluke / USA
Model:	1529 5615
Serial number:	B2C801 887861
Other identification:	ID: PHT-01-18 ID: PHT-01-27
Calibration information	
Date of calibration:	17/05/2020 , Due To : 17/05/2021
Place of calibration:	PH LAB. 1
Method(s) of calibration:	Calibration method using - PROC-TC-012 (C)
Calibrated quantity:	Temperature °C
Results of calibration:	Attached a complete result in Annex 1 of this certificate
Measurement uncertainty:	The reported expanded uncertainty is based on UKAS M3003 Standard and the standard Uncertainty multiplied by coverage factor k=2 to give confidence level of 95%
Metrological traceability:	The traceability of measurement results to the SI units is assured by the National standard maintained at Central Organization for standardization and Quality Control through calibration at :- UME (G1KS-0127)
Environmental conditions of calibration:	Temp. 31.27° C RH.% 27%
Observations, opinions or recommendations:	The results in Annex 1 should be taken into consideration



Approved By :
Hanaa Mohammed
 Head Of Physics Section
 17/05/2020

1 of 2
 This certificate is issued in accordance with the laboratory accreditation requirements, it provides traceability of measurement to recognized national standards, and to the units of measurement realized at the COSQC or other recognized national standards laboratories. This certificate may not be reproduced other than in full by photographic process. This certificate refers only to the particular item submitted for calibration.



Calibration Certificate
Central Organization for Standardization and Quality Control (COSQC)
Metrology Department - Physics Section (FOR-TC-012)
P.O. Box13032 Algaderia street, Baghdad ,Tel:7785180 - E-Mail : cosqc@cosqc.gov.iq

Certificate No.: PHT 283/2020
Date of issue: 17/05/2020

Annex 1

Results

Set °C	Ref. °C (R)	UUC °C (M)	Error °C (M)-(R)	Uncertainty ±°C
50	49.87	49.6	-0.32	0.36
100	100.88	99.7	-1.22	0.35
150	148.08	149.4	1.35	0.17

Calibrated By :
Khalid Naser
17/05/2020

Revised By :
Ali Hassan
17/05/2020

Approved By :
Hanaa Mohammed
17/05/2020

2 of 2

This certificate is issued in accordance with the laboratory accreditation requirements. It provides traceability of measurement to recognized national standards, and to the units of measurement realized at the COSQC or other recognized national standards laboratories. This certificate may not be reproduced other than in full by photographic process. This certificate refers only to the particular item submitted for calibration

Ref. PROC. TC-012

A.3 High-Speed Camera (AOS)



Baden-Daettwil, 30th November 2021

To whom it may concern

CERTIFICATE OF CALIBRATION

We confirm that the delivered

Q-PRI camera with serial# 2121011648

has the following factory installed calibration files, which are valid and loaded in the camera:

2121011648_calib-coefficients_low.coeff
2121011648_calib-coefficients_high.coeff

Manufacturer
AOS Technologies AG

A handwritten signature in black ink that reads "S. Trost".

Stephan Trost
Managing Director

Appendix (B)

List of Publications

- 1- Salam H. Mahdi, Zaid M. AL-Dulaimi.(2022). Flame Speed and Laminar Burning Velocity in Syngas/Air Mixtures: A Review. International Journal of Design & Nature and Econdynamics.



Flame Speed and Laminar Burning Velocity in Syngas/Air Mixtures: A Review

Salam H. Mahdi*, Zaid M. Al-Dulaimi

Department of Mechanical Power Engineering, Technical Engineering College, Al-Furat Al-Awsat Technical University, Najaf 54001, Iraq

Corresponding Author Email: Salam_mahdi_ms_etcm@student.atu.edu.iq

<https://doi.org/10.18280/i2m.210302>

ABSTRACT

Received: 6 May 2022
Accepted: 7 June 2022

Keywords:
flame parameters, syngas, flame speed, combustion systems, laminar burning velocity

Flame speed and laminar burning velocity (LBV) are important properties of fuel combustion. Both have an impact on how combustion systems are designed and operated. As a result, understanding how LBV and flame speed fluctuate as a function of thermodynamic conditions is critical for understanding the impact of practical applications in all combustion systems. Working pressures and temperatures are far higher than those found in the environment. Several studies on flame speed and LBV have been conducted. This study, however, includes a thorough literature analysis of approaches and procedures used to measure these two parameters, as well as the effects of operational factors for various fuels, with a focus on biofuels, for the sake of review simplicity.

1. INTRODUCTION

Traditionally, coal and oil have traditionally been the main energy sources in recent decades, and they are directly burned to generate electric and kinetic energy in automobiles and power plants. As a result of the increased concern for environmental protection, more stringent emission laws have been enacted for automotive and power plant exhaust gas emissions. Clean combustion research has recently caught people's attention as a possible solution to this problem.

One of the most significant characteristics of a reacting premixed mixture is LBV, and precise data on it is always in demand for combustion applications. Since the late 1970s, scientists have made significant progress in their understanding of the effects of flame stretch on LBV [1]. Syngas is gaining appeal as a cleaner alternative fuel.

Syngas is a gasification product largely composed of H₂, CH₄, CO₂, N₂, CO, and other components, with a small amount of H₂S [2]. Rather than solely in gas turbines, syngas can also be utilized to create power.

However, internal combustion engines are also used. The lack of a consistent fuel supply [3], gas turbine [4], is one of the most critical challenges for syngas-fired IC engines. Fluctuations in the composition of syngas are an issue in this and other combustion systems. Because of the many fuel sources and processing circumstances, syngas composition is quite complex [5]. Hundreds of chemical processes, turbulence vortex patterns, and acoustic field interactions all contribute to the combustion process. Furthermore, because of its complex geometry and operating approach, the combustion process is more difficult to comprehend. As a result, several fundamental study topics have been created, such as laminar flame dynamics, to examine various features of the combustion process [6], flame-turbulence interaction [7], chemical reaction process [8], and so on.

One of the most widely used pieces of equipment is the constant-volume combustion bomb (Figure 1), which ignites the combustible mixture in the domain center and produces a

laminar spherically premixed flame that spreads outwardly [9]. One of the most important and well-studied subjects in laminar flame dynamics is the laminar spherically premixed flame of the combustion bomb. This article looks at a variety of factors influence the laminar burning velocity and flame speed for biofuel/air mixtures: a review study. such as initial pressure, initial temperature, flame temperature, initial ignition energy, etc. While the laminar flame speed is the most important parameter for understanding combustion properties. Wrinkled structures may emerge on the flame front when the pressure is increased or hydrogen is introduced to the lean combustible mixture. In this case, the wrinkled structure on the surface of a laminar spherically premixed flame will be looked at.

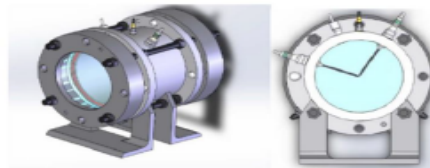


Figure 1. Constant volume combustion chamber [9]

2. FLAME PARAMETER CHARACTERISTICS AND FUNDAMENTALS

A flammable combination's LBV is a critical property. refers to the rate at which an adiabatic, unstretched, premixed planar flame propagates relative to the unburned mixture [10]. The cumulative impact of mixture diffusivity, exothermicity, and reactivity determines the LBV of a premixed fuel-oxidizer mixture [11, 12]. As compared to unburned mixes, the burning velocity in the lamina LBV is the speed at which a steady,

2- Salam H. Mahdi, Zaid M. AL-Dulaimi.(2022). Numerical Study of Laminar Burning Velocity of CH₄/air Mixture with H₂ Dilution and different Initial Pressure.AIP.



1st International Conference on Achieving the Sustainable Development Goals

(6th – 7th) June 2022 in Istanbul- Turkey

Final Acceptance Letter

Manuscript Number: 98

Dear: Salam Hasan Mahdi

Co-Authors: Zaid Maan H. Al-Dulaimi

Congratulations!

It's a great pleasure to inform you that, after the peer review process, your manuscript entitled

(Numerical Study of Laminar Burning Velocity of CH₄/air Mixture with H₂ Dilution and different Initial Pressure)

had been **ACCEPTED** for participating in the **1st International Conference on Achieving the Sustainable Development Goals**, and considered for publication in **(AIP Conference proceeding)**.

Thank you for your valuable participation in the ICASDG2022 conference.

A handwritten signature in green ink, appearing to read "Ahmed G. Wadday".



Prof. Dr. Ahmed G. Wadday
ICASDG2022 Scientific Committee Chair | AIP Conference Proceeding Editor
6th – 7th June 2022 | Istanbul | Turkey

الخلاصة

تعتبر هذه الدراسة مهمة جدًا للاحتراق ، فالاحتراق من أكبر المشاكل في حياتنا ، حيث يلعب دورًا أساسيًا في البيئة والاقتصاد. من أهم الخصائص التي تحدد الاحتراق هو حساب سرعة اللهب الأساسية. حيث يتم حساب سرعة اللهب الرقائقي لتحديد هذه السرعة. تعد سرعة اللهب الرقائقي أحد أهم العوامل التي تحدد نوع الوقود المستخدم في الاحتراق. تعتمد سرعة اللهب بشكل أساسي على نسبة الكثافة غير المحترقة إلى نسبة الكثافة المحترقة. في هذه الدراسة ، تمت دراسة سرعة اللهب الرقائقي وسرعة احتراق اللهب المخلوط مسبقًا لمختلف أنواع الوقود تجريبيًا وعدديًا. في هذه الدراسة تم استخدام برنامج Traker لتحليل سرعة اللهب الممتد ، وبرنامج CHEMKIN-PRO لحساب درجة حرارة اللهب الثابت ونسبة الكثافة ، والتي تستخدم لحساب سرعة الاحتراق الرقائقي. أولاً ، قمنا بتقييم سرعات الاحتراق الرقائقي لمزيج الميثان / الهواء لتأكيد نتائج التصميم التجريبي. كشفت المقارنة عن اتفاق قوي مع النتائج الواردة في الأدبيات ، مما يؤكد الدقة الممتازة للتصميم التجريبي وتقنيات القياس. تم تقييم سرعة الاحتراق الرقائقي (LBV) لمزيج الميثان/هيدروجين/ثاني أكسيد الكربون/الهواء الممزوج مسبقًا باستخدام CHEMKIN-PRO. بدرجة حرارة ابتدائية (303 كلفن)، وضغوط (0.1 ميغا باسكال ، 0.15 ميغا باسكال ، 0.2 ميغا باسكال) ، ونسب تكافؤ (0.8-1.2). كانت الدراسة التجريبية عبارة عن تصميم وبناء غرفة حجم ثابت اشتعال مركزيًا (CVC) تم استخدامه لحساب سرعة اللهب غير الممتدة (S_I) ، وسرعة اللهب الممتدة (S_n) ، وسرعة الاحتراق الرقائقي (S_u). باستخدام تقنية schlieren وكاميرا عالية السرعة تسجل عملية الاحتراق. أجريت التجارب في قنبلة ذات حجم ثابت بنصف قطر داخلي 150 ملم وطول 510 ملم، باستخدام أنواع مختلفة من الوقود النقي (الميثان) ومزيج الميثان / الهيدروجين بنسب مزج تتراوح من 10٪ إلى 30٪ بالحجم. أجريت التجارب عند ضغوط أولية قدرها 0.1 ميغا باسكال ، ودرجات حرارة أولية 303 ± 3 كلفن ، ونسب تكافؤ من 0.8 إلى 1.2 لخليط الهواء / الوقود. وجد أن إضافة ثاني أكسيد الكربون إلى خليط الميثان / الهواء بنسبة 30٪ من حجم الوقود سيقال من سرعة الاحتراق الرقائقي LBV بنسبة 36٪ (38 سم / ثانية - 28 سم / ثانية) ، بينما وجد أن إضافة الهيدروجين إلى الميثان / خليط الهواء بنسبة 30٪ من حجم الوقود سيرفع LBV بنسبة 29٪ (38 سم / ثانية - 48 سم / ثانية). من ناحية أخرى ، استنتج أنه يجب إضافة الهيدروجين بأكثر من

30% من حجم خليط الميثان / الهواء لتجاوز التأثير السلبي لمضاعفة الضغط الأولي. أخيرًا ، تم العثور على زيادة الضغط الأولي لإبطاء LBV. بهذه الطريقة، سوف يضاعف الضغط الأولي إضافة عنصر الهيدروجين مع أقصى نسبة مستخدمة في العمل الحالي.



تأثير المتغيرات المختلفة على عوامل الاحتراق باستخدام غرفة الاحتراق بالحجم الثابت

رسالة

مقدمة الى قسم هندسة تقنيات ميكانيك القوى

كجزء من متطلبات نيل درجة الماجستير في هندسة تقنيات ميكانيك القوى / الحراريات

تقدم بها

سلام حسن مهدي

ماجستير في هندسة تقنيات ميكانيك القوى

اشراف

الاستاذ المساعد الدكتور

زيد حسن معن

أيلول / 2022



جمهورية العراق
وزارة التعليم العالي والبحث العلمي
جامعة الفرات الاوسط التقنية
الكلية التقنية الهندسية – نجف

تأثير المتغيرات المختلفة على عوامل الاحتراق باستخدام غرفة الاحتراق
بالحجم الثابت

سلام حسن مهدي

ماجستير في هندسة تقنيات ميكانيك القوى

2022